Identification and characterization of *Dorea ammoniilytica* as a novel deoxycholic acid-producing bacterial species in the human gut microbiota

(ヒト腸内細菌叢における新規デオキシコール酸生産細菌種

Dorea ammoniilytica の同定と特性の評価)

北海道大学大学院農学院
農学専攻生命フロンティアコース博士後期課程

Ni Wayan Eka Putri Gayatri Kastawa

January 2026

Table of Contents

List of Tables

List of Figures

Chapter I. General Introduction

General Introduction

1. Bile acids

Bile acids (BAs) are cholesterol-derived, amphipathic molecules that aid in the breakdown of dietary lipids. The detergent-like properties of BAs allow them to promote lipid and fat-soluble vitamin absorption when secreted into the intestinal lumen during digestion (Lefebvre *et al*. 2009). Beyond this classical digestive role, BAs are now recognized as important signaling molecules that regulate diverse metabolic processes, including glucose and lipid metabolism, energy homeostasis, and immune function (Chen *et al*. 2023; Xu *et al*. 2023; Zhang *et al*. 2024; Thibaut *et al*. 2022; Zhao *et al*. 2025). Various derivation of bile acids are presented in humans and rodent as a result of additional modifications that will be discussed later (**Figure 1-1**).

1.1. Primary BA synthesis

In humans, BAs are synthesized from cholesterol in the liver via two major pathways: the classic (neutral) pathway and the alternative (acidic) pathway **(Figure 1-2)**. Together, these pathways regulate cholesterol catabolism and maintain BA homeostasis. The classic pathway represents the predominant route of BA synthesis in humans, accounting for approximately 90% of total BA production (Russell, 2003). This pathway is initiated by cholesterol 7α-hydroxylase (CYP7A1), a microsomal enzyme that catalyzes the rate-limiting step in BA biosynthesis. Through a series of enzymatic reactions, cholesterol is primarily converted into the two major primary BAs, cholic acid (CA; 3α,7α,12α-trihydroxy-5β-cholan-24-oic acid) and chenodeoxycholic acid (CDCA; 3α,7α-dihydroxy-5β-cholan-24-oic acid) (Ridlon *et al*. 2006). The activity of CYP7A1 is tightly regulated by negative feedback mechanisms involving BA-activated receptors, particularly the farnesoid X receptor (FXR), which suppresses BA synthesis to prevent toxic accumulation (Russell, 2003; Chiang and Ferrell 2019).

The alternative, or acidic, pathway contributes a smaller but physiologically significant portion of BA pool. This pathway is initiated by sterol 27-hydroxylase (CYP27A1), a mitochondrial enzyme expressed in the liver as well as in extrahepatic tissues. The alternative pathway preferentially contributes to CDCA synthesis and is thought to play an important role under specific physiological or pathological conditions, including altered cholesterol metabolism. In addition, cholesterol 24-hydroxylase (CYP46A1), primarily expressed in the brain, contributes indirectly to BA synthesis by facilitating cholesterol turnover (Russell, 2003; Chiang and Ferrell 2018).

1.2. Conjugation and enterohepatic circulation

Before secretion from the liver to the small intestine via the gallbladder, primary BAs are conjugated in hepatocytes with the hydrophilic amino acids glycine or taurine, forming conjugated BAs such as glycocholic acid (GCA), taurocholic acid (TCA), glycochenodeoxycholic acid (GCDCA), and taurochenodeoxycholic acid (TCDCA) (Garidel *et al*. 2007). In humans, glycine conjugation predominates over taurine conjugation, a species-specific feature that influences BA solubility and intestinal behavior (Hardison, 1978). Conjugation lowers the pKa of BAs, increasing their solubility and reducing passive diffusion across cell membranes, thereby limiting cytotoxicity and enhancing their retention within the enterohepatic circulation. Conjugated BAs are secreted into bile, concentrated in the gallbladder, and released into the duodenum in response to food intake. Nutrient ingestion stimulates the release of cholecystokinin from enteroendocrine cells, triggering gallbladder contraction and BA secretion (Di Ciaula *et al*. 2017). In the small intestine, BAs facilitate lipid digestion through the formation of mixed micelles, enabling efficient absorption of dietary lipids, cholesterol, and fat-soluble vitamins (A, D, E, and K) (Ridlon *et al*. 2016).

Following their intestinal function, the majority of BAs are efficiently reabsorbed in the distal ileum via active transport mechanisms. Approximately 95% of secreted BAs are recycled and returned to the liver through the portal circulation, a process known as enterohepatic circulation **(Figure 1-3)** (Ridlon *et al*. 2006). Hepatic uptake of BAs allows their reuse in subsequent digestive cycles, contributing to the tight regulation of the BA pool. This highly efficient recycling system is essential for maintaining BA homeostasis and limiting de novo synthesis. Nevertheless, a small fraction of BAs, approximately 5%, escapes ileal reabsorption and enters the large intestine. (Ridlon *et al*. 2006; Ridlon *et al*. 2016). In the large intestine, BAs that escape enterohepatic circulation are exposed to dense and metabolically diverse gut microbial communities. These microorganisms can modify BAs via a range of biochemical reactions, yielding secondary BAs with distinct structural and functional properties.

1.3. Structural diversity and physicochemical properties of human BAs

In addition to the conjugated primary BAs, humans and rodents possess a diverse pool of BA derivatives generated through further enzymatic modifications, including oxidation, epimerization, and dehydroxylation **(Fig. 1-4)** (Ridlon *et al*. 2006). Human BAs are characterized by hydroxyl groups typically located at the C-3, C-7, and C-12 positions of the steroid nucleus, as well as a side chain terminating in a carboxyl group. Structural diversity among BAs arises from differences in (1) side chain length and modifications, (2) the stereochemistry of the A/B ring fusion, and (3) the number, position, and orientation of hydroxyl groups on the steroid backbone. These structural features strongly influence the physicochemical properties of BAs, including their solubility, hydrophobicity, and biological activity (Monte *et al*. 2009).

BAs vary considerably in hydrophobicity, which affects their detergent strength, cytotoxicity, and interactions with biological membranes **(Figure 1-5)** (Modica *et al*. 2010). More hydrophobic BAs exhibit more potent membrane-disrupting properties and are generally more cytotoxic, whereas hydrophilic BAs are less damaging to host tissues. These differences have important implications for BA signaling, host tolerance, and microbial selection within the gut environment (De Aguiar *et al*. 2013).

1.4. Biotransformation of BAs

The human gastrointestinal (GI) tract represents the most significant interface (250-400 m^2) between the host, environmental factors, and antigens in the human body. Consequently, the human GI tract harbors an abundance of microorganisms that pose a significant threat to gut integrity (Bengmark, 1998). The number of microorganisms in the GI tract has been estimated to exceed 10^{14} cells, which is higher than the number of human cells. In addition, gut microbiota can carry out a variety of bile salt biotransformations (Bäckhed *et al*.; Ridlon *et al*. 2016).

Microbial enzymes can modify primary BAs through deconjugation, oxidation/epimerization of C-3, C-7, or C-12 hydroxy groups, and 7α/β dehydroxylation to produce secondary BAs (Ridlon *et al*. 2016). Before their production, the deconjugation of the BAs, which removes taurine and glycine from conjugated primary BAs, is necessary. The gut microbiota can oxidize and epimerize hydroxy groups at the C-3, C-7, and C-12 positions of BAs, yielding iso-bile (β-hydroxy) acids **(Figure 1-6)** (Ridlon *et al*. 2016). The BA 7α/β-dehydroxylation is a representative conversion reaction from primary BAs (CA and CDCA) to secondary BAs by the gut microbiota. It comprises a multi-step biochemical pathway called 7α-dehydroxylation by anaerobic gut bacteria that produces deoxycholic acid (DCA; 3α, 12α-

dihydroxy-5β-cholan-24-oic acid) from CA and lithocholic acid (LCA; 3α-hydroxy-5β-cholan-24-oic acid) from CDCA (Ridlon *et al*. 2016).

1.4.1. Deconjugation of BAs

BA conjugation refers to the amide linkage of primary BAs to taurine or glycine at the C-24 side chain. This process occurs in the liver prior to secretion into the gastrointestinal tract. The BA profile in the small intestine closely resembles the biliary pool. In contrast, fecal and cecal BA profiles consist predominantly of unconjugated and secondary BAs, reflecting the activity of bile salt hydrolases (BSHs) and further BA transformations mediated by the gut microbiota (Ridlon *et al*. 2016). BSHs catalyze the hydrolysis of the C-24 N-acyl bond, releasing free BAs and their corresponding amino acids. These enzymes belong to the N-terminal nucleophilic hydrolase family, which also includes penicillin amidases, and are characterized by a catalytic N-terminal cysteine residue (Tanaka *et al*. 2000). BSHs are oxygen-insensitive, intracellular enzymes with an optimal pH range of 5 to 6. In some bacteria, BSH activity provides a source of energy and metabolic building blocks for biosynthesis (Coleman and Hudson 1995; Tanaka *et al*. 2000; Kim *et al*. 2004). Following deconjugation, glycine can be further metabolized to ammonia and carbon dioxide, while taurine catabolism produces ammonia, carbon dioxide, and sulfite (Ridlon *et al*. 2016). Most BSH-harboring bacteria in the gut are Gram-positive, including members of the genera *Clostridium*, *Enterococcus, Bifidobacterium*, and *Lactobacillus*. Among Gram-negative bacteria, BSH activity has been primarily identified in the genus *Bacteroides* (Ridlon *et al*. 2006; Ridlon *et al*. 2016). Importantly, BSH is a prerequisite for gut microbiota production of secondary BA (Ridlon *et al*. 2006). High BSH gene expression under an animal-based diet was associated with a significant increase in DCA levels in human feces (David *et al*. 2014) .

1.4.2. Production of secondary BAs from primary BAs by intestinal bacteria in the gastrointestinal tract

During enterohepatic circulation, approximately 5% of BAs escape the circulation and enter the colon, where they can be transformed into various secondary BAs by some members of gut microbiota. One of the main biotransformations of primary BA by gut microbiota is oxidation/epimerization of the hydroxy group at C-3, C-7, and C-12 positions. Another predominant biotransformation is 7α-dehydroxylation, as its products, DCA and LCA, predominate in human feces (Ridlon *et al*. 2006).

1.4.2.1. Oxidation and epimerization of the hydroxy group

Oxidation and epimerization of the C-3, C-7, and C-12 hydroxy groups of the BAs in the gastrointestinal tract are carried out by gut microbiota harboring genes encoding hydroxysteroid dehydrogenases (HSDHs), which belong to the short-chain dehydrogenase/reductase superfamily. These enzymes catalyze the reversible oxidation of a hydroxy group to a carbonyl group at the specific carbon position in the BA molecule (Bortolini *et al*. 1997; Ridlon *et al*. 2006). Epimerization of BA hydroxy groups requires HSDHs, which produce a stable oxo-BA intermediate, α-hydroxy group ↔ oxo ↔ β-hydroxy group. The oxidation/reduction potential of the cellular environment appears to influence the extent of epimerization and accumulation of the oxo-BA intermediate. Oxo-BA formation may be advantageous in bacteria on the mucosal surface of the gut, which has a higher redox potential than that in the intestine lumen (Ridlon *et al*. 2006). The epimerization of the BAs 7α-hydroxy group reduces the toxicity of CDCA to gut microbiota. Ursodeoxycholic acid (UDCA), the 7β-epimer of CDCA, is more hydrophilic and less toxic to gut microbiota (Heuman *et al*. 1989; Matsuoka and Moroi, 2002; Watanabe *et al*. 2017).

The 3α- and β-HSDHs specifically catalyze the reversible, stereospecific oxidation/reduction of 3α- and 3β-OH groups of BA molecules. For example, Ruminococcus gnavus can epimerize the C-3 hydroxy group of DCA to form 3-iso-DCA through 3-oxo-DCA as an intermediate to reduce toxicity (Devlin and Fischbach 2015). 7α- and β-HSDHs reversibly catalyze the dehydrogenase reaction specific to the 7α- and β-hydroxy group at the C-7 position of BA molecules. 7α-HSDH is an essential enzyme that converts primary BAs into 7-oxo-BAs that are not substrates for 7α-dehydroxylation (Ridlon *et al*. 2016). Previous studies have demonstrated that *Bacteroides intestinalis* isolated from human feces is a secondary BA producer that converts CA and DCA into 7-oxo-DCA and 7-oxo-LCA, respectively, via 7α-HSDH activity (Fukiya *et al*. 2009). Additionally, *R. gnavus* N53 produces UDCA from 7-oxo-LCA by the 7β-HSDH (Lee *et al*. 2013). Oxidation/epimerization at the C-12 position of BAs by 12α- and β-HSDHs are rarely found. Biotransformation of the 12-hydroxy group mainly found among the genus Clostridium (Macdonald *et al*. 1979).

1.4.2.2. 7α/β dehydroxylation of BAs

The term of secondary BAs typically denotes BAs that have undergone fundamental microbial transformation in the gut, most notably the removal of the hydroxy group at C-7, a process known as 7α/β-dehydroxylation (Ridlon *et al*. 2006). The 7α-dehydroxylation reaction catalyzes the removal of 7α-hydroxy group of the BA molecules, while 7β-dehydroxylation reaction removes 7β-hydroxy group of BAs. Some intestinal bacteria are capable of both 7α/β-dehydroxylation, while others possess only 7α-dehydroxylation activity, reflecting the diversity of enzymatic capabilities within the gut microbiome (White *et al*. 1981). Notably, 7α/β-dehydroxylation is restricted to unconjugated BAs (free BAs), which require prior deconjugation of taurine- or glycine-conjugated BAs by BSHs (Ridlon *et al*. 2006),

The 7α-dehydroxylation is quantitatively the most active BA transformation in the intestine, mediated by spesific enzymes encoded by the bile acid-inducible (*bai*) gene cluster. This cluster includes multiple genes (*bai*A–*bai*I) that act in a coordinated, ordered sequence to remove the 7α-hydroxy group from CA and CDCA, ultimately producing DCA and LCA, respectively **(Figure 1-7)** (Funabashi *et al*. 2020). In contrast, 7β-dehydroxylation results in the production of LCA from urso deoxycholic acid (UDCA) (White *et al*. 1981; Ridlon and Bajaj, 2015). Both 7α/β-dehydroxylation share common enzymes including BaiGBAF. However, they are differentiated at specific steps involving BaiCD vs. BaiH, and Bai E vs. BaiI (Ridlon and Bajaj 2015; Kang *et al*. 2019).

2. Deoxycholic acid

DCA has been detected at substantial levels in fecal and cecal samples, accounting for approximately 34% of the total BA pool **(Figure 1-3)** (Ridlon *et al*. 2006). Among secondary BAs, DCA is particularly significant due to its significant effects on the composition and function of the gut microbiota. Its increased hydrophobicity resulted in bactericidal activity approximately 10 times higher than that of CA, allowing DCA to act as a potent regulator of microbial populations in the intestinal lumen **(Figure 1-8)** (Kurdi *et al*. 2006; Watanabe *et al*. 2017). This regulatory function is especially critical in conditions of high dietary fat intake, where DCA concentrations are elevated and modulate microbial ecology in the rat cecum (Islam *et al*. 2011; Watanabe *et al*. 2025).

In addition to its role in microbial regulation, DCA has multiple physiological effects on the host. Its amphipathic nature enables efficient emulsification of dietary lipids, facilitating the digestion and absorption of fats and fat-soluble vitamins. Furthermore, DCA functions as a signaling molecule by activating nuclear receptors, including the FXR, and membrane-bound receptors such as the Takeda G protein-coupled BA receptor 1 (TGR5) (Jalil *et al*. 2025).

Activation of these receptors influences a range of metabolic and immunological pathways, including lipid and glucose metabolism, energy homeostasis, and inflammatory responses.

Despite these beneficial roles, excessive accumulation of DCA has a carcinogenic effect on the liver and colon. Its high hydrophobicity makes it cytotoxic, inducing oxidative stress, membrane disruption, and DNA damage in intestinal epithelial cells. Chronic exposure to elevated DCA levels has been linked to the development of colorectal cancer (Cao *et al*. 2017; Cong *et al*. 2024) and hepatocellular carcinoma (Yoshimoto *et al*. 2013). Over recent decades, it has become evident that aspects of the 'western lifestyle' including diets low in fiber and high processed carbohydrates and saturated fats, increased both the amount of bile entering the GI tract and the hydrophobicity of the BA pool. These changes affect host metabolic function and increase the risk to human health (Wahlström *et al*. 2016; Trauner and Fuchs, 2022). Given the potent and multiphasic biological effects of DCA, it is crucial to understand and characterize DCA-producing bacteria in the human intestine.

3. DCA producers

The study of DCA-producing bacteria traces back to early 20th century studies that established the chemical structure of BAs. By the mid-1950s to 1960s, gnotobiology animal studies definitively demonstrated that DCA is a secondary BA, meaning the host liver does not synthesize it but is instead a product of microbial biotransformation in the gut (Bergström *et al*. 1960; Sjövall, 2004). In the 1960s, radiolabeling experiments further elucidated the stereochemistry of this transformation, leading to the discovery of a multi-step enzymatic process known as the Hylemon-Björkhem pathway, also referred to as the 7α-dehydroxylating pathway. This specialized pathway is primarily carried out by a small group of low abundance gut bacteria (Ridlon *et al*. 2023).

DCA-producing bacteria abundance in the gut was estimated to be only ~0.0001% of the total gut microbiota (Ridlon *et al*. 2006). Over the years, several DCA-producing bacteria have been discovered in the human gut, highlighting the complexity and diversity of microbial contributions to BA metabolism. Several studies have identified several species of DCA-producing bacteria, such as *Clostridium scindens* (Morris *et al*. 1985; Tawthep *et al*. 2017; Devendran *et al*. 2019), *Peptacetobacter hiranonis* (Kitahara *et al*. 2001; Chen *et al*. 2020), *Clostridium hylemonae* (Kitahara *et al*. 2000; Ridlon *et al*. 2010), *Dorea* sp. (Bai *et al*. 2022), and *Eubacterium* sp. c-25 (Song *et al*. 2021), which was recently classified as *Claveliimonas bilis* (Hisatomi *et al*. 2023).

Among these, *C. scindens* has been frequently used as a reference or model species in studies of DCA biosynthesis. *C. scindens* possesses the *bai* operon, which encodes enzymes responsible for the 7α-dehydroxylation of primary BAs, a critical step in DCA formation. Its well-characterized enzymatic pathway and growth characteristics have made it a benchmark organism for exploring the molecular and physiological mechanisms underlying DCA production. A study in healthy Japanese subjects demonstrated that *C. scindens* was present at extremely low abundance in fecal samples, approximately ~$10^{5.5}$ cells per gram of feces, and that its prevalence did not significantly correlate with fecal DCA concentrations (Kitahara *et al*. 2004). These observations suggest that there may be less-characterized bacterial taxa that play substantial roles in shaping the pool of secondary BAs in the human intestine. This highlights a gap in our current knowledge and indicates that additional, possibly novel DCA-producing bacteria are likely still present in the human gut. Identifying these bacteria is essential not only to understand better how gut microbes metabolize BAs, but also to clarify how the gut microbiome affects host physiology and disease through the production of secondary BAs.

4. Study motivation and objective

DCA was produced in the human gut via a multi-step 7α-dehydroxylation pathway catalyzed by specific bacteria. Despite the physiological importance of this process, only a limited number of 7α-dehydroxylating bacteria have been isolated and studied. In contrast, recent metagenomic analysis of the human gut microbiota have substantially expanded our understanding of the genetic potential of them. The presence of *bai* genes has been reported in bacterial taxa that were not previously recognized as DCA producers (Vital *et al*. 2019). These *bai* genes are typically organized into a gene cluster that encodes the key enzymes required for the 7α-dehydroxylation pathway. The widespread detection of *bai* gene-containing metagenomic assembly genomes suggests that the capacity for DCA production may be more widely distributed among gut bacteria than previously known. However, most of these candidate organisms remain uncultured, and their predicted metabolic function have not been experimentally confirmed. As a result, a significant gap remains between metagenomic predictions and direct functional evidence of DCA production by the intestinal bacteria. This knowledge gap is critical because DCA is known to play a key role in shaping gut microbial communities and influencing host physiology in both beneficial and harmful effects. Therefore, a deeper understanding of the bacteria responsible for DCA production is essential for clarifying how gut microbial metabolism contributes to host health and disease.

Motivated by the limited number of characterized DCA-producing bacteria and the widespread metagenomic evidence of unrecognized contributors, this study aims to screen, identify, and characterize previously unrecognized DCA-producing bacteria in the human gut microbiota. Human fecal samples were used DCA-producing bacteria screening. Human fecal samples were serially diluted and cultured to test DCA production at decreasing bacterial densities. This approach allowed assessment of DCA-producing activity within the gut microbiota. Candidate strains were then analyzed using genomic and functional assays to

confirm their ability to produce DCA. Through this integrated approach, *Dorea ammoniilytica* was identified as a novel DCA-producing bacterium. Characterization of this species provides direct experimental evidence supporting the existence of underexplored DCA-producing bacteria in the human gut.

5. Figures and tables

a

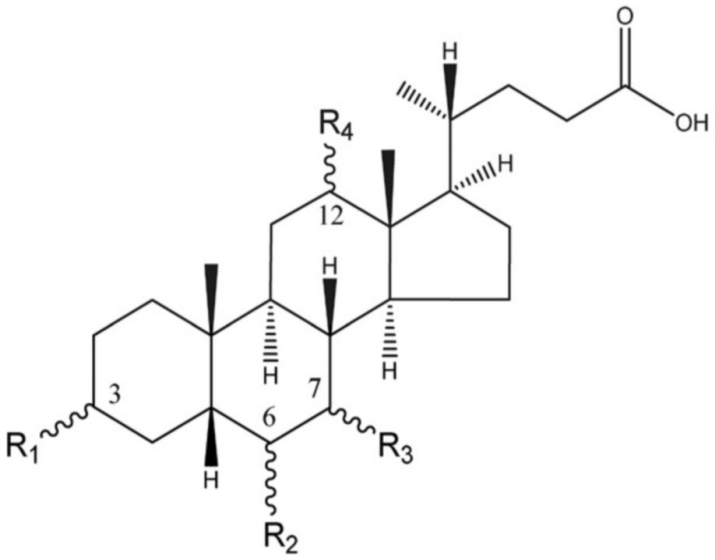

b

Name	R_1	R_2	R_3	R_4	Type[a]
3α, 7α, 12α-trihydroxy-5β-cholan-24-oic acid (Cholic acid; CA)	αOH	H	αOH	αOH	Common
3α, 7α, dihydroxy-5β-cholan-24-oic acid (Chenodeoxycholic acid; CDCA)	αOH	H	αOH	H	Common
3α, 12α, dihydroxy-5β-cholan-24-oic acid (Deoxycholic acid; DCA)	αOH	H	H	αOH	Common
3α-hydroxy-5β-cholan-24-oic acid (Lithocholic acid; LCA)	H	H	αOH	H	Common
3α, 7β, 12α-trihydroxy-5β-cholan-24-oic acid (Ursocholic acid; UCA)	αOH	H	βOH	αOH	Common
3α, 7β, dihydroxy-5β-cholan-24-oic acid (Ursodeoxycholic acid; UDCA)	αOH	H	βOH	H	Common
3α, 12α, dihydroxy-7-oxo-5β-cholan-24-oic acid (7-oxo-deoxycholic acid; 7-oxo-DCA)	αOH	H	=O	αOH	Common
3α-hydroxy-7-oxo-5β-cholan-24-oic acid (7-oxo-lithocholic acid; 7-oxo-LCA)	αOH	H	=O	H	Common
3α-hydroxy-12-oxo-5β-cholan-24-oic acid (12-oxo-lithocholic acid; 12-oxo-LCA)	αOH	H	H	=O	Common
3-oxo-12α-hydroxy-5β-cholan-24-oic acid (3-oxo-12α)	=O	H	H	αOH	Common

[a] The bile acids present in both humans and rodents were termed "common").

Figure. 1-1. General structure of bile acids and list of common bile acid derivatives found in humans.

(a) Schematic representation of the core bile acids structure and (b) a list of representative bile acid derivatives identified in humans and/or rodents. Adapted from Watanabe *et al*. 2017.

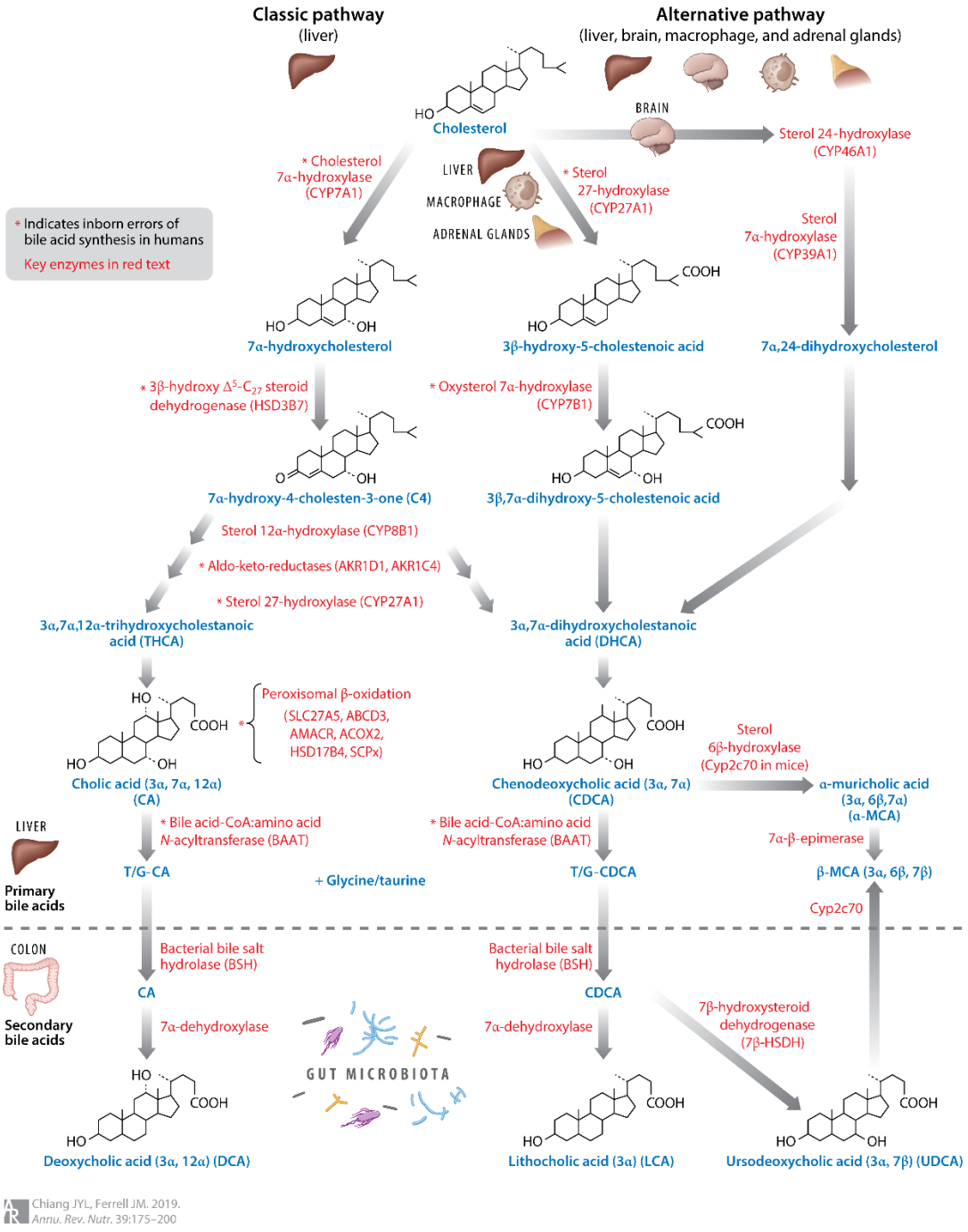

Figure 1-2. Classical and alternative bile acid synthesis pathways.

Diagram illustrating the classical (neutral) and alternative (acidic) bile acid synthesis pathway in the liver, highlighting the key enzymes and intermediates. Adapted from Chiang and Ferrell, 2019.

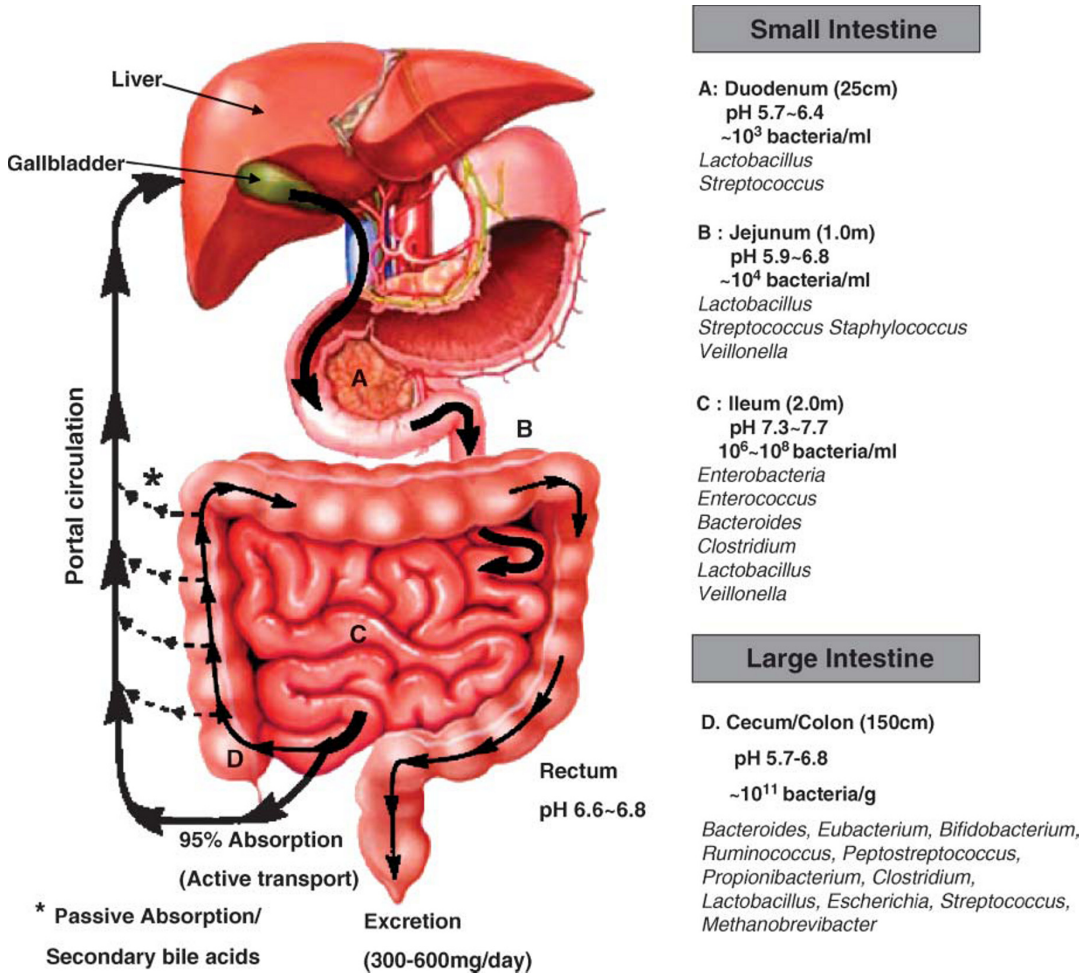

Figure 1-3. Gastrointestinal tract anatomy, enterohepatic circulation of bile and predominant microbial genera.

Schematic representation of the gastrointestinal tract anatomy, enterohepatic circulation of bile, and the predominant microbial genera present in each intestinal region. Adapted from Ridlon *et al*. 2006.

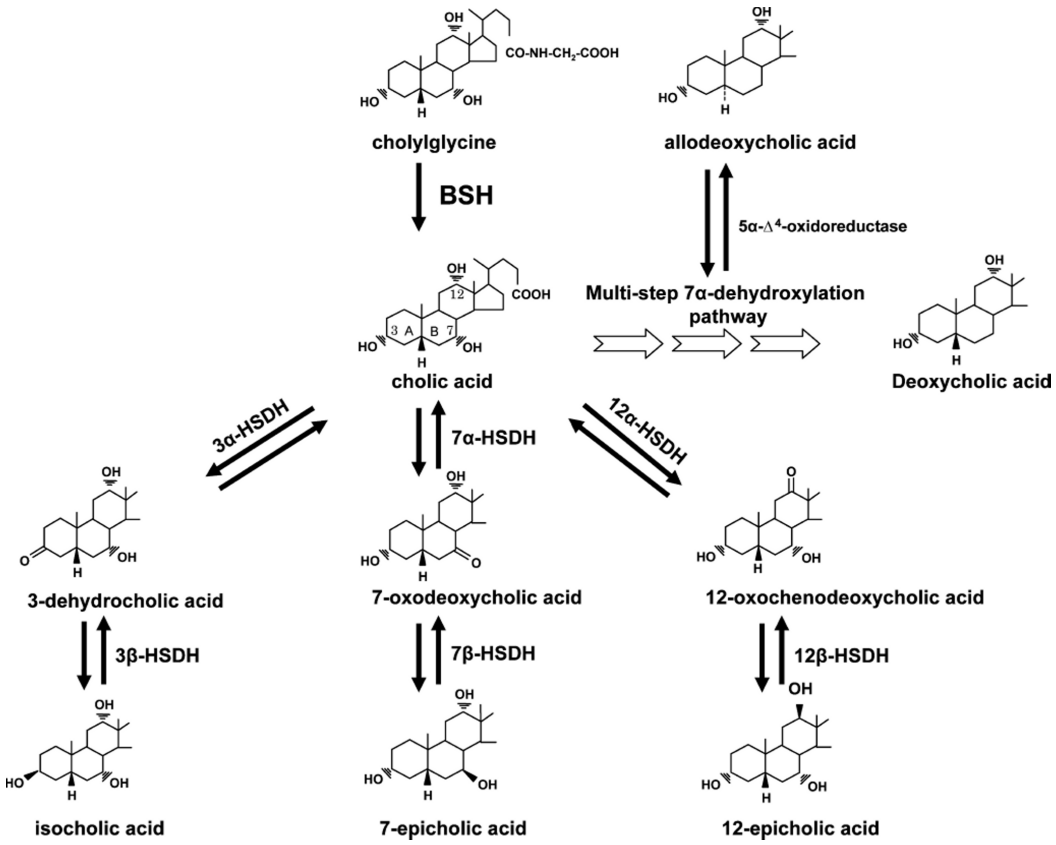

Figure 1-4. Bile salts transformation reaction in the gastrointestinal tract.

Illustration of the bile salts transformation pathways in the gastrointestinal tract, demonstrated using cholic acid as an example. Adapted from Ridlon *et al*. 2006.

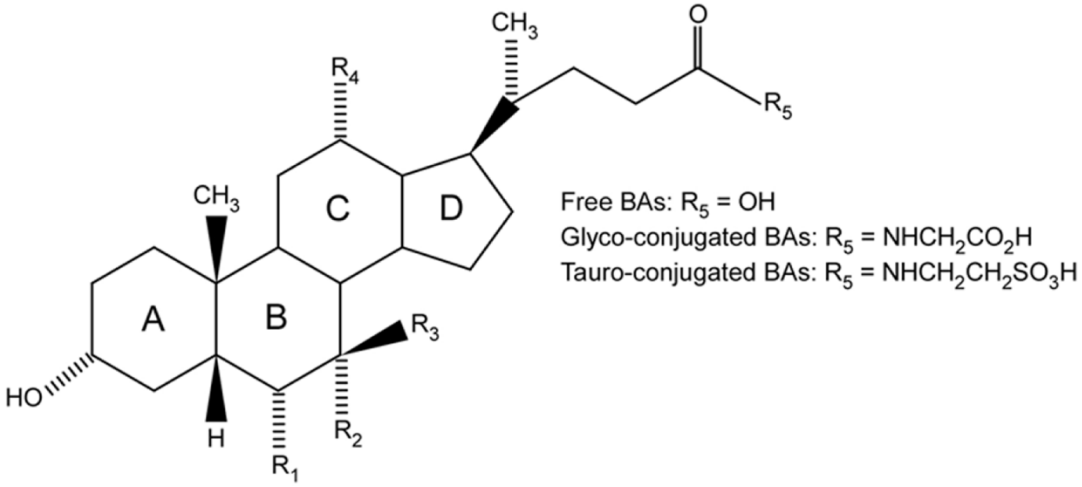

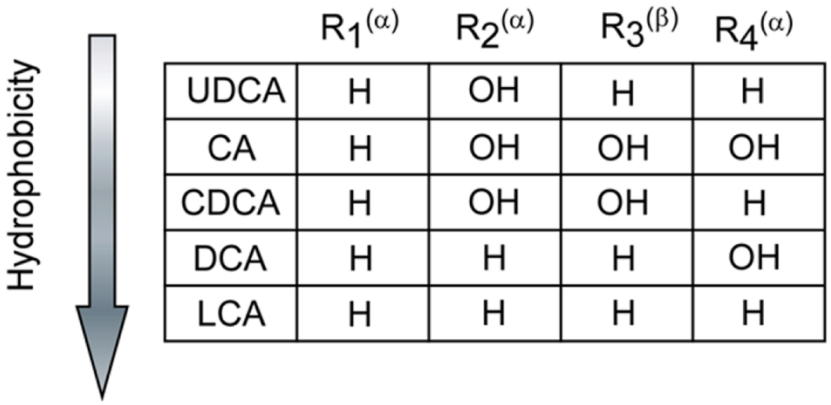

	$R_1^{(\alpha)}$	$R_2^{(\alpha)}$	$R_3^{(\beta)}$	$R_4^{(\alpha)}$
UDCA	H	OH	H	H
CA	H	OH	OH	OH
CDCA	H	OH	OH	H
DCA	H	H	H	OH
LCA	H	H	H	H

Figure 1-5. Hydrophobicity profiles of common bile acids and their associated side modifications.

Comparison of hydrophobicity among common bile acids, showing how specific side-chain modification influence their hydrophobicity profiles. Adapted from Modica *et al*. 2010.

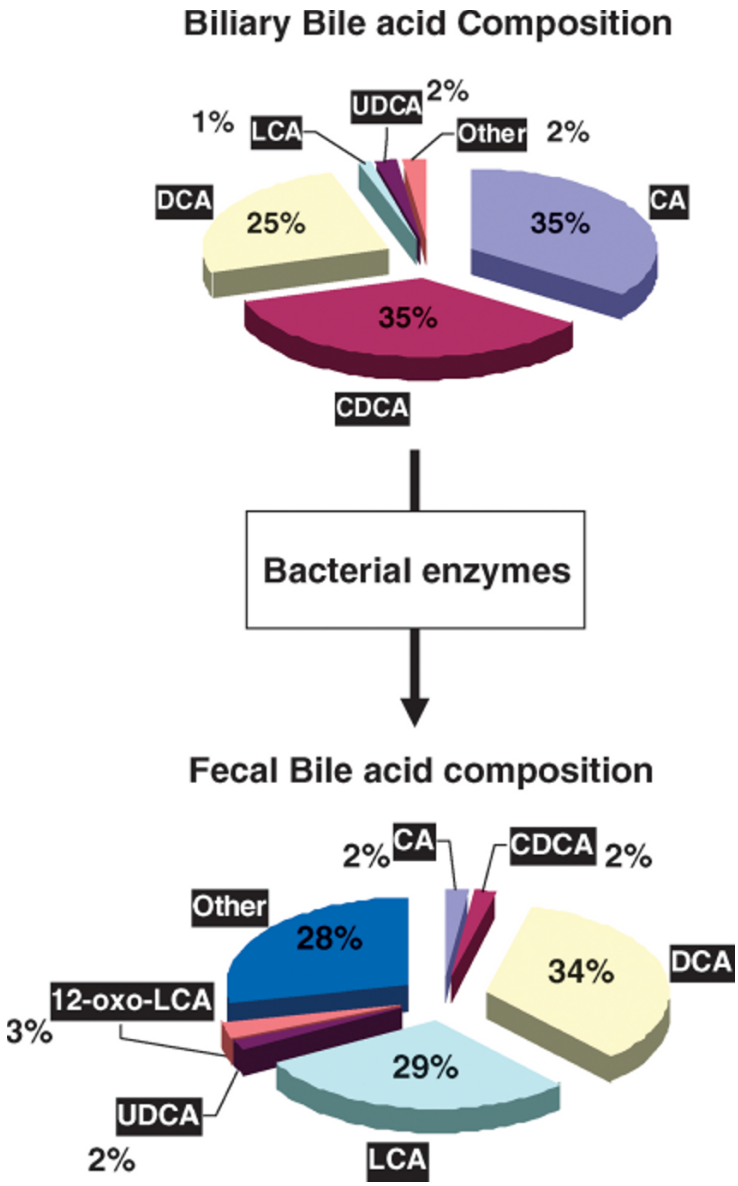

Figure 1-6. Fecal and gallbladder bile acids composition in healthy humans.

Comparison of bile acid composition in fecal samples and gallbladder bile from healthy human subjects. Adapted from Ridlon *et al*. 2006.

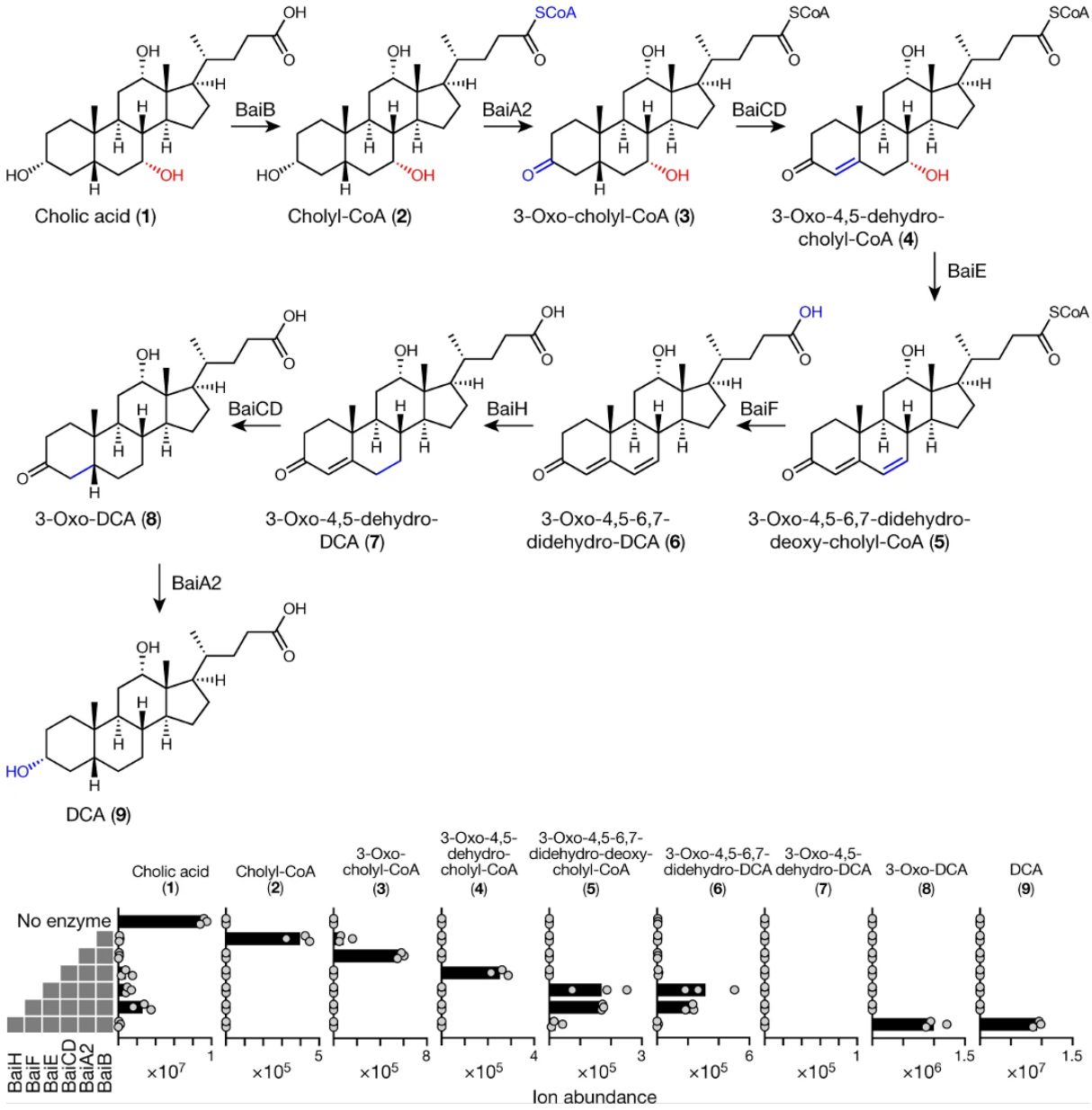

Figure 1-7. *bai* gene-mediated 7α-dehydroxylation pathway of CA to DCA

Top: Complete proposed pathway for the 7α-dehydroxylation of CA to DCA. **Bottom**: LC-MS ion abundances of DCA (9) and pathway intermediates (1-8) produced in a stepwise reconstitution assay using the indicated enzymes. Adopted from Funabashi *et al*., 2020.

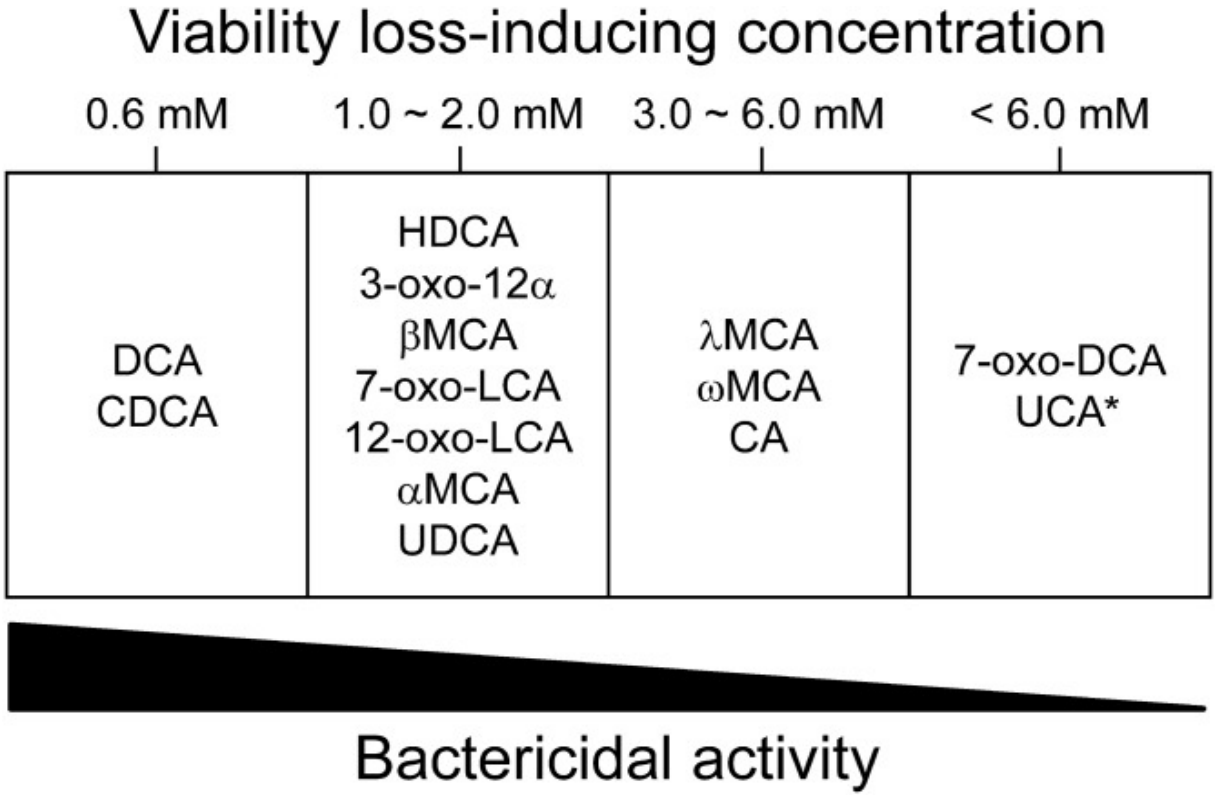

Figure 1-8. Bactericidal activity of free bile acids.

Illustration of the bactericidal activity of various free bile acids against gut bacteria. Adapted from Watanabe *et al*. 2017.

Chapter II. Screening of DCA-producing bacteria

1. Screening of DCA-producing bacteria

1.1. Objective

The human gut harbors a diverse microbial ecosystem that profoundly influences host physiology. Among its many functions, certain gut microbiota member has the ability to convert CA to DCA, which act as signaling molecules regulating metabolic pathways, immune responses, and intestinal homeostasis. Alterations in DCA levels have been associated not only with GI disorders but also with systemic metabolic diseases, highlighting the broader importance of understanding the microbes that drive its production.

Despite their physiological significance, DCA-producing bacteria have been characterized in only a few species, and it remains unclear whether these organisms fully represent the diversity of microorganisms capable of DCA production in the human gut. While recent metagenomic studies indicate that DCA-producing capability may be widespread among diverse gut taxa, direct evidence demonstrating active DCA production by these bacteria is limited.

To address this gap, this study aimed to screen unidentified DCA-producing bacteria in the human gut. In this study, screening approach using freshly obtained fecal samples from healthy donors were applied to detect active DCA-producing populations within complex microbial communities. This study also examines changes in microbial community composition associated with DCA production to assess whether this activity is linked to specific taxonomic groups or community configurations in the healthy gut microbiota. By integrating activity-based screening with microbial community profiling, this work establishes a functionally driven framework for identifying candidate DCA-producing bacteria and provides a foundation for future works aimed at targeted isolation and characterization.

1.2. Materials and methods

1.2.1. Bile acids

The bile acids used in this study were purchased from the following companies: sodium salts of CA, DCA, CDCA, LCA, GCA, and TCA, Merck KGaA (Darmstadt, Germany); 7-oxo-deoxycholic acid, Steraloids, Inc. (Newport, RI, USA). Nordeoxycholic acid (NDCA; 24-nor-3α,7α-dihydroxy-5β-cholan-23-oic acid) was purchased from MP Biomedicals, LLC (Santa Ana, CA, USA) for use as the internal standard for liquid chromatography-mass spectrometry (LC-MS) analysis.

1.2.2. Analysis of BA

BA were extracted from 100 µl of culture broth with five volumes of ethyl acetate after acidification using 30 µl of 3 M hydrochloric acid. The sample was then vortexed for 1 minute and centrifuged at 21,500×*g* for 5 minutes to induce phase separation. The organic phase was collected and dried by centrifugal evaporation, reconstituted with 10 µl of methanol, and spotted onto the silica plate for Thin-layer chromatography (TLC) analysis, which was conducted as described in a previous study (Tawthep *et al*. 2017).

For LC-MS analysis, dried BA samples were purified using Oasis HLB 1cc extraction cartridges (Waters Corp., Milford, MA, USA). BAs were then eluted in 1 mL of methanol, and 5 µL was used for LC-MS analysis, according to the method described in a previous report (Tawthep *et al*. 2017). Briefly, BAs were separated using the Dionex UltiMate 3000 UPLC system (Thermo Fisher Scientific) with an ACQUITY UPLC® BEH C18 column as the main column (100 × 2.0 mm i.d., 1.7 µm thickness, Waters Corp.). A 2-minute isocratic flow protocol using a solvent mixture composed of a 50:50 solvent A (20% acetonitrile) and solvent B (80% acetonitrile), both containing 10 mM ammonium acetate, was used for the separation of CA, DCA, 7-oxo-DCA, and NDCA. Mass analysis was conducted using the Q Exactive Plus

Hybrid Quadrupole-Orbitrap Mass Spectrometer (Thermo Fisher Scientific) equipped with an electrospray ionization probe in the negative ion mode. NDCA was used as an internal standard for the quantification of each BA. Conversion yield (%) of DCA and 7-oxo-DCA from CA was calculated by dividing each BA concentration by the total BA concentration of CA, DCA, and 7-oxo-DCA.

1.2.3. Fecal sample preparation and culture conditions

Fecal samples were obtained from seven healthy adult human donors (C, K-P). Immediately after defecation, samples were aseptically collected into sterile 50 mL conical tubes and immediately transferred to sealed pouches containing AnaeroPack oxygen absorber (Mitsubishi Gas Chemical Co., Inc., Tokyo, Japan) to minimize oxygen exposure. The fecal samples were maintained under anaerobic conditions until further processing. Prior to cultivation, 0.1 g of each fecal sample was used for serial dilution (10^{-1} to 10^{-6}) in sterile 1× phosphate-buffered saline (PBS) under strict anaerobic condition using anaerobic chamber (Coy Laboratory Products Inc., Grass Lake, MI, USA) containing mixed gas (N_2 : CO_2 : H_2 = 80 : 10 : 10). The remaining diluted fecal suspensions were mixed with glycerol solution (final glycerol concentration: 15 % (w/v)) and stored at -80°C for further analysis.

At total of 100 μL aliquots of each diluted fecal suspension were inoculated into anaerobic tubes containing 5 mL of Gifu Anaerobic Medium (GAM; Nissui Pharmaceutical Co. Ltd., Tokyo, Japan; **Table 2-1**) at pH 8.0 supplemented with 1 mM cholic acid sodium salt (CA-Na). The cultures were incubated at 37°C for 72 h under strict anaerobic conditions to allow bacterial growth and BA transformation. Bacterial growth was monitored by measuring the optical density at 660 nm (OD_{660}) over 72 h using a SPECTRONIC $20D^+$ spectrophotometer (Thermo Fisher Scientific, Inc., Waltham, MA, USA). Detailed illustration of the experimental

workflow is shown in **Figure 2-1**. This human study was approved by the Ethical Committee in the Research Faculty of Agriculture, Hokkaido University (no. 2021-001).

1.2.4. Cell dilution culture

Fecal cultures that are confirmed to produce DCA were selected for further cell-dilution culture experiments. Cell dilution was performed to precisely control the bacterial population size in glycerol stock. The number of viable cells in glycerol stocks was quantified by colony-forming unit (CFU) analysis. Briefly, glycerol stocks were serially diluted (10^{-1} to 10^{-8}) using 1× PBS. Aliquots of 10 μL from each dilution were spotted onto GAM agar plates and incubated anaerobically at 37°C for 24-72 h. After incubation, colonies were enumerated, and CFU values were calculated for each dilution. Based on CFU quantification, glycerol stocks were further diluted to contain defined bacterial cell densities (e.g., 10^7, 10^6, 10^5, and 10^4 CFU/mL) using 15% (v/v) glycerol solution. A total of 20 μL of each diluted glycerol stock was inoculated into each well of a 96-deep well plate containing 1 mL GAM medium supplemented with 1 mM CA-Na. Cultures were incubated anaerobically at 37°C and subsequently subjected to BA analysis.

1.2.5. Genomic DNA Extraction and 16S rRNA Gene Amplicon Sequencing

Diluted glycerol stocks that were confirmed to produce DCA were selected for further analyses. Prior to DNA extraction, frozen glycerol stocks were thawed briefly on ice and aseptically inoculated into 5 mL of GAM medium. Cultures were incubated at 37°C for 72 h under strict anaerobic conditions. Following incubation, cultures were collected for genomic DNA extraction as described below.

Bacterial cultures were transferred into conical tubes and centrifuged at 9,000×*g* for 5 min at 4°C. The resulting bacterial pellets were washed with 1× PBS, then with washing buffer,

and centrifuged again under the same conditions (9,000×*g* for 5 min at 4°C). DNA extraction was performed by resuspending the washed bacterial pellets in lysis buffer. The resuspended cell suspension was transferred into 2 mL sterile screw-cap tubes containing 0.3 g of beads (YGB01 0.1 mm, Yasui Kiaki Co., LTD.) Cells are disrupted using a bead shaker (2,500 rpm, 80 s (ON/OFF = 20s / 10s). Following bead beating, the samples were incubated at 70°C using a heat block, then centrifuged at ~18,700×*g* for 10 min at 4°C. The supernatant was transferred to a new 2 mL microcentrifuge tube, and 300 µL of lysis buffer was added to the remaining pellet. The steps of pellet disruption and lysis buffer addition were repeated three times, and the resulting supernatants were combined. To the collected supernatant, 260 µL of 10 mM ammonium acetate solution was added, mixed thoroughly, and incubated on ice for 5 min, followed by centrifugation at ~18,700×*g* for 10 min at 4°C. The supernatant was transferred to a new 2 mL microtube, and 1 µL of RNase A (10 mg/mL) was added. Samples were incubated at 37°C for 1 h to remove RNA. After RNase treatment, the supernatant was divided equally into two microtubes. An equal volume of phenol/chloroform/isoamyl alcohol (25:24:1, PCI) was added to each tube, mixed thoroughly by vortex, and centrifuged at ~18,700×*g* for 5 min at 4°C. The aqueous phase was transferred to new microtubes, and an additional extraction with an equal volume of PCI (25:24:1) was performed, followed by centrifugation under the same conditions. The aqueous phases from the same sample were combined into a new microtube. DNA was precipitated by adding an equal volume of 2-propanol, then incubated on ice for 30 min. Samples were centrifuged at ~18,700×*g* for 15 min at 4°C, and the supernatant was carefully discarded. The DNA pellet was washed with 1 mL of 70% (v/v) ethanol, briefly vortexed, and centrifuged at ~18,700×*g* for 2 min at 4°C. After ethanol removal, the pellet was dried by vacuum centrifugation. Finally, DNA was resuspended in 50 µL of TE buffer and was ready to use for further analysis.

16S rRNA gene amplicon sequencing was conducted at Bioengineering Lab Co., Ltd. (Kanagawa, Japan), along with the sequencing workflow. A brief description of the methodology is summarized here. DNA concentrations were quantified using a Synergy LX microplate reader (Agilent Technologies) in combination with the QuantiFluor dsDNA System (Promega). Sequencing libraries were prepared using a two-step tailed PCR method using the primers indicated in **Table 2-2**, after which library concentrations were measured using a Synergy H1 microplate reader (Agilent Technologies) and the QuantiFluor dsDNA System (Promega). Library quality and fragment size distributions were assessed using a Fragment Analyzer with the dsDNA 915 Reagent Kit (Agilent Technologies). Sequencing was performed using either the NextSeq 1000 system with the NextSeq 1000/2000 P1 Reagents (600 cycles) kit or the MiSeq system with the MiSeq Reagent Kit v3 (Illumina), generating paired-end reads of 2 × 300 bp. Sequencing data were analyzed using QIIME 2 (v2024.2), where denoising and chimera removal were performed using the DADA2 plugin, and taxonomic assignment was conducted using the SILVA database (v138).

1.3. Results

1.3.1. Fecal microbiota cultures and DCA production

Fecal microbiota cultures derived from healthy donors displayed considerable variation in DCA production, as assessed by TLC analysis, reflecting differences in baseline secondary BA metabolism among individuals. Among the donor samples, feces from donors L, N, and O consistently showed clear DCA-producing activity after 72 h of incubation, with detectable production observed across nearly all fecal dilution series **(Table 2-3).** Despite similar growth, as measured by OD_{660} values, among the cultures (**Figure 2-2**), only certain cultures produce DCA, indicating that DCA production on each culture depends on the presence of DCA-producing bacteria.

To evaluate DCA production at lower bacterial densities, the investigation was continued using diluted cell cultures. The lowest dilution of the fecal suspension was selected to quantify viable bacterial cells and the CFU was determined. This dilution reduces the complexity of the microbial community and allowed detection of DCA-producing bacteria at low bacterial density.

1.3.2. Diluted cell cultures and assessment of DCA-producing activity

Following the CFU measurements **(Table 2-4)**, bacterial cells were serially diluted to concentrations ranging from 10^7 to 10^4 cells. Each diluted cell suspension was inoculated into 96-deep well plates containing 1 mL of GAM medium supplemented with CA-Na. TLC clearly observed DCA production after 72 h of culture. DCA was detected on the well containing 10^7 and 10^5 cells **(Figure 2-3)**. To further evaluate the DCA-producing capacity of these populations, we selected the lowest cell concentration (10^5) stock that produced DCA. These bacterial cells were analyzed under identical culture conditions. Interestingly, while diluted cultures from donors N and O were unable to produce detectable DCA in this follow-up assay, the culture from donor L continued to produce DCA, indicating the presence of a robust DCA-producing population. Based on these results, further investigation focused on the diluted culture from donor L to characterize the bacterial composition responsible for DCA production. Comparing the microbial communities of DCA-positive and DCA-negative cultures provide insight into the specific taxa potentially associated with DCA production in the human gut. DCA production was confirmed again using TLC and LC-MS analyses (**Figure 2-4**). Among the four initially identified cultures, one consistently produced DCA across repeated analyses.

1.3.3. Microbial community composition linked to DCA production

Taxonomic analysis revealed five major bacterial phyla in both culture types: Firmicutes, Bacteroidota, Proteobacteria, Actinobacteria, and Fusobacteria, with notable differences in their relative abundances **(Figure 2-5)**. Based on DCA production confirmed by TLC and LC-MS analyses (Figure 2-4), samples were categorized into one DCA-positive culture and seven DCA-negative cultures. Comparative analysis revealed differences in relative abundance of several bacterial genera between the DCA-positive culture and the DCA-negative cultures. The DCA positive culture contained genera including uncultured bacteria, *Paraeggerthella*, *Lachnoclostridium, Fusicatenibacter, Escherichia-Shigella*, *Erysipelatoclostridium, Enterococcus, Dorea, Blautia, Bifidobacterium,* and *Bacteroides* (**Figure 2-6**). A total of 79 amplicon sequence variants (ASVs) were detected across the cultures. Observed ASVs from diluted cell culture samples were listed and analyzed using BLASTn to predict species-level identities (**Table 2-5**).

No ASV corresponded to the known DCA-producing bacteria. Among the ASVs detected specifically in the DCA-positive culture, BLASTn analysis of the ASV_44 sequence revealed *Dorea ammoniilytica* and *Ruminococcu*s sp. 653 as the top-hit taxa (**Table 2-5**). ASV_44 accounted for approximately 1.13% of the total bacterial composition in the culture. *Dorea* has previously been reported as DCA-producing bacteria (Bai *et al*. 2022). However, this activity has been described only at the genus level, without assignment to a specific species. Based on this observation, these bacteria were selected for further investigation.

1.4. Discussion

The results of this study revealed that DCA production in human fecal cultures is highly variable and donor-dependent, reflecting the complexity and individuality of gut microbial composition and metabolism. This variability is consistent with previous reports showing that

the levels of secondary BAs, particularly DCA, differ substantially among individuals, likely due to differences in microbial community structure, functional capacity, and host factors (Kitahara *et al*. 2004; Martin *et al*. 2018). Such variation highlights the dynamic, donor-specific nature of BA metabolism in the human gut.

Across fecal samples and diluted cell culture, only one culture consistently produced DCA across repeated assays, suggesting that robust DCA production depends on specific bacterial populations. This culture produces ~16% DCA after 72 h, with DCA spots also observed in TLC analysis (**Figure 2-4**). Microbial community composition of DCA-producing and non-DCA-producing diluted cell cultures was analyzed using 16S rRNA amplicon sequencing.

BLASTn analysis of ASV_44, which was detected in the DCA-producing culture, identified *Dorea ammoniilytica* and Ruminococcus sp. 653 as the top hit taxa (**Table 2-5**) in the DCA-positive culture suggests that bacteria related to these taxa may be involved in DCA production. Previous study by Bai *et al*. (2022) reported that members of the genus *Dorea* possess DCA-producing activity, however, this activity was demonstrated only at the genus level and not assigned to a specific species. The detection of ASV_44 with high similarity to *D. ammoniilytica* in the DCA-positive culture therefore highlights this species as a candidate for further study. Although *Ruminococcus* sp. 653 has not been characterized as DCA producer, its close phylogenetic relationship to *D. ammoniilytica* suggest possible functional similarity.

Notably, consistent DCA production was observed only in the culture in which ASV_44 was detected, whereas this ASV was absent from DCA negative culture. this association indicates that DCA production in the present screening system may depend on the presence of the specific bacterial taxa. Several factors, including culture conditions and dilution, may influence the detection of DCA-producing bacteria. Some bacterial populations might be

sensitive to stress, nutrient availability, or cell density, which could explain why only certain donor cultures maintained consistent DCA production.

Therefore, the association between consistent DCA production and the presence of ASV_44 provides a rationale for selecting bacteria related to *D. ammoniilytica* and *Ruminococcus* sp. 653 for futher characterization. these bacteria were therefore selected for detailed investigation of their DCA-producing activity in Chapter III.

1.5. Conclusion

This study demonstrates that DCA production in human fecal cultures is donor dependent and restricted to specific bacterial populations. While no ASVs matched previously described DCA-producing species, BLASTn analysis identified ASV_44 annotated with high similarity to *D. ammoniilytica* and *Ruminococcu*s sp. 653, in the consistently DCA-producing culture. The detection of this ASV suggests that DCA production may be associated with specific bacterial species. These findings emphasize the importance of targeted isolation and functional characterization to identify contributors to DCA production.

1.6. Figures and Tables

Table 2-1. Composition of gifu anaerobic medium (GAM)

Medium composition	Agar medium	Liquid medium	
Peptone	10	10	g
Soya peptone	3	3	g
Proteose peptone	10	10	g
Digested serum	13.5	13.5	g
Yeast extract	5	5	g
Meat extract	2.2	2.2	g
Liver extract	1.2	1.2	g
Glucose	3	3	g
KH_2PO_4	2.5	2.5	g
NaCl	3	3	g
Starch soluble	5	5	g
L-cysteine hydrocloride	0.3	0.3	g
$NaC_3H_4O_2S$	0.3	0.3	g
Agar	15	-	g
Distilled water up to	1000	1000	mL

All media were autoclaved at 115ºC for 15 minutes. Semi-solid media were filtered to remove agar particles before autoclaving. All media were anaerobically treated prior to use.

Table 2-2. Primers used for 16S rRNA amplicon sequencing

Primer name	Sequence (5' → 3')
1st-515f_MIX❖2	ACACTCTTTCCCTACACGACGCTCTTCCGATCT-NNNNN-GTGCCAGCMGCCGCGGTAA
1ST-806R_MIX❖2	GTGACTGGAGTTCAGACGTGTGCTCTTCCGATCT-NNNNN-GGACTACHVGGGTWTCTAAT
2ndF	AATGATACGGCGACCACCGAGATCTACAC-Index2-ACACTCTTTCCCTACACGACGC
2ndR	CAAGCAGAAGACGGCATACGAGAT-Index1-GTGACTGGAGTTCAGACGTGTG

Primer sequences and target regions for bacterial 16S rRNA amplicon amplification. To improve sequencing quality, mixed primers containing 0-5 random nucleotides (N) at the 5′ end were used (❖2). Primers were used in PCR for sequencing library preparation.

Table 2-3. DCA-producing activity in fecal dilution cultures analyzed by TLC

Sample code[a]	Fecal dilution[b]						Detection method[c]
	10^{-1}	10^{-2}	10^{-3}	10^{-4}	10^{-5}	10^{-6}	
Donor_C	-	-	-	-	-	-	TLC
Donor_K	-	-	-	-	-	-	TLC
Donor_L	+	+	+	+	+	+	TLC
Donor_M	-	-	-	-	-	-	TLC
Donor_N	+	+	+	+	+	+	TLC
Donor_O	+	+	+	+	+	-	TLC
Donor_P	-	-	-	-	-	-	TLC

[a] Alphabets represent donors identity.

[b] Fecal dilution of each donor. The presence (+) or absence (-) of DCA was determined based on the spot detection on the TLC plate.

[c] DCA production of all samples were analyzed by TLC.

Table 2-4. CFU of fecal-derived bacterial culture stocks used for DCA production assays

Sample Code[a]	CFU/ml[b]	Serial cell dilution[c]	
		From	to
Donor_L	4.90E+09	1.00E+07	1.00E+04
Donor_N	5.23E+08	1.00E+06	1.00E+03
Donor_O	3.60E+08	1.00E+07	1.00E+04

[a] Alphabets represent donors identity.

[b] Colony forming unit (CFU) of viable cells in each glycerol stock.

[c] Diluted cells for diluted cell culture of each glycerol stock.

Table 2-5. Species identified in DCA-producing and non-DCA-producing cultures

ASV_ID[a]	Top hit name[b]	Identity (%)[c]	Composition in the culture (%)[d]							
			1	2	3	4	5	6	7	8
ASV_2	*Bacteroides vulgatus* strain NMBE-13 16S ribosomal RNA gene, partial sequence	253/253(100%)	0.4808	–	0.8882	–	–	–	–	–
ASV_3	*Phocaeicola vulgatus* strain FDAARGOS_1098 chromosome	253/253(100%)	0.0683	–	0.1491	–	–	–	–	–
ASV_5	*Bacteroides uniformis* CL03T12C37 chromosome, complete genome	253/253(100%)	–	–	0.1968	0.1853	–	–	–	–
ASV_8	*Bacteroides thetaiotaomicron* partial 16S rRNA gene, strain 2368	253/253(100%)	–	–	0.1628	–	–	–	–	–
ASV_9	*Bacteroides fragilis* partial 16S rRNA gene, isolate 93N_17396	253/253(100%)	53.1336	28.766	27.143	22.2712	0.2717	0.3775	0.3465	0.1632
ASV_10	*Bacteroides ovatus* strain PC329 16S ribosomal RNA gene, partial sequence *Bacteroides xylanisolvens* H-Alg2 gene for 16S rRNA, partial sequence	253/253(100%) 253/253(100%)	0.011	–	–	–	0.3955	0.694	–	–
ASV_11	*Bacteroides ovatus* partial 16S rRNA gene, strain VPI-3049	253/253(100%)	0.0134				0.328	0.5889	0.4809	0.1265
ASV_12	*Bacteroides ovatus* strain V975 16S ribosomal RNA gene, partial sequence *Bacteroides kribbi* strain 27824 16S ribosomal RNA gene, partial sequence	253/253(100%) 253/253(100%)	–	–	–	–	1.1719	1.992	1.7021	0.3951
ASV_13	*Bacteroides* sp. strain Y2-T-103 16S ribosomal RNA gene, partial sequence *Bacteroides ovatus* strain W16008 16S ribosomal RNA gene, partial sequence	253/253(100%) 253/253(100%)	–	–	–	–	0.1609	0.2811	0.2023	–
ASV_14	*Parabacteroides distasonis* strain BFG-238 chromosome, complete genome	253/253(100%)	0.05	–	–	–	–	–	–	–
ASV_15	*Parabacteroides distasonis* strain PB-SUZFK 16S ribosomal RNA gene, partial sequence	253/253(100%)	–	–	–	–	1.3936	2.3364	0.9864	1.6994
ASV_16	*Parabacteroides distasonis* strain FDAARGOS_615 chromosome *Parabacteroides* sp. strain BB1-J-100 16S ribosomal RNA gene, partial sequence	253/253(100%) 253/253(100%)	0.1751	–	–	0.144	–	–	–	–

Table 2-5. (Continued)

ASV_ID[a]	Top hit name[b]	Identity (%)[c]	Composition in the culture (%)[d]							
			1	2	3	4	5	6	7	8
ASV_19	*Escherichia coli* strain Ecol_422, complete genome	253/253(100%)	0.0391	–	–	0.1066	–	–	–	–
ASV_21	*Escherichia coli* strain DS18053-2 16S ribosomal RNA gene, partial sequence	252/253(99%)	9.0434	0.1481	0.1551	0.1814	0.1564	0.1434	0.1299	0.1506
ASV_22	*Escherichia coli* strain DS18053-2 16S ribosomal RNA gene, partial sequence	252/253(99%)	9.0434	16.4657	17.1526	20.7756	17.704	15.8409	15.4283	16.2338
ASV_23	*Agathobaculum desmolans* partial 16S rRNA gene *Butyricicoccus* sp. strain Y1-J-104 16S ribosomal RNA gene, partial sequence	253/253(100%) 253/253(100%)	–	–	–	–	0.1474	0.2044	0.2564	0.2342
ASV_24	Uncultured Ruminococcaceae bacterium clone HC_776.29-1 16S ribosomal RNA gene, partial sequence Uncultured Lachnospiraceae bacterium clone MS107A1_B11 16S ribosomal RNA gene, partial sequence	253/253(100%) 253/253(100%)	–	–	–	–	0.2132	0.327	0.3294	0.3476
ASV_27	*Eggerthella lenta* strain R-29733 16S ribosomal RNA gene, partial sequence	252/252(100%)	0.094	–	–	–	–	–	–	–
ASV_30	*Anaerostipes hadrus* DSM 3319 partial 16S rRNA gene	253/253(100%)	–	–	–	–	0.7038	0.9693	1.1773	0.6098
ASV_31	*Anaerostipes hadrus* YIT13225 gene for 16S rRNA, partial sequence	253/253(100%)	–	–	–	–	3.2434	4.4934	5.4129	2.7306
ASV_32	*Blautia* sp. strain HA2174 16S ribosomal RNA gene, partial sequence *Blautia argi* strain C2-GN-1-2-64 16S ribosomal RNA gene, partial sequence	253/253(100%) 253/253(100%)	–	0.125	17.2815	11.3474	–	–	–	–
ASV_35	*Fusicatenibacter saccharivorans* partial 16S rRNA gene	253/253(100%)	–	2.3105	2.259	5.0917	–	–	–	–
ASV_37	*Dorea longicatena* strain DSM 13814 chromosome, complete genome	253/253(100%)	–	–	–	–	2.7478	2.7302	2.5284	2.9156
ASV_39	*Enterocloster bolteae* partial 16S rRNA gene *Enterocloster clostridioformis* strain FDAARGOS_739 chromosome	253/253(100%) 253/253(100%)	0.3301	0.9005	0.3502	0.4885	–	–	–	–

Table 2-5. (Continued)

ASV_ID[a]	Top hit name[b]	Identity (%)[c]	Composition in the culture (%)[d]							
			1	2	3	4	5	6	7	8
ASV_40	*Clostridium clostridioforme* strain D4 16S ribosomal RNA gene, partial sequence *Enterocloster clostridioformis* k19-0097-F3 DNA, complete genome	253/253(100%) 253/253(100%)	5.2896	3.4427	1.3111	1.8807	–	–	–	–
ASV_43	*Dorea formicigenerans* partial 16S rRNA gene *Clostridiaceae bacterium* DJF_LS13 16S ribosomal RNA gene, partial sequence	253/253(100%) 253/253(100%)	–	11.4134	9.8149	9.6107	–	–	–	–
ASV_44	*Dorea ammoniilytica* strain CLA-AA-H147 16S ribosomal RNA gene, partial sequence *Ruminococcus* sp. 653 gene for 16S ribosomal RNA, partial sequence	253/253(100%) 253/253(100%)	1.1288	–	–	–	–	–	–	–
ASV_46	*Slackia isoflavoniconvertens* strain HE8 16S ribosomal RNA, partial sequence	253/253(100%)	–	–	–	–	0.1598	–	–	–
ASV_47	*Collinsella aerofaciens* strain D6-34 16S ribosomal RNA gene, partial sequence	253/253(100%)	–	–	–	–	2.1109	1.9612	2.5654	3.4229
ASV_49	*Eggerthella hongkongensis* strain HKU11 16S ribosomal RNA gene, partial sequence *Paraeggerthella hongkongensis* strain W04029A2-2 16S ribosomal RNA gene, partial sequence	252/252(100%) 252/252(100%)	0.3301	0.2162	–	0.1407	–	–	–	–
ASV_50	*Blautia* sp. strain 26-15 16S ribosomal RNA gene, partial sequence *Blautia segnis* strain BX17 16S ribosomal RNA gene, partial sequence	253/253(100%) 253/253(100%)	–	0.144	–	0.216	–	–	–	–
ASV_52	*Sutterella wadsworthensis* strain SFAD58 chromosome, complete genome	253/253(100%)	–	–	–	–	2.1733	2.4903	2.2907	2.4781
ASV_53	*Bifidobacterium adolescentis* strain NB2B-16-TSAB chromosome	253/253(100%)	4.3902	12.9294	12.2899	11.8526	9.3775	7.8031	8.2051	7.0954
ASV_54	*Bifidobacterium breve* strain 2240 16S ribosomal RNA gene, partial sequence *Bifidobacterium longum* subsp. infantis strain BINF chromosome, complete genome	253/253(100%) 253/253(100%)	–	0.2678	–	0.3723	0.1969	0.1545	0.1863	0.1666
ASV_55	*Bifidobacterium faecale* strain RACS_DI100 16S ribosomal RNA gene, partial sequence	253/253(100%)	4.3902	–	–	–	–	–	–	–

Table 2-5. (Continued)

ASV_ID[a]	Top hit name[b]	Identity (%)[c]	Composition in the culture (%)[d]							
			1	2	3	4	5	6	7	8
ASV_56	*Bifidobacterium pseudocatenulatum* strain 1708 16S ribosomal RNA gene, partial sequence	253/253(100%)	–	–	–	–	10.0835	10.2859	10.7728	11.1527
	Bifidobacterium kashiwanohense strain BSM11-1 16S ribosomal RNA gene, partial sequence	253/253(100%)								
ASV_59	*Erysipelatoclostridium ramosum* DSM 1402 partial 16S rRNA gene	466/466(100%)	8.4894	6.008	–	–	0.4214	0.3821	0.4046	0.3052
	Thomasclavelia ramosa strain JCM 1298 16S ribosomal RNA, partial sequence	252/252(100%)								
ASV_60	*Flavonifractor plautii* strain 265 16S ribosomal RNA, partial sequence	253/253(100%)	–	0.2589	–	–	–	–	–	–
ASV_62	*Acidaminococcus intestini* strain UO.H1096 16S ribosomal RNA gene, partial sequence	253/253(100%)	–	–	–	–	0.1024	0.115	0.11	0.1025
ASV_63	*Acidaminococcus intestini* strain UO.H1096 16S ribosomal RNA gene, partial sequence	252/252(100%)	–	–	–	–	26.4114	25.9613	26.4421	27.3796
ASV_66	*Enterococcus malodoratus* strain V1873 16S ribosomal RNA gene, partial sequence	253/253(100%)	–	–	–	–	1.3131	1.1685	1.3693	1.3255
	Enterococcus avium strain V3063 16S ribosomal RNA gene, partial sequence	253/253(100%)								
ASV_67	*Enterococcus faecium* strain RU26-2 16S ribosomal RNA gene, partial sequence	252/252(100%)	16.6017	16.0421	10.2272	14.7315	14.8274	15.0162	16.3104	18.7978
	Enterococcus faecalis strain DZ-09 16S ribosomal RNA gene, partial sequence	252/252(100%)								
ASV_68	*Lactiplantibacillus plantarum* strain CAU6365 16S ribosomal RNA gene, partial sequence	252/252(100%)	16.6017	–	–	–	–	–	–	0.1105
ASV_69	*Enterobacter cloacae* strain 312502 clone 78 16S ribosomal RNA gene, partial sequence	253/253(100%)	0.1031	–	–	–	–	–	–	–
	Enterococcus faecium strain 340 16S ribosomal RNA gene, partial sequence	252/253(99%)								
	Enterococcus mundtii strain A96 16S ribosomal RNA gene, partial sequence	252/253(99%)								
ASV_70	*Phascolarctobacterium faecium* strain 1-DE-D30-67 16S ribosomal RNA gene, partial sequence	252/252(100%)	0.0018	–	–	–	1.105	1.2213	1.0719	1.0175

Table 2-5. (Continued)

ASV_ID[a]	Top hit name[b]	Identity (%)[c]	Composition in the culture (%)[d]							
			1	2	3	4	5	6	7	8
ASV_71	*Mitsuokella multacida* strain p4-22-X_9_D7 16S ribosomal RNA gene, partial sequence	252/252(100%)	–	–	–	–	0.3173	0.1928	–	–
ASV_72	*Mitsuokella multacida* DSM 20544 partial 16S rRNA gene	252/252(100%)	–	–	–	–	1.7964	0.906	–	–
ASV_73	*Eubacterium ramulus* strain DJF_CR50 16S ribosomal RNA gene, partial sequence	251/253(99%)	0.0079	–	–	–	–	–	–	–
ASV_74	*Eubacterium ventriosum* strain CLA-AA-H195 16S ribosomal RNA gene, partial sequence	253/253(100%)	–	–	–	0.1809	–	–	–	–
ASV_76	*Mediterraneibacter faecis* JCM 15917 DNA, complete genome *Ruminococcus faecis* JCM 15917 partial 16S rRNA gene	253/253(100%) 253/253(100%)	–	–	–	–	0.2324	0.3955	0.4861	0.3596
ASV_78	*Fusobacterium ulcerans* strain PM5-10 16S ribosomal RNA gene, partial sequence	252/252(100%)	–	–	–	–	0.1176	0.1678	–	–

[a] List of identified amplicon sequence variant (ASV) in the samples.

[b] Top hit bacterial species based on BLASTn analysis.

[c] identity and similarity of the ASVs sequences from both cultures.

[d] Values indicate the relative abundance (%) of bacteria ASVs within each culture. 1 correspond to DCA-positive culture, and 2-8 correspond to DCA-negative cultures.

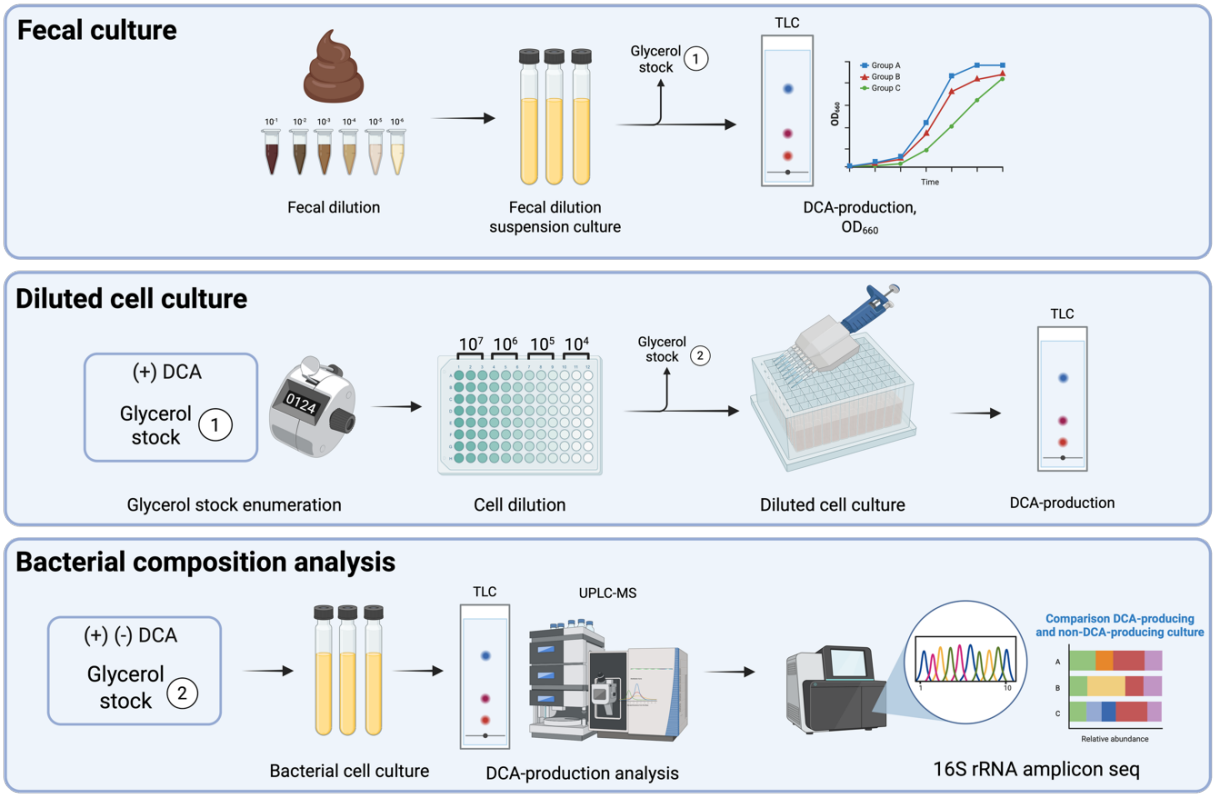

Figure 2-1. Experimental workflow for screening of DCA-producing bacteria

The screening process began with fecal culture under anaerobic conditions. Cultured samples were diluted to 10^7 to 10^4 cells, and bacterial composition was analyzed to identify potential DCA-producing bacteria. Created with BioRender.

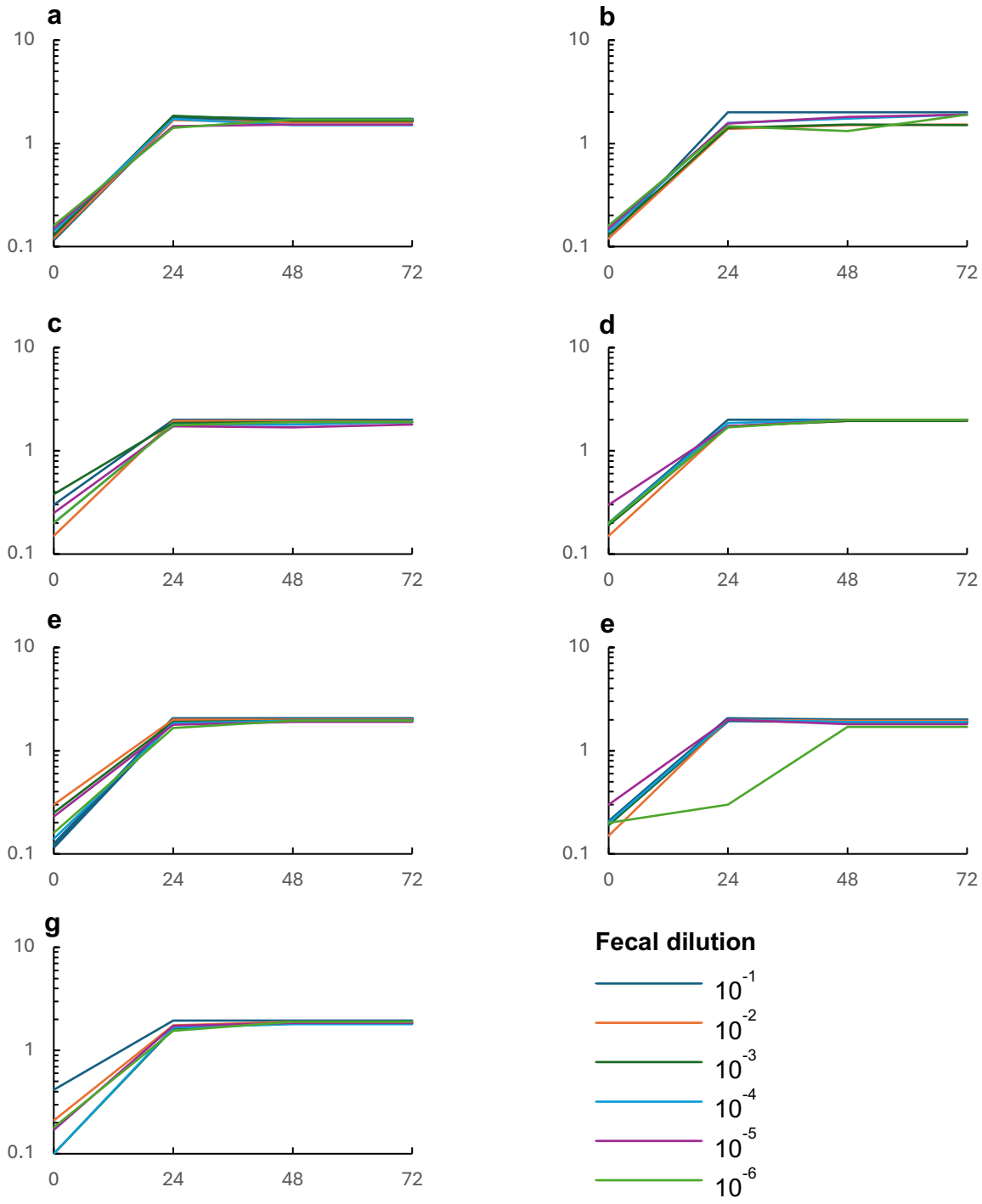

Figure 2-2. OD_{660} of fecal-derived cultures from seven donors

Optical density at 660 nm (OD_{660}) was measured for fecal-derived cultures serially diluted from 10^{-1} to 10^{-6} (n=1; colored line). (a) represent feces culture from donor C, (b – g) represent feces donor from donor K-P (n=1).

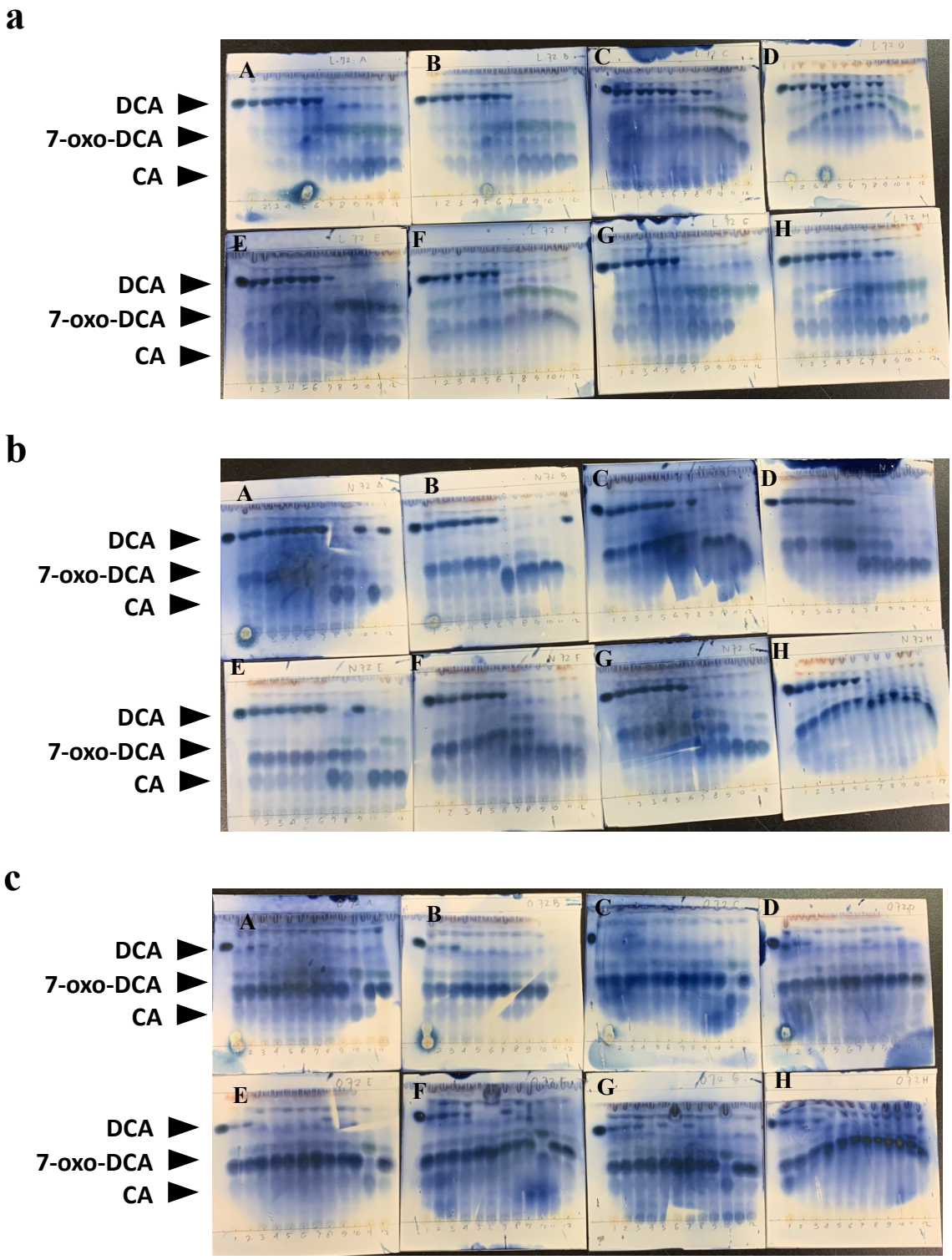

Figure 2-3. TLC analyzed DCA production in diluted cell culture

Diluted cell suspensions (10^7 - 10^4) were inoculated into 96-deep-well plates containing GAM medium supplemented with CA-Na and incubated for 72 h. Columns 1-3, 4-6, 7-9, and 10-12 correspond to cell concentration of 10^7, 10^6, 10^5, and 10^5, respectively (rows A-H). Representative TLC profiles are shown for diluted cultures from (**a**) donor L, (**b**) donor N, and (**c**) donor O (n = 1).

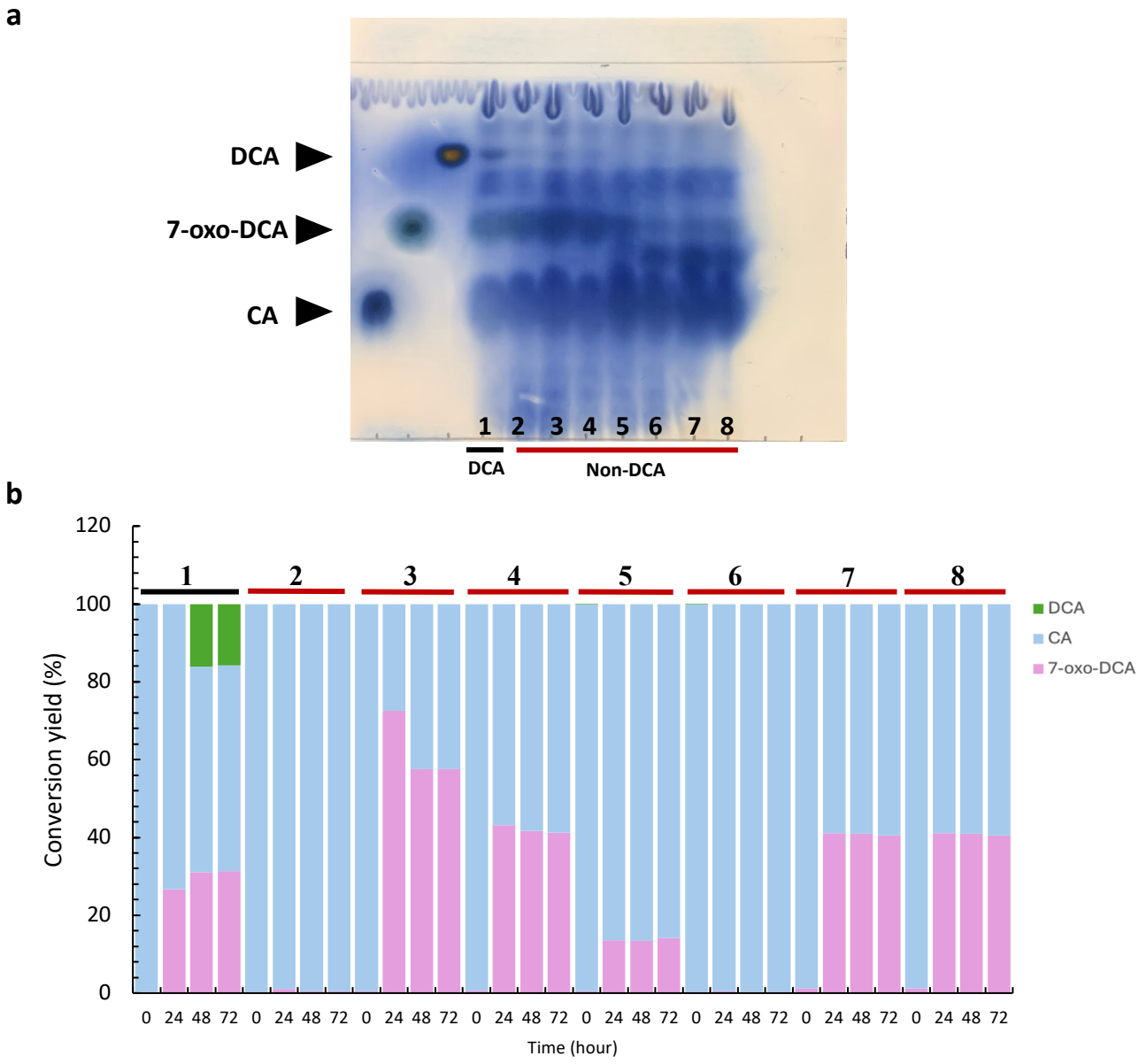

Fig 2-4. TLC and LC-MS analysis of BAs in diluted cell cultures

DCA production in diluted cell culture samples was initially reconfirmed after 72 h of culture by TLC **(a)** and LC-MS **(b)**. Sample 1 represents DCA-positive culture, whereas samples 2-8 represent DCA-negative cultures. Representative TLC results and BA quantification data by LC–MS analysis are shown (*n*=1).

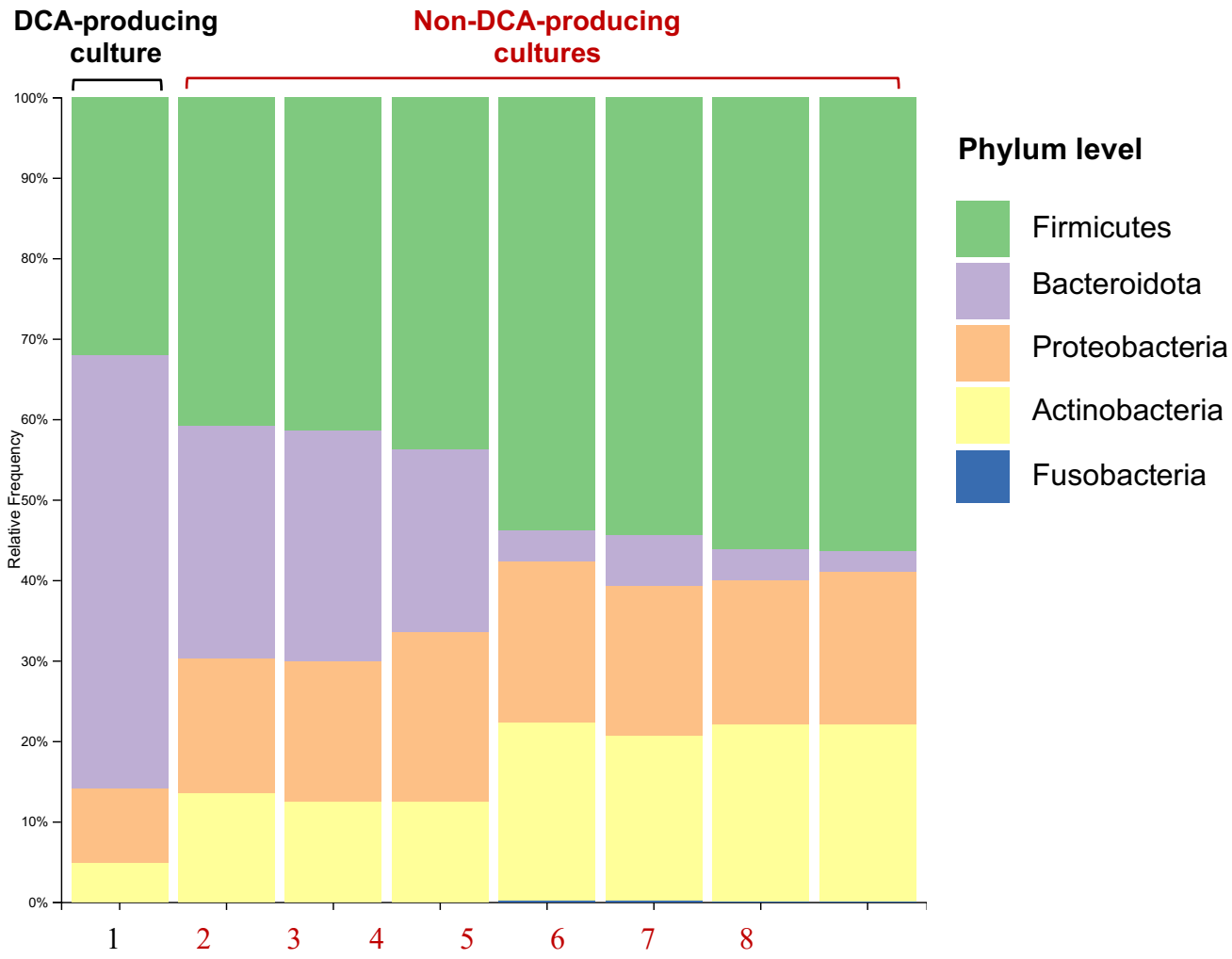

Figure 2-5. Phylum-level composition (%) in DCA-producing and non-DCA-producing cultures

Bar plot showing the relative abundance of bacterial phyla in diluted cell cultures. Sample 1 represents DCA-positive cultures, and samples 2-8 represent DCA-negative cultures.

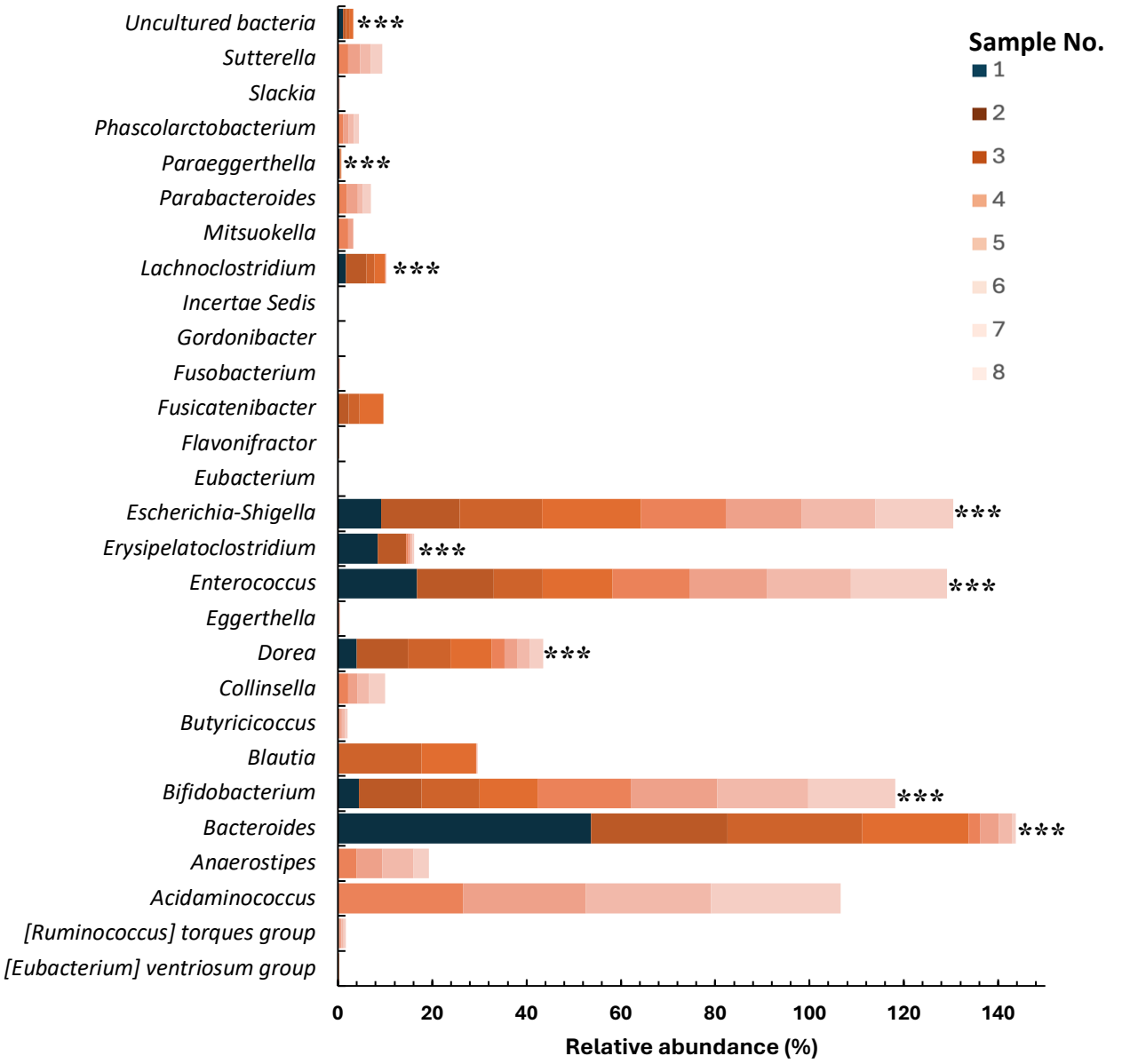

Figure 2-6. Genus-level composition (%) in DCA-producing and non-DCA-producing cultures

Bar plot showing the relative abundance (%) of bacterial genera in diluted cell cultures. Sample 1 correspond to DCA-positive culture, and samples 2-8 correspond to DCA-negative cultures. Dark blue bars indicate higher DCA production, while dark to light terracotta bars indicate culture with no detectable DCA. Genera marked with asterisks (***) were detected in DCA-producing culture.

Chapter III. Identification and characterization of novel DCA-producing bacteria

3. Identification and characterization of novel DCA-producing bacteria

This chapter is adapted from:

Ni Wayan Eka Putri Gayatri Kastawa, Yasuhiro Gotoh, Isaiah Song, Tomoya Maeda, Satoru Fukiya, Identification and characterization of *Dorea ammoniilytica* as a novel deoxycholic acid-producing bacterial species in the human gut microbiota, Bioscience, Biotechnology, and Biochemistry, 2025.

3.1. Background

Among the secondary BAs, DCA is particularly important due to its effects on the gut microbiota and host physiology. DCA exerts ten times higher bactericidal activity than CA due to its greater hydrophobicity (Kurdi *et al*. 2006; Watanabe *et al*. 2017). Thus, DCA works as a major regulatory factor of the gut microbiota in the rat cecum (Islam *et al*. 2011), especially in high-fat diet feeding conditions (Watanabe *et al*. 2025). An elevated level of DCA is involved in the development of colon cancer (Cao *et al*. 2017; Cong *et al*. 2024) and liver diseases such as liver cancer (Yoshimoto *et al*. 2013).While we have gained insights into the mechanisms of DCA production in specific DCA-producing bacteria in vitro, much remains unclear about how DCA production occurs and is regulated in the human intestine, which we defined as the "in vivo DCA production mechanism." Understanding this mechanism is crucial for controlling its production and preventing dysbiosis and disease development.

To clarify the "in vivo DCA production mechanism," it is essential to elucidate the diversity of DCA-producing bacteria present in the human intestine and to understand their characteristics. As stated in General Introduction, their abundance was estimated to be only about 0.0001% of the total gut microbiota (Ridlon *et al*. 2006), and extensive research has identified several species of DCA-producing bacteria.

In Chapter II, ASV_44 annotated by BLASTn as *Dorea ammoniilytica* and *Ruminococcus* sp. 653 was detected exclusively in the DCA positive culture. To date, DCA-producing bacteria within the genus *Dorea* have been reported only at the genus level, and no specific species has been functionally characterized for this activity (Bai *et al*. 2022). Genus *Dorea* was first proposed as a novel genus in the family Lachnospiraceae in 2002 (Taras *et al*. 2002). They are Gram-positive, rod-shaped, and nonmotile, and produce ethanol, formate, and acetate as major end-products of glucose fermentation. However, they do not produce lactate and butyrate (Taras *et al*. 2002). Currently, only six species have been validly identified in this genus, and most of their functions have yet to be characterized.

Thus, this study aimed to identify and characterize DCA-producing Dorea species by investigating genomic and physiological properties. Through sequence similarity analysis, we identified two candidate isolates from human feces, *Dorea ammoniilytica* JCM 34808^T and *Ruminococcus* sp. JCM 18685, and their DCA-producing abilities were evaluated. Whole-genome sequencing was performed to elucidate their taxonomic classification and metabolic potential, complemented by physiological assessments.

3.2. Materials and methods

3.2.1. Bacterial strains and culture conditions

Dorea ammoniilytica JCM 34808^T and *Ruminococcus* sp. JCM 18685 were provided by the Japan Collection of Microorganisms (JCM), RIKEN BRC, which is participating in the National BioResource Project of MEXT, Japan. All strains were stored at -80 ^oC in 15% (v/v) glycerol solution and cultured anaerobically in Gifu Anaerobic Medium (GAM; **Table 2-4**) in an anaerobic chamber (Coy Laboratory Products Inc., Grass Lake, MI, USA) filled with mixed anoxic gas (N_2:CO_2:H_2 = 80:10:10). The anaerobic conditions were established by treating the medium overnight using sealed pouches containing AnaeroPack oxygen absorbers (Mitsubishi

Gas Chemical Co., Inc., Tokyo, Japan). For pre-cultures, bacterial glycerol stocks were inoculated into the GAM broth (pH 6.9). Anaerobic conditions in the culture tubes were maintained by flushing the mixed anoxic gas into the headspace of the liquid medium through a butyl rubber stopper on the tube lid using a 25G syringe tip. The tubes were then cultured at 37°C in the anaerobic chamber. These pre-cultures were subsequently inoculated into fresh GAM (pH 6.9 or pH 8.0) to achieve an initial optical density at 660 nm (OD_{660}) of 0.05 for the test culture. Bacterial growth was monitored over 72 h using a SPECTRONIC $20D^{+}$ spectrophotometer (Thermo Fisher Scientific, Inc., Waltham, MA, USA). The sodium salt of CA was added as a substrate for the BA transformation experiments at a final concentration of 1 mM to assess to what extent the tested strains can convert CA to DCA at high substrate concentrations. Additionally, the tested strains were cultured under the same conditions with the addition of 0.1 mM sodium salt CDCA to evaluate their capacity to convert CDCA to LCA. Conversion analysis of conjugated BAs was conducted by culturing the strain in GAM (pH 6.9) for 48 and 72 h in the presence of 1 mM glycocholic acid (GCA; 3α,7α,12α-dihydroxy-5β-cholan-24-oic acid N-(carboxymethyl)-amide) or taurocholic acid (TCA; 3α,7α,12α-trihydroxy-5β-cholan-24-oic acid N-(2-sulfoethyl)-amide). Additional CA conversion experiments to evaluate DCA-producing ability were conducted in the same culture conditions used in a previous report on *Dorea* sp. (Bai *et al*. 2022).

Precultured cells were inoculated at initial OD_{660}=0.01 into peptone yeast glucose (PYG) medium (pH 7.2; **Table 3-3**) containing 0.1 mM CA and anaerobically cultured at 37°C for 24 h and 48 h. Carbohydrate utilization ability was evaluated by measuring the OD_{660} at 24 h when cultured in GAM Semisolid without Dextrose medium (Nissui Pharmaceutical Co. Ltd.; pH 6.9; **Table 3-4**). Agar was removed by filtration using filter paper before autoclaving, and each tested carbohydrate was added at 1% (w/v) after autoclaving.

3.2.2. Bile acids analysis

DCA production by the candidate strains was evaluated using LC-MS and TLC analysis. BA analysis was conducted as described in Chapter II (Section 1.2.1 and 1.2.2).

3.2.3. Morphological and biochemical characterization

Morphology of the candidate bacteria was examined using an optical microscope BX50 (Olympus Corp., Tokyo, Japan) after Gram staining of the cultured cells in GAM (pH 6.9). Biochemical characterization of the candidate strains, focusing on enzymatic activities, was conducted using the API RAPID ID 32A system (bioMérieux Japan, Ltd., Tokyo, Japan) according to the manufacturer's instructions. Briefly, bacterial suspensions were prepared by harvesting fresh anaerobic colonies and suspending them in the suspension medium provided with the API kit to a McFarland turbidity of 4.0. Each suspension was homogenized before inoculating the respective API strip pits. The strips were incubated at 37°C for 4 to 4.5 h in anaerobic conditions. After incubation, biochemical reactions were evaluated by observing color changes or other visual indicators, with some tests requiring the addition of reagents provided with the kit. Reactions were recorded as positive, negative, or weakly positive based on the intensity of the color changes or reactions.

3.2.4. Complete genome sequence analysis

High-molecular-weight genomic DNA was extracted from bacterial cells using the Monarch® HMW DNA Extraction Kit for Tissue (New England Biolabs, Ipswich, MA, USA) according to the manufacturer's protocol with some modifications. Briefly, bacterial cell pellets obtained from overnight cultures were resuspended in 500 µL of TES buffer (30 mM Tris-HCl, 1 mM EDTA, 50 mM NaCl, pH 8.0). Subsequently, 500 µL of 25% (w/v) sucrose solution containing egg white lysozyme (FUJIFILM Wako Pure Chemical Corp., Osaka,

Japan) at a final concentration of 30 mg/mL was mixed with the cell suspension and incubated for 1 h at 37°C. Subsequently, 500 μL of TES buffer containing 12.5% (w/v) sucrose and achromopeptidase (FUJIFILM Wako Pure Chemical Corp., Osaka, Japan) at a final concentration of 9 mg/mL was mixed with the suspension and incubated for 30 min at 37°C. Then, cells were harvested and resuspended in STET buffer [8% (w/v) sucrose, 5% (w/v) Triton X-100, 50 mM EDTA, 50 mM Tris-HCl, pH 8.0] and subjected to HMW genomic DNA extraction. Finally, DNA was eluted in Tris-EDTA buffer (10 mM Tris-HCl, 0.5 mM EDTA, pH 9.0). The concentration of genomic DNA was quantified using a Qubit 3.0 fluorometer (Thermo Fisher Scientific). Long-read sequencing libraries were prepared with the Native Barcoding Kit 96 V14 (Oxford Nanopore Technologies (ONT), Oxford, UK) and sequenced using the R10.4.1 flow cell on the PromethION platform (ONT). Read data in FASTQ format were generated using Dorado v7.6.8 (ONT) with the Super-accurate basecalling model v4.3.0, filtered using NanoFilt v2.7.1 with a threshold of ≥3 kb at a quality score of ≥20, and the first 100 bp were trimmed. Short-read sequencing libraries were prepared using the TruSeq DNA PCR-free kit (Illumina Inc., San Diego, CA, USA) and sequenced on the Illumina NovaSeq 6000 platform to generate paired-end sequence reads (2× 150 bp). The Illumina reads were trimmed using atria v4.0.0 (Chuan *et al*. 2021) with the default parameters. The filtered long reads were assembled along with the trimmed Illumina reads of each strain using the microPIPE pipeline (Murigneux *et al*. 2021). The assembled genome sequences were annotated using DFAST v1.2.18 (Tanizawa, Fujisawa and Nakamura 2018).

3.2.5. Bioinformatic analysis

BLAST sequence similarity analysis (blastn, blastp, and tblastn) was used for the identification of candidate DCA-producing strains, putative *bai* genes in the genome, and taxonomic information. The usage of each BLAST analysis was mentioned in the

corresponding parts of the Results. Multiple sequence alignment of 16S rRNA gene sequences from candidate strains, known DCA-producing bacteria, and related taxa was carried out using ClustalW (Thompson et al. 1994), and a phylogenetic tree was constructed using the maximum likelihood method with the Tamura-Nei substitution model (Tamura and Nei, 1993) in MEGA11 (Tamura et al. 2021). The robustness of the tree was evaluated using 1,000 bootstrap replicates, with all other parameters set to their default values. Species-level identification and whole-genome comparisons were carried out using Average Nucleotide Identity (ANI), calculated with ANIb algorithm (Richter *et al*. 2016), with reference genomes obtained from public databases. The resulting ANI matrix was visualized as a half-matrix heatmap in R (version 4.4.2) using the ggplot2 package (Wickham 2016). Putative *bai* genes were identified based on the amino-acid sequence similarity of the known Bai proteins encoded in Cl. scindens ATCC 35704 using the local blastp program in GENETYX Ver. 12 (Genetyx Corp., Tokyo, Japan). The operon structure, including gene order and transcriptional direction, was manually assessed using the graphical genome display feature of the GENETYX platform. Promoter prediction in the *bai* operon region was conducted using the BPROM program (Solovyev and Salamov 2011) in Softberry (http://www.softberry.com/). Alignment and comparison of the genomic structure of the two strains were conducted using the DiGAlign program (Nishimura *et al*. 2024). Metabolic pathway reconstruction was conducted using the KEGGMapper reconstruction function (https://www.kegg.jp/kegg/mapper/) (Kanehisa and Sato 2020) based on the results of BlastKOALA analysis (https://www.kegg.jp/blastkoala/) at default settings (Kanehisa *et al*. 2016).

3.2.6. Statistical analysis

Statistical analysis of the differences between the averaged OD_{660} values in the carbohydrate utilization tests was performed using the Tukey-Kramer post-hoc test following one-way ANOVA. Statistical significance was set at $p < 0.05$.

3.3. Results

3.3.1. Identification of the candidate DCA producers

Based on the screening results described in Chapter II, *Dorea ammoniilytica* and *Ruminococcus* sp. 653 as a candidate for DCA-producing bacteria were selected for further identification and characterization. A microbial tblastn analysis using the amino acid sequence of six Bai enzymes (BaiB, BaiA2, BaiCD, BaiE, BaiF, and BaiH) encoded in *Cla. bilis* c-25 was conducted, since bacterial species harboring a similar *bai* operon structure to this strain were detected in the human gut microbiota in our previous study (Song *et al*. 2021). This analysis detected homologous genes in the draft genome sequences of bacteria, including metagenome-assembled genomes. Among the detected candidates, *D. ammoniilytica* Sanger_02 (GenBank Accession no. GCA_025567415.1) (Hitch *et al*. 2021), harbors homologous *bai* gene sequences, whose gene order and direction were also the same as observed in Cla. bilis c-25 genome (**Table 3-1**). In Chapter II, ASV_44 annotated as *D. ammoniilytica* was detected in the DCA positive culture. based on this association and the conserved *bai* operon structure, D. *ammoniilytica* Sanger_02 as the first candidate DCA-producing bacterium. This strain, deposited in the JCM as *D. ammoniilytica* JCM 34808^T, was then used for further analysis.

To identify additional closely related candidate strains, a BLASTn analysis was performed against the non-redundant nucleotide database to identify additional closely related

isolates to *D. ammoniilytica* JCM 34808^T using the 16S rRNA gene sequence of this strain (Locus_tag: OCV65_12415; 1531 bp). Four entries showed over 99.5% nucleotide identity to the query sequence (**Table 3-2**). Among them, *Ruminococcus* sp. 653 (JCM 18685) has not been characterized, aside from the deposition of its partial 16S rRNA gene sequence to the public database (GenBank accession no. AB744233). Notably, *Ruminococcus* sp. 653 was also detected in the DCA positive culture in Chapter II. Accordingly, *Ruminococcus* sp. JCM 18685 was selected as the second candidate DCA-producing bacterium. No genomic information was available for this strain until this study.

The cell morphology of these two strains was examined using light microscopy after Gram staining. Both strains were Gram-positive and their cells measured approximately 2-3 μm in length, were rod-shaped (bacilli), and were observed singly or in short chains (**Figure 3-1**).

3.3.2. DCA production ability of the candidate strains

The growth and BA conversion dynamics of *D. ammoniilytica* JCM 34808^T and *Ruminococcus* sp. JCM 18685 were investigated in GAM broth at initial pH levels of 6.9 and 8.0 to evaluate their ability to produce DCA (**Figure 3-2**). In the first 6 h of culture at both pH conditions for *D. ammoniilytica*, CA levels greatly decreased, while the production of 7-oxo-DCA (~12%) and DCA (33-36%) conversely increased. This rapid conversion occurred in parallel with exponential growth (**Figure 3-2 a and b**). As the culture progressed up to 72 h, CA was entirely converted to DCA, achieving a conversion yield of 98%. This occurred despite a slight decrease in OD_{660} after 6 h, indicating that BA transformation continued during the stationary phase. These observations also imply that *D. ammoniilytica* rapidly activated the enzymes of the 7α-dehydroxylation pathway during the exponential growth phase.

Ruminococcus sp. JCM 18685 showed similar profiles at pH 6.9 (**Fig. 3-2 c**). CA levels decreased rapidly in the exponential growth phase, which was accompanied by the production of 7-oxo-DCA (14%) and DCA (81%). CA was completely converted to DCA (99%) by 72 h (Fig. 1c). In contrast, at pH 8.0, CA gradually decreased over 12-72 h, accompanied by comparatively low production of DCA (22-66%) irrespective of the higher maximum OD_{660} observed than at pH 6.9 (**Figs. 3-2 c and d**). These results suggested that *Ruminococcus* sp. 653 has a differential response to environmental pH compared to *D. ammoniilytica*.

Additionally, under the same culture conditions using GAM medium supplemented with 0.1 mM CDCA, LCA production was detected in *D. ammoniilytica* (**Figure 3-3 a and c**) and *Ruminococcus* sp. JCM 18685 (**Figure 3-3 b and d**). In both strains, LCA was first detected after 6 h of incubation and remained detectable until the end of the culture period. The detection of DCA and LCA in these experiments clearly demonstrated that both strains possess potent production activity of secondary BAs from CA and/or CDCA through 7α-dehydroxylation.

3.3.3. Complete genome sequencing and genomic rearrangement

Complete genome sequences of *D. ammoniilytica* JCM 34808^T and *Ruminococcus* sp. JCM 18685 were obtained to clarify their taxonomic positions and identify genetic determinants of their phenotypic traits, particularly the ability to convert CA to DCA. Both strains exhibit similar genomic features, except for an extended 14.3 kbp in *Ruminococcus* sp. JCM 18685 and a corresponding increase in the number of coding sequences (**Table 3-5**). The genomic alignment analysis revealed that most of the genomic regions shared ≥95% nucleotide identity, indicating high genomic similarity between the two strains. Despite this, a single large inversion (approximately 2.24 Mbp) was detected in both genomes, spanning 81.25% of the *D.*

ammoniilytica genome and 77.23% of the *Ruminococcus* sp. genome, respectively (**Figure 3-4**).

3.3.4. Identification of genes responsible for BA transformation

Genome sequences of both strains were explored to identify genes responsible for BA transformation, especially for BA 7α-dehydroxylation. The blastp similarity analysis using the Bai protein amino acid sequences of *Cl. scindens* ATCC 35704 as queries indicated that both strains possess a complete set of *bai* gene homologs except for *bai*G (encodes a BA transporter) (**Figure 3-5**). An alternative to *bai*G, a gene encoding a conjugated bile salt major facilitator superfamily (MFS) transporter, exists between *bai*B and *bai*F, as observed in *Cla. bilis* (Song *et al*. 2021; Hisatomi *et al*. 2023). A homolog of *bai*I was also detected at distinct loci separate from the *bai* operon. The *bai* operon structure is identical in both strains, corresponding to *Cla. bilis* (Song *et al*. 2021; Hisatomi *et al*. 2023) and secondary BA-producing strains of *Dorea* (Bai et al. 2022), while differing from the *bai* operon structure of Cl. scindens (**Figure 3-5**). Prediction of promoter sequences recognized by sigma70 detected four possible transcription promoters for the following genes in the *bai* operon: *bai*CD-*bai*E; *bai*H; barAB; *bai*A2-*bai*B-MFS transporter-*bai*F (**Figure 3-5**). These results suggested that the *bai* operon in *D. ammoniilytica* is segmented into four transcriptional units. In addition to the 7α-dehydroxylation genes, *D. ammoniilytica* possesses genes encoding a bile salt hydrolase (Damm_09290), which can deconjugate glycine or taurine from amino acid-conjugated primary BAs, and 7α-HSDH (Damm_13310). The same genes were also detected in *Ruminococcu*s sp. and identified as R653_18280 and R653_13570, respectively. The presence of the latter genes in both strains corroborates their ability to produce 7-oxo-DCA as observed in the CA conversion analysis (**Fig. 3-2**).

Additional analysis was conducted to compare amino acid sequences between novel and known-DCA producing bacteria. Local BLASTp analysis of Bai amino acid sequences was performed using *D. ammoniilytica* JCM 34808^T as the query. Bai sequences from *Ruminococcus* sp. JCM 18685, and *Dorea* sp. (Bai *et al*. 2022) showed very high amino acid sequence identity (>99%) to *D. ammoniilytica* (**Table 3-6**). In contrast, Bai amino acid sequences from *Cla. bilis* exhibited lower identity values, ranging from 74% to 83%, while retaining the same *bai* operon structure.

Lower levels of sequence similarity were observed for other known DCA producers. *Cl. scindens* displayed 38-77% amino acid identity, *C. hylemonae* showed 33-60% identity, and *P. hiranonis* exhibited 38-75% identity. In addition, the BaiG-like MFS transporter gene was not detected in *Cl. scindens*, *C. hylemonae*, or *P. hiranonis*, which harbor the original BaiG gene (**Table 3-6**).

3.3.5. Taxonomic identification of two strains

To identify the taxonomic positions of the two strains, their metabolic capabilities were first evaluated using the API RAPID ID 32A system. Both strains exhibited consistent and reproducible biochemical profiles across three independent replicates, with identical results between strains (**Table 3-7**). Positive reactions were observed in both strains for α-galactosidase, β-galactosidase, utilization of D-mannose and D-raffinose, glutamic acid decarboxylase, and proline arylamidase. Positive reactions for α- and β-galactosidases indicate that both strains can hydrolyze these galactoside linkages, the former of which corresponds to the ability to utilize D-raffinose.

Subsequently, a phylogenetic tree was constructed using 16S rRNA gene sequences (**Figure 3-6**). *D. ammoniilytica* JCM 34808^T and *Ruminococcus* sp. JCM 18685 clustered in the same clade as *Dorea* sp. AF36-15AT and *Dorea* sp. AM 58-8, which were recently

identified as DCA-producing bacteria (Bai *et al*. 2022). They were also separated from other known DCA-producing bacteria (*Cla. bilis, Cl. scindens, Cl. hylemonae*, and *P. hiranonis*) (Kitahara *et al*. 2001; Ridlon *et al*. 2010; Tawthep *et al*. 2017; Devendran *et al*. 2019; Song *et al*. 2021; Hisatomi *et al*. 2023), and possible DCA producer, *Sporofaciens musculi* (Rasmussen *et al*. 2021; Song *et al*. 2021). Other Dorea species were not clustered together within this cluster, indicating the distinct evolutionary lineages present within the genus. Likewise, this cluster, which includes *Ruminococcus* sp. JCM 18685, was phylogenetically distant from other species of *Ruminococcus*, *Mediterraneibacter*, and *Faecalicatena* (**Figure 3-6**).

Finally, an ANI analysis was conducted to further classify *D. ammoniilytica* JCM 34808^T and *Ruminococcus* sp. JCM 18685 and to differentiate them from other DCA-producing bacteria (**Figure 3-7**). The ANI value between *D. ammoniilytica* JCM 34808^T and *Ruminococcus* sp. JCM 18685 was 95.71%, slightly over the commonly accepted intra-species cutoff (≥ 95%) (Goris *et al*. 2007; Jain *et al*. 2018), suggesting that these strains belong to the same species of *D. ammoniilytica*. Although the sequences used for ANI analysis were draft genomes, *Dorea* sp. AM 58-8 and AF36-15AT also showed over 95% ANI to those strains, suggesting that these two *Dorea* strains also belong to *D. ammoniilytica*. As expected from the phylogenetic analysis (**Figure 3-7**), lower ANI values (65.46% to 73.91%) were observed when comparing *D. ammoniilytica* and *Ruminococcus* sp. JCM 18685 to other DCA-producing bacteria, highlighting their genomic distinctiveness and reflecting their unique evolutionary niches in the gut microbiota.

3.3.6. Reconstruction of the carbohydrate utilization pathways

The ability of intestinal bacteria to utilize carbohydrates is crucial for understanding their ecological niches in the gut environment. Thus, carbohydrate utilization pathways were reconstructed to characterize *D. ammoniilytica* JCM 34808^T (**Figure 3-8**). Reconstruction

analysis revealed that all genes of the glycolytic pathway from glucose to acetyl-CoA were conserved (**Figure 3-8 a**). Additionally, D-fructose, D-mannose, D-sorbitol, and D-mannitol can be funneled into the glycolytic pathway via conversion to D-fructose-6-phosphate (**Figure 3-8 b**). This corroborates the D-mannose utilization observed in the biochemical analysis (**Table 3-7**). Sucrose can be hydrolyzed to D-fructose and D-glucose, both of which can feed into the glycolytic pathway (**Figure 3-8 c**). D-galactose can also be utilized via conversion to D-glucose-6-phosphate. In addition, α-galactoside (raffinose and melibiose) and β-galactoside (lactose) utilization pathways were also conserved (**Figure 3-8 d**), supporting the activities of both α- and β-galactosidases in the biochemical analysis (**Table 3-7**). Strach can be utilized by the action of glycogen/starch/α-glucan phosphorylase (EC 2.4.1.1; Damm_26320). Ethanol and acetate can be produced from acetyl-CoA as fermentation products (**Figure 3-8 e**). No genes for lactate and butyrate production were detected. These characteristics are consistent with the definition of properties of the genus *Dorea* (Taras *et al*. 2002). Utilization of the above-indicated carbohydrate sources was evaluated by growth assays in the presence of each carbohydrate as a sole carbohydrate source (**Figure 3-9**). Significant increases in averaged OD_{660} values were observed in the presence of D-glucose, D-fructose, D-galactose, D-mannose, D-mannitol, and starch. In contrast, no significant increases in growth were detected in the presence of D-sorbitol, raffinose, melibiose, and lactose (**Figure 3-9**). These results showed that both strains can utilize these monosaccharides, D-mannitol, and starch, all of which were deduced from metabolic pathway reconstruction analysis.

3.4. Discussions

This study identified *D. ammoniilytica* JCM 34808^T and *Ruminococcus* sp. JCM 18685 as members of *D. ammoniilytica*, a novel DCA-producing species that is taxonomically distinct from known DCA producers. Here, we clarified the morphology, growth, and BA

transformation profiles, biochemical characteristics, and genomic information of these two strains.

The same-species classification was supported by several criteria. First, both strains are Gram-positive and exhibit similar morphology, appearing rod-shaped and often arranged in chains under microscopic observation (**Figure 3-1**). Second, both strains share identical biochemical profiles, as determined using the API RAPID ID 32A system (**Table 3-7**). Third, phylogenetic analysis using the 16S rRNA gene sequences placed both strains within the same clade (**Figure 3-6**). Fourth, whole-genome ANI analysis revealed 95.71% identity, exceeding the intra-species threshold of ≥95% (Goris *et al*. 2007; Jain *et al*. 2018) (**Figure 3-7**). Despite their differences in historically assigned genus, both strains were clearly identifiable as *D. ammoniilytica* in this study.

Phylogenetic analysis and ANI analysis indicated that both strains are distinct from other known DCA producers, such as *Cl. scindens*, *Cl. hylemonae, Cla. bilis*, and *P. hiranonis* (**Figure 3-6, 3-7**). In contrast, recently identified DCA-producing *Dorea* strains, *Dorea* sp. AM58-8 and AF36-15AT, were clustered into the same clade in phylogenetic analysis (**Figure 3-6**). Draft genomic sequences of these strains indicated over 95% ANI values when compared with the genomes of *D. ammoniilytica* strains (**Figure 3-7**). These results suggested that these strains are closely related to *D. ammoniilytica*. Although these Dorea strains had already been reported to produce DCA, no physiological or taxonomical characterization was conducted in that study (Bai *et al*. 2022). Moreover, only their draft genomic sequences are available. In contrast, this study taxonomically identified the two strains as a novel DCA-producing species, *D. ammoniilytica*, and the previously reported *Dorea* strains would also be included in this species. Complete genome sequencing and biochemical characterization revealed that *D. ammoniilytica* possesses broader carbohydrate utilization ability than previously characterized DCA-producing bacteria, as discussed below. Moreover, the two *D. ammoniilytica* strains

exhibited considerably higher DCA production activity compared to the reported *Dorea* strains. *Dorea* sp. AM58-8 and AF36-15AT were reported to have low DCA production activity: only about 5% of CA was converted to DCA over 48 h of incubation (Bai *et al*. 2022). In contrast, *D. ammoniilytica* strains showed almost complete conversion of CA to DCA within 48 h (**Figure 3-10**) when cultured under the same conditions used in a previous report (Bai *et al*. 2022). These findings highlight the *D. ammoniilytica* strains as previously unrecognized but highly efficient DCA-producing species, differentiating them from the closely related DCA-producing *Dorea* strains.

Biochemical and metabolic pathway reconstruction analysis revealed that *D. ammoniilytica* can utilize D-glucose and is predicted to utilize D-fructose, D-galactose, D-mannose, D-sorbitol, D-mannitol, sucrose, α-galactosides, β-galactosides, and starch (**Table 3-7**). Culture analysis in the presence of each carbohydrate as a sole carbohydrate source verified that *D. ammoniilytica* strains can utilize these monosaccharides, D-mannitol, and starch (Fig. 6). These carbohydrate utilization properties are similar to those of other DCA-producing bacteria, except for the utilization of polymeric starch: *Cla. bilis* can utilize D-glucose, sucrose, and trehalose (Hisatomi *et al*. 2023); *Cl. scindens* ATCC 35704 can utilize six monosaccharides (D-glucose, D-fructose, D-mannose, D-galactose, D-ribose, and D-xylose), two sugar alcohols (dulcitol and D-sorbitol), and one disaccharide (lactose) (Devendran *et al*. 2019). These results suggest that DCA-producing bacteria share a similar ecological niche with regards to carbohydrate sources within the human gut.

The *bai* gene operon structure, segmented into four putative transcriptional units, was conserved among both strains of *D. ammoniilytica*, the two *Dorea strains*, and *Cla. bilis* (Fig. 3). This structure is different from that shared in *Cl. scindens* (**Figure 3-5**), *Cl. hylemonae*, and *P. hiranonis*, where *bai* genes are arranged in a single operon (Ridlon *et al*. 2016). It is intriguing why the segmented operon structure is conserved in the phylogenetically distant

species, *D. ammoniilytica* and *Cla. bilis* (**Figure 3-6**). One possible reason is that these operons may have been acquired through horizontal gene transfer. This inference comes from BLAST analyses of the amino acid sequences of six Bai proteins (BaiB, BaiA2, BaiCD, BaiE, BaiF, and BaiH) in *D. ammoniilytica*. Their sequences were found to be more similar to those of *Cla. bilis* than to those of *Cl. scindens*: *Cla. bilis* exhibits over 70% amino acid identity (**Table 3-1**). Another possible reason is their advantage in regulating DCA production. Bai enzymes act to produce DCA in the following order: BaiB, BaiA2, BaiCD, BaiE, BaiF, BaiH, BaiCD, and BaiA2 (Funabashi *et al*. 2020). When these genes are organized in a single operon, the transcript abundance of each *bai* gene is expected to be similar. This has indeed been reported in the RNA-Seq analysis of *Cl. scindens* ATCC 35708 (Devendran *et al*. 2019). In contrast, in the segmented operon found in *D. ammoniilytica*, the transcript abundance of each transcription unit may vary. In fact, in *Cla. bilis* c-25, which has a similar operon structure, the transcript levels of *bai*B and *bai*CD—encoding enzymes that act in the first half of the reaction pathway—have been reported to be 15-20 times higher than that of *bai*H, which works in the latter half (Song *et al*. 2021). While the reaction rates of each enzyme must be considered, the segmented *bai* operon may contribute to efficient DCA production by allowing for differential regulation of the enzymes required for each step. Further analysis of the gene expression and regulatory mechanisms of the *bai* operon will help clarify the functional significance of this operon structure.

Comparison of Bai amino acid sequences among *D. ammoniilytica, Ruminococcus* sp., and *Dorea* strains revealed very high sequence similarity, with amino acid identities over 99%, indicating strong conservation of Bai proteins across these taxa (**Table 3-6**). No major sequence differences were detected among the compared strains. However, as described above, *D. ammoniilytica* exhibited substantially higher DCA production than the Dorea strains (**Figure 3-10**). This discrepancy suggests that variation in DCA production is unlikely to be

explained by differences in Bai amino acid sequences alone and may instead be associated with factors such as *bai* gene expression levels.

D. ammoniilytica possesses genes encoding bile salt hydrolase (Damm_09290) and 7α-HSDH (Damm_13310) in addition to the *bai* genes. The former enzyme is responsible for the production of free BAs from primary BAs conjugated with glycine or taurine, which are synthesized in the liver (Ridlon *et al*. 2006). The gene encoding this enzyme is not conserved among the DCA-producing bacteria; only *P. hiranonis* is known to possess this gene (Kim *et al*. 2022). This suggests that *D. ammoniilytica* can utilize conjugated CA as a substrate for DCA production. This was confirmed through conversion analysis using GCA or TCA as a substrate (**Figure 3-11**). Although conversion was qualitatively evaluated by TLC analysis, it was evident that these strains produced DCA from conjugated CA (**Figure 3-11**). Unconjugated CA was also detected in the process. These findings are consistent with the known phenomenon that conjugated CA is used as a substrate for DCA production only after it has been deconjugated by the action of bile salt hydrolase (Ridlon *et al*. 2006). Given its potent DCA-producing activity from both conjugated and unconjugated CA, *D. ammoniilytica* may represent a major DCA producer in the human gut. Further population-level analysis of this species will help clarify its contribution to DCA production.

3.5. Conclusions

This study demonstrated that *D. ammoniilytica* JCM 34808^T and *Ruminococcus* sp. JCM 18685 belong to the same species, *D. ammoniilytica*, a novel species of DCA-producing bacteria. This discovery expands the known diversity of secondary BA producers in the human gut microbiome. Further studies of this species will provide new insight into intestinal BA metabolism and its implications for host health and disease.

3.6. Tables and Figures

Table 3-1. Identified putative *bai* genes in *Dorea ammoniilytica* Sanger_02 by tblastn analysis using the deduced amino acid sequence of Bai proteins in *Claveliimonas bilis* c-25.

Bai protein	In *Claveliimonas bilis* c-25[a]	Gene in *D. ammoniilytica*[b]	Protein in *D. ammoniilytica*[a]	Annotation	Score	Expect	Identities	Positives	Gaps	Frame
BaiF	BCZ28401.1	OCV65_09735	MCU6700506.1	CoA transferase	823 bits(2126)	0	383/452(85%)	415/452(91%)	0/452(0%)	-1
BaiB	BCZ28403.1	OCV65_09745	MCU6700508.1	bile acid--CoA ligase BaiB	776 bits(2005)	0	369/491(75%)	430/491(87%)	0/491(0%)	-3
BaiA2	BCZ28404.1	OCV65_09750	MCU6700509.1	SDR family oxidoreductase	400 bits(1028)	5.00E-129	206/254(81%)	227/254(89%)	0/254(0%)	-2
BaiH	BCZ28407.1	OCV65_09765	MCU6700512.1	NAD(P)/FAD-dependent oxidoreductase	949 bits(2453)	0	483/666(73%)	553/666(83%)	5/666(0%)	-2
BaiCD	BCZ28408.1	OCV65_09770	MCU6700513.1	FAD-dependent oxidoreductase	1068 bits(2762)	0	514/640(80%)	577/640(90%)	0/640(0%)	+2
BaiE	BCZ28409.1	OCV65_09775	MCU6700514.1	nuclear transport factor 2 family protein	287 bits(734)	9.00E-91	130/168(77%)	153/168(91%)	0/168(0%)	+1

[a] GenBank accession no. was indicated.

[b] Locus_tag in the genome of *D. ammoniilytica* Sanger_02

Table 3-2. Entries of 16S rRNA genes that showed high nucleotide identity to that of *Dorea ammoniilytica* Sanger_02

Description	Scientific Name	Max Score	Total Score	Query Cover	E value	Per. Ident	Acc. Len	Accession
Corynebacterium sp. Marseille-P4122 partial 16S rRNA gene, strain Marseille-P4122	*Corynebacterium dentalis*	2748	2748	98%	0	99.87%	1494	LT897837.1
Corynebacterium dentalis strain Marseille-P4122 16S ribosomal RNA, partial sequence	*Corynebacterium dentalis*	2748	2748	98%	0	99.87%	1494	NR_179631.1
Clostridium sp. Marseille-P3820 partial 16S rRNA gene, strain Marseille-P3820	*Clostridium* sp. Marseille-P3820	2660	2660	95%	0	99.59%	1453	LT838232.1
Ruminococcus sp. 653 gene for 16S ribosomal RNA, partial sequence	*Ruminococcus* sp. 653	2628	2628	94%	0	99.65%	1438	AB744233.1

Table 3-3. Composition of peptone yeast glucose (PYG) medium (modified)

Medium composition (DSMZ, 104)		
Trypticase peptone	5	g
Peptone	5	g
Yeast extract	10	g
Beef extract	5	g
Glucose	5	g
K_2HPO_4	2	g
Tween 80	1	ml
Salt solution (see below)	40	ml
Resazurin	1	mg
*Vitamin K1 solution (see below)	0.20	ml
*Haemin solution (see below)	10	ml
Cysteine-HCl × H2O	0.50	g
Distilled water up to	950	ml

*The vitamin K1, haemin solution and the cysteine are added after the medium has been boiled and cooled under CO_2. Adjust pH to 7.2 using 8 N NaOH. Distribute under N_2 and autoclave (121^{o}C, 15 minutes).

Salt solution		
$CaCl_2 \times 2\ H_2O$	0.25	g
$MgSO_4 \times 7\ H_2O$	0.50	g
K_2HPO_4	1	g
KH_2PO_4	1	g
$NaHCO_3$	10	g
NaCl	2	g
Distilled water up to	1000	ml

*Haemin solution:

Dissolve 50 mg haemin in 1 ml 1 N NaOH; make up to 100 ml with distilled water. Store refrigerated

*Vitamin K1 solution:

Dissolve 0.1 ml of vitamin K1 in 20 ml 95% ethanol and filter sterilize. Store refrigerated in a brown bottle.

Table 3-4. Composition of semi-solid gifu anaerobic medium (GAM)

Medium composition	Liquid medium	
Peptone	10	g
Soya peptone	3	g
Proteose peptone	10	g
Digested serum	13.5	g
Yeast extract	5	g
Meat extract	2.2	g
Liver extract	1.2	g
Glucose	3	g
KH_2PO_4	2.5	g
NaCl	3	g
Starch soluble	5	g
L-cysteine hydrocloride	0.3	g
$NaC_3H_4O_2S$	0.3	g
Agar	2	g
Distilled water	1000	mL

Semi-solid medium was filtered to remove agar particles before autoclaving and autoclaved at 115^{o}C for 15 minutes. Medium was anaerobically treated prior to use.

Table 3-5. Completed sequenced genome information

	Dorea ammoniilytica JCM 34808^T	*Ruminococcus* sp. JCM 18685
Genome size (bp)	2,753,170	2,896,198
GC content (%)	43.4	43.1
No. of CDSs	2,672	2,760
Average Protein Length	308.8	312.6
Coding ratio (%)	89.9	89.4
No. of rRNAs	10	10
No. of tRNAs	53	53

Table 3-6. Heatmap table of Bai amino acid sequence identities (%) between *Dorea ammoniilytica* JCM 34808^T, Ruminococcus sp. JCM 18685, *Dorea* strains, and known DCA-producing bacteria

	BaiB	BaiCD	BaiE	BaiF	BaiG-like	BaiH	BaiI	BaiA2
Dorea ammoniilytica	-	-	-	-	-	-	-	-
Ruminococcus sp. 653	99.23 (0)	95.74 (0)	98.92 (6e-141)	99.78 (0)	99.77 (0)	99.25 (0)	100 (3e-167)	99.61 (0)
Dorea sp. AM58-8	99.23 (0)	99.84 (0)	100 (7e-143)	99.34 (0)	99.30 (0)	100 (0)	99.45 (0)	98.83 (0)
Dorea sp. AF36-15AT	99.62 (0)	99.84 (0)	100 (7e-143)	99.34 (0)	99.30 (0)	100 (0)	100 (2e-144)	99.61 (0)
Cla. bilis	74.61 (0)	80.16 (0)	77.38 (3e-102)	82.74 (0)	76.94 (0)	75.52 (0)	75.54 (2e-111)	81.89 (8e-156)
C. scindens	49.21 (3e-176)	54.91 (0)	77.38 (9e-102)	43.07 (3e-114)	ND	67.12 (0)	46.93 (2e-54)	38.37 (2e-56)
C. hylemonae	50.69 (2e-179)	54.45 (0)	60.36 (5e-77)	44.83 (9e-120)	ND	33.48 (1e-111)	45.81 (1e-53)	38.96 (1e-48)
P. hiranonis	50.2 (0)	56.47 (0)	57.40 (2e-72)	44.06 (6e-117)	ND	68.93 (0)	74.73 (8e-103)	37.96 (4e-55)

BLAST Expect values are given in parentheses. Darker boxes indicate higher degree of similarity.

Table 3-7. Biochemical characteristics of *Dorea ammoniilytica* JCM 34808^T and *Ruminococcus* sp. JCM 18685 using the API Rapid ID 32 A system

Enzyme activity and substrates	D1	D2	D3	R1	R1	R3
Urease	-	-	-	-	-	-
Arginine dihydrolase	-	-	-	-	-	-
α-Galactosidase	+	+	+	+	+	+
β-Galactosidase	+	+	+	+	+	+
β-Galactosidase 6 phospate	-	-	-	-	-	-
α-Glucosidase	-	-	-	-	-	-
β-Glucosidase	-	-	-	-	-	-
α-Arabinosidase	-	-	-	-	-	-
β-Glucuronisidase	-	-	-	-	-	-
N-Acetyl-β-glucosaminidase	-	-	-	-	-	-
Mannose	+	+	+	+	+	+
Raffinose	+	+	+	+	+	+
Glutamic acid decarboxylase	+	+	+	+	+	+
α-Fucosidase	-	-	-	-	-	-
Nitrates reduction	-	-	-	-	-	-
Indole	-	-	-	-	-	-
Alkaline phospatase	-	-	-	-	-	-
Arginine arylamidase	-	-	-	-	-	-
Proline arylamidase	+	+	+	+	+	+
Leucyl glycine arylamidase	-	-	-	-	-	-
Phenylalanine arylamidase	-	-	-	-	-	-
Leucine arylamidase	-	-	-	-	-	-
Pyroglutamic acid	-	-	-	-	-	-
Tyrosine arylamidase	-	-	-	-	-	-
Alanine arylamidase	-	-	-	-	-	-
Glycine arylamidase	-	-	-	-	-	-
Histidine arylamidase	-	-	-	-	-	-
Glutamyl glutamic acid	-	-	-	-	-	-
Serine arylamidase	-	-	-	-	-	-

D1, D2, D3 represent biological replicates of *Dorea ammoniilytica* JCM 34808^T . R1, R2, R3 represent biological replicates of *Ruminococcus* sp. JCM 18685. +, Positive; -, Negative. Adapted from Kastawa *et al*. 2025.

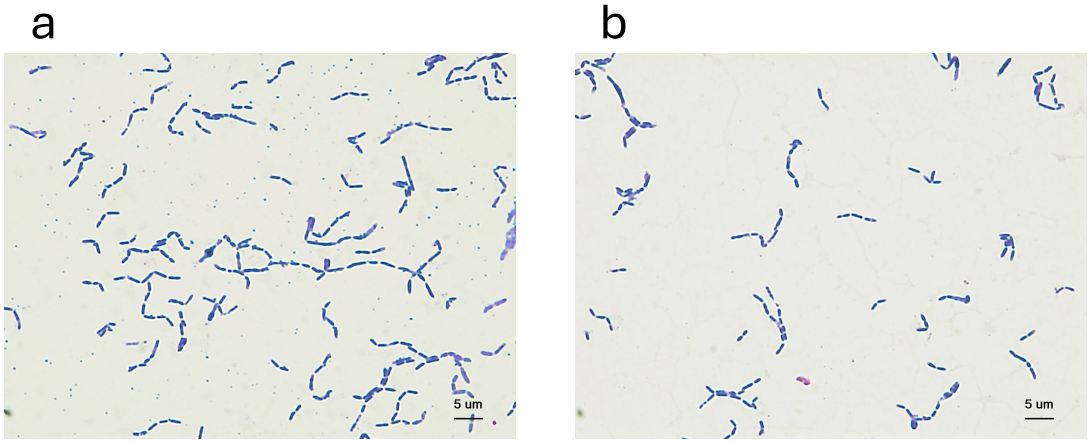

Figure 3-1. Cell morphology of *Dorea ammoniilytica* JCM 34808^T and *Ruminococcus* sp. JCM 18685

Cell morphology of *Dorea ammoniilytica* JCM 34808^T **(a)** and *Ruminococcus* sp. JCM 18685 **(b)** was examined by light microscopy following Gram staining. Adapted from Kastawa *et al*. 2025.

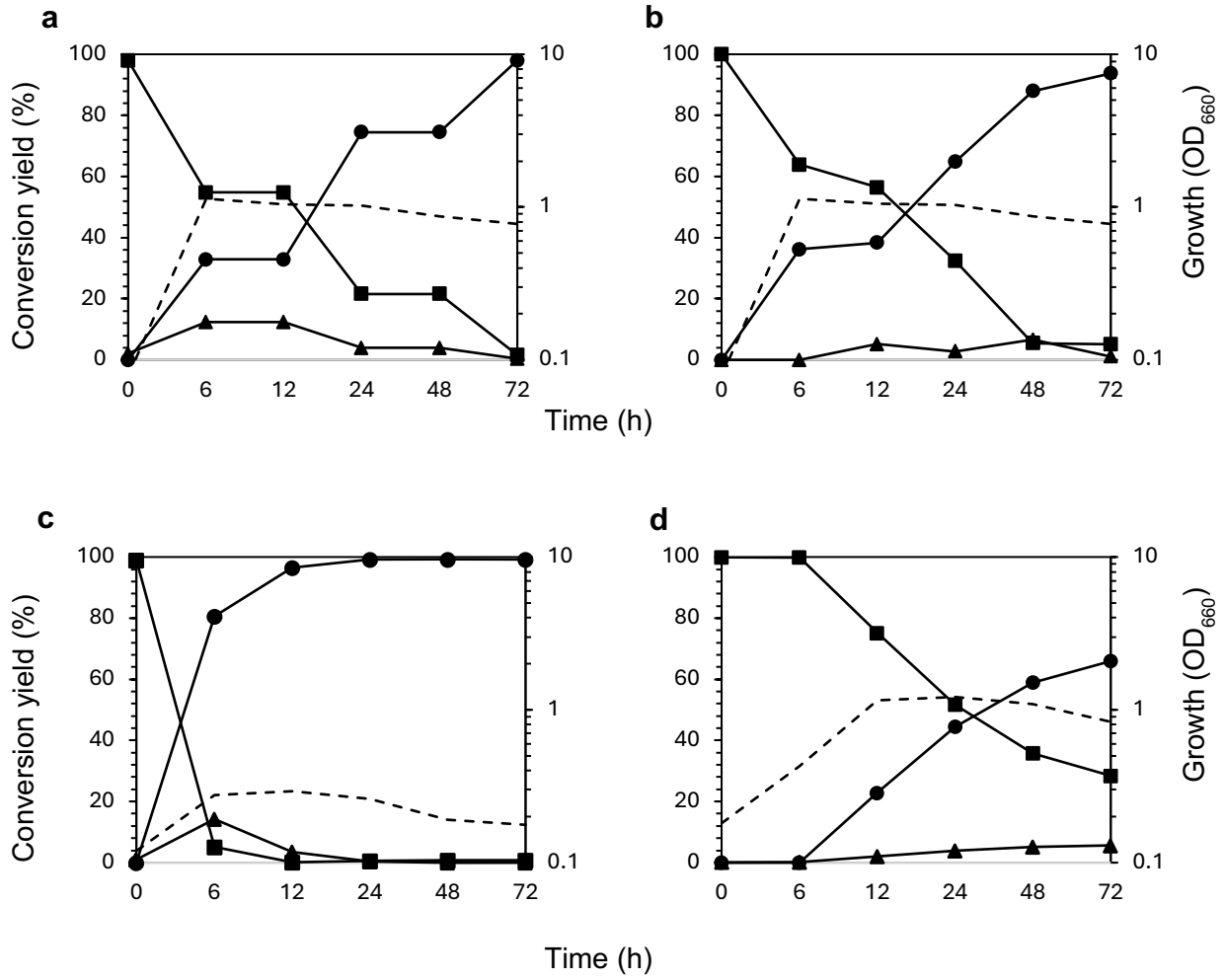

Figure 3-2. Time-course analysis of the growth and CA conversion profile of two candidate DCA-producing strains under different pH conditions.

The bacterial strains were anaerobically cultured in GAM medium at initial pH 6.9 (a and c) and 8.0 (b and d) in the presence of CA-Na. a and b, *Dorea ammoniilytica* JCM 34808^{T}; c and d, *Ruminococcus* sp. JCM 18685. Bacterial growth was measured by optical density at 660 nm (OD_{660}; dotted line). The conversion yield was calculated by dividing each BAs concentration by the total concentration of CA, DCA, and 7-oxo-DCA. These are represented by squares, circles, and triangles, respectively. Data were presented as the mean values from three independent experiments. Adapted from Kastawa *et al*. 2025.

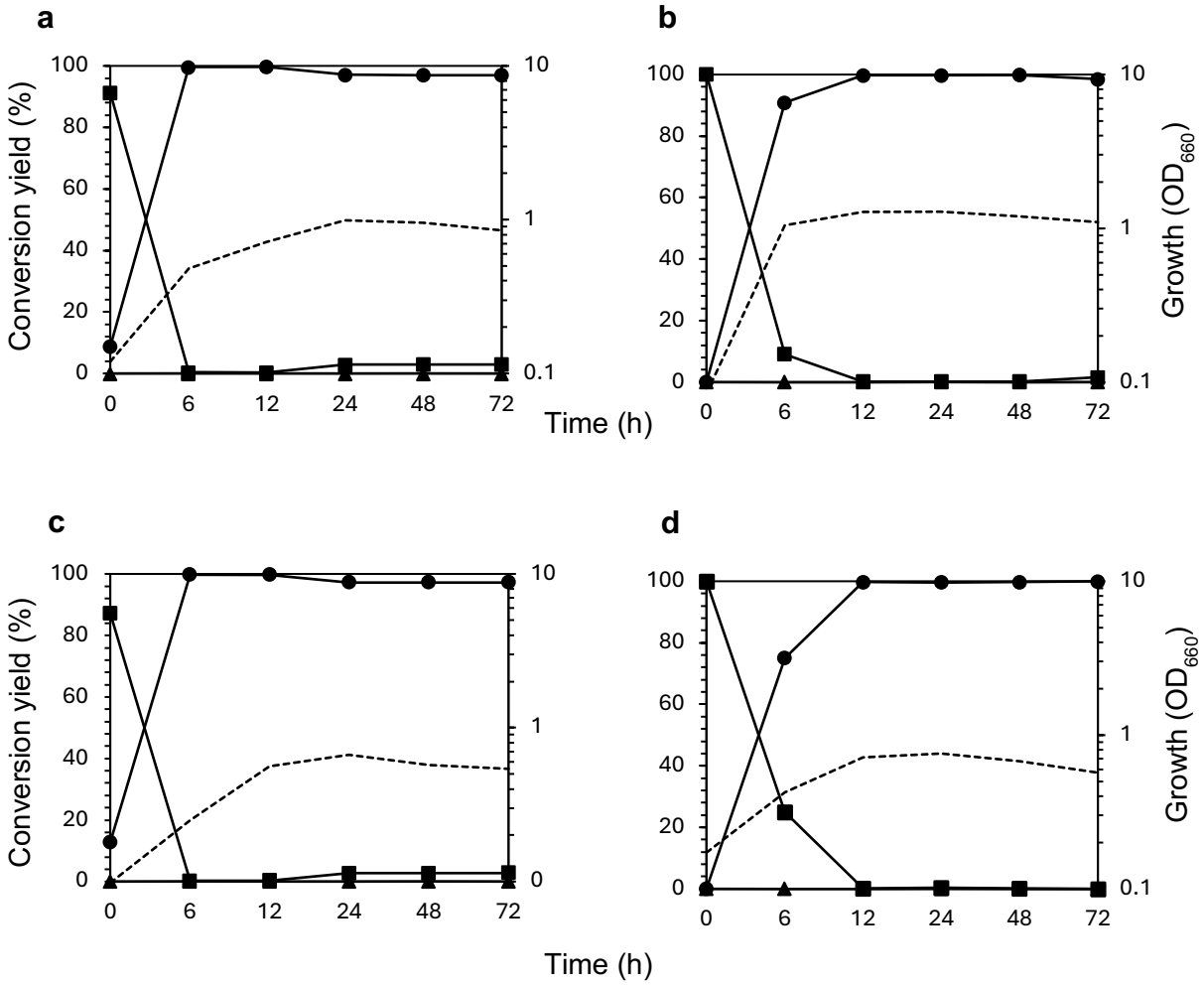

Figure 3-3. Time-course analysis of the growth and CDCA conversion profile of two candidate DCA-producing strains under different pH conditions.

The bacterial strains were anaerobically cultured in GAM medium at initial pH 6.9 (a and c) and 8.0 (b and d) in the presence of CDCA. a and b, *Dorea ammoniilytica* JCM 34808^T; c and d, *Ruminococcus* sp. JCM 18685. Bacterial growth was measured by optical density at 660 nm (OD_{660}; dotted line). The conversion yield was calculated by dividing each BAs concentration by the total concentration of CDCA, LCA, and 7-oxo-LCA. These are represented by squares, circles, and triangles, respectively. Data were presented as the mean values from three independent experiments.

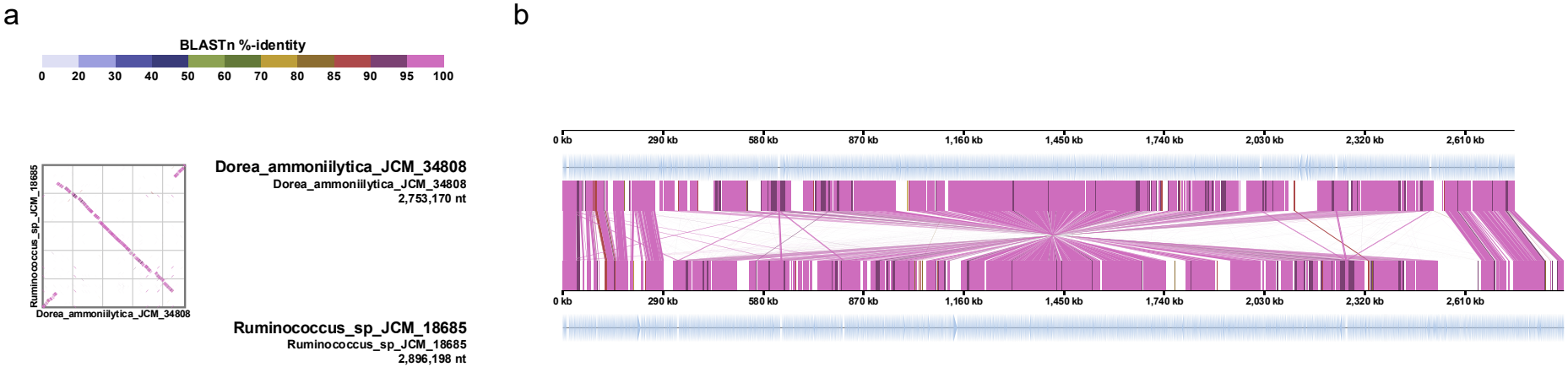

Figure 3-4. Large genomic inversion in the genomes of two DCA-producing strains.

Genomic sequences of two DCA-producing strains were compared using the genome alignment viewer DiGAlign (Nishimura *et al*. 2024) following the results of the blastn sequence similarity analysis. a) Scatter plot of the homologous regions between the two genomes. The color bar indicates the nucleotide sequence identity as determined by blastn analysis. b) Genome alignment between *D. ammoniilytica* JCM 34808^{T} (upper) and *Ruminococcus* sp. JCM 18685 (lower). Homologous genes are connected by lines, with the color representing the nucleotide sequence identity. Genes are visualized as directional arrowheads colored in light blue, with the top and bottom tracks representing the two genomes. Adapted from Kastawa *et al*. 2025.

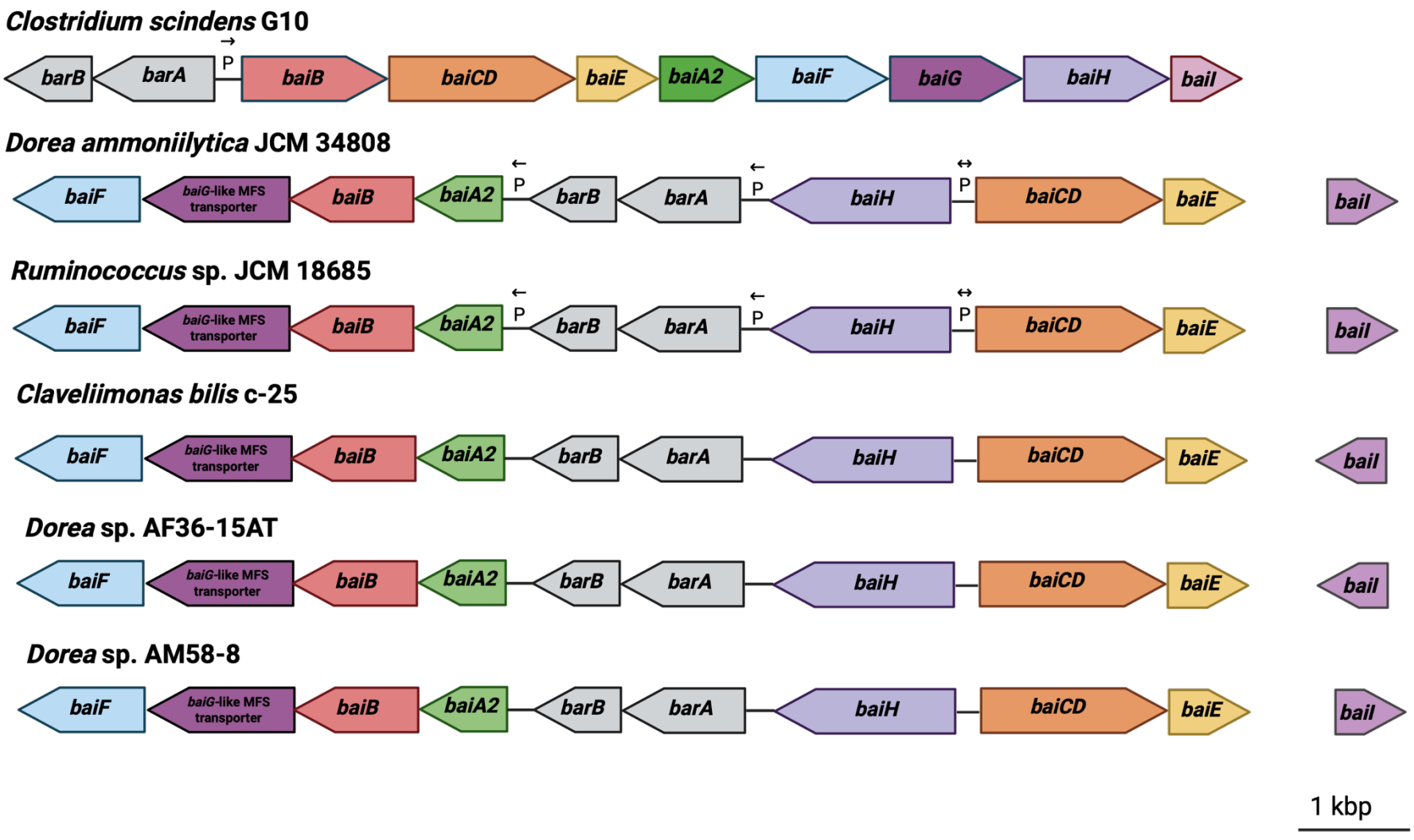
Clostridium scindens G10
barB
barA
P
baiB
baiCD
baiE
baiA2
baiF
baiG
baiH
baiI
Dorea ammoniilytica JCM 34808
baiF
baiG-like MFS transporter
baiB
baiA2
P
barB
barA
P
baiH
P
baiCD
baiE
baiI
Ruminococcus sp. JCM 18685
baiF
baiG-like MFS transporter
baiB
baiA2
P
barB
barA
P
baiH
P
baiCD
baiE
baiI
Claveliimonas bilis c-25
baiF
baiG-like MFS transporter
baiB
baiA2
barB
barA
baiH
baiCD
baiE
baiI
Dorea sp. AF36-15AT
baiF
baiG-like MFS transporter
baiB
baiA2
barB
barA
baiH
baiCD
baiE
baiI
Dorea sp. AM58-8
baiF
baiG-like MFS transporter
baiB
baiA2
barB
barA
baiH
baiCD
baiE
baiI
1 kbp

Cont.

Figure 3-5. *bai* gene arrangements of *Dorea ammoniilytica* JCM 34808^T, *Ruminococcus* sp. JCM 18685 and other DCA-producing bacterial strains.

The *bai* gene arrangements as observed in *Dorea ammoniilytica* JCM 34808^T, *Ruminococcus* sp. JCM 18685, and other DCA-producing bacterial strains, such as *Clostridium scindens* G10, *Claveliimonas bilis*, *Dorea* sp. AF36-15AT, and *Dorea* sp. AM58-8. The operon structures are shown based on the conserved gene content across these species, with homologous genes color-coded to illustrate shared functions. Predicted promoter regions are indicated upstream of several operons as "P" with the arrows showing the direction of transcription. Created in BioRender. Kastawa, N. (2025) https://BioRender.com/tsj1eyk. Adapted from Kastawa *et al*. 2025.

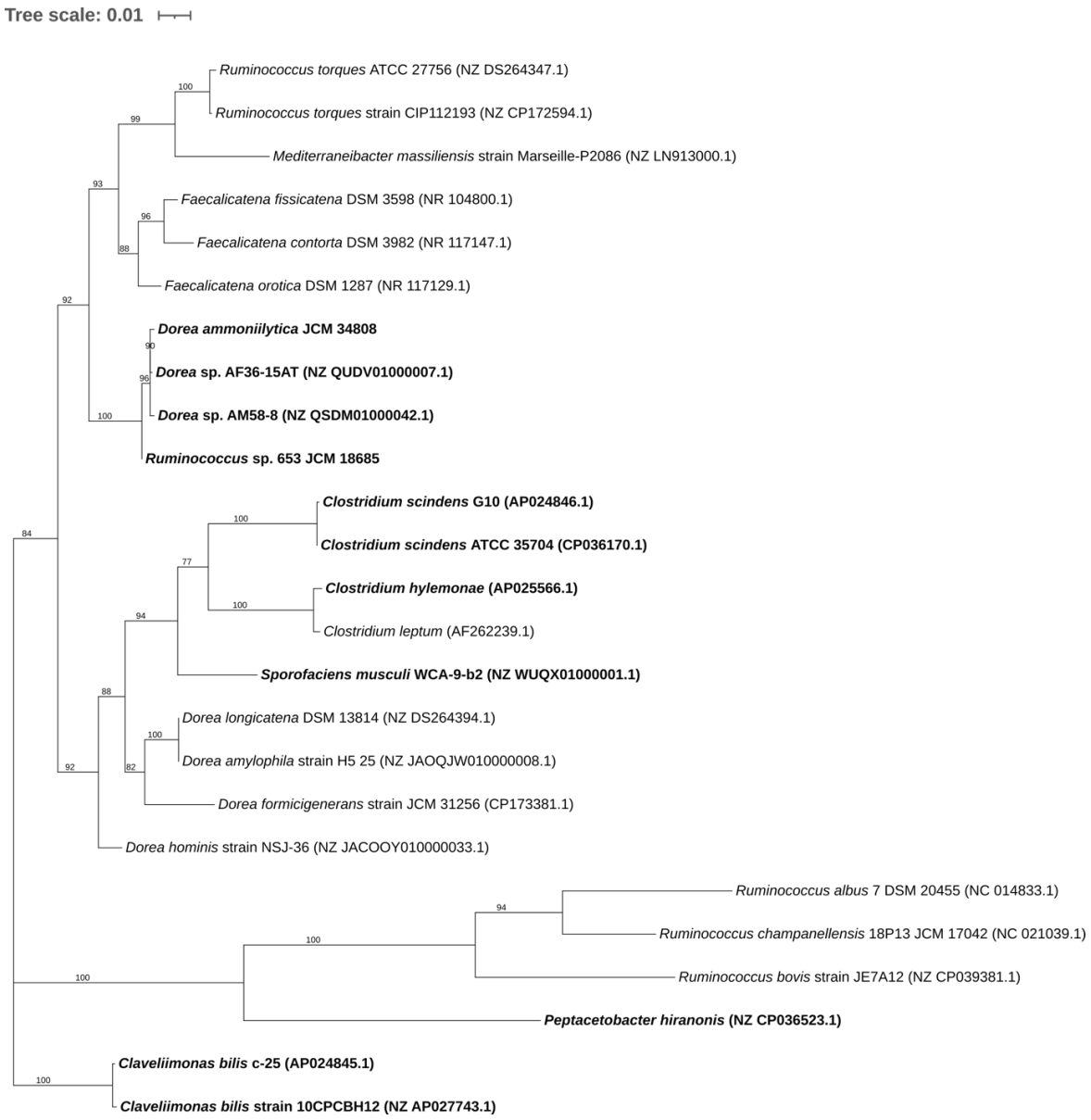

Figure 3-6. Phylogenetic tree based on 16S rRNA gene sequences of *Dorea ammoniilytica* JCM 34808^T, *Ruminococcus* sp. JCM 18685 and other strains related to DCA-producing bacterial species.

Evolutionary relationship between *D. ammoniilytica* JCM 34808^T, *Ruminococcus* sp. JCM 18685, and other related bacterial species. Strains capable of DCA production are indicated in bold. The tree was constructed in MEGA 11 (Tamura *et al*. 2021) using the Tamura-Nei model (Tamura and Nei, 1993) with 1,000 bootstrap replicates. Bootstrap values are shown next to the corresponding branches. Adapted from Kastawa *et al*. 2025.

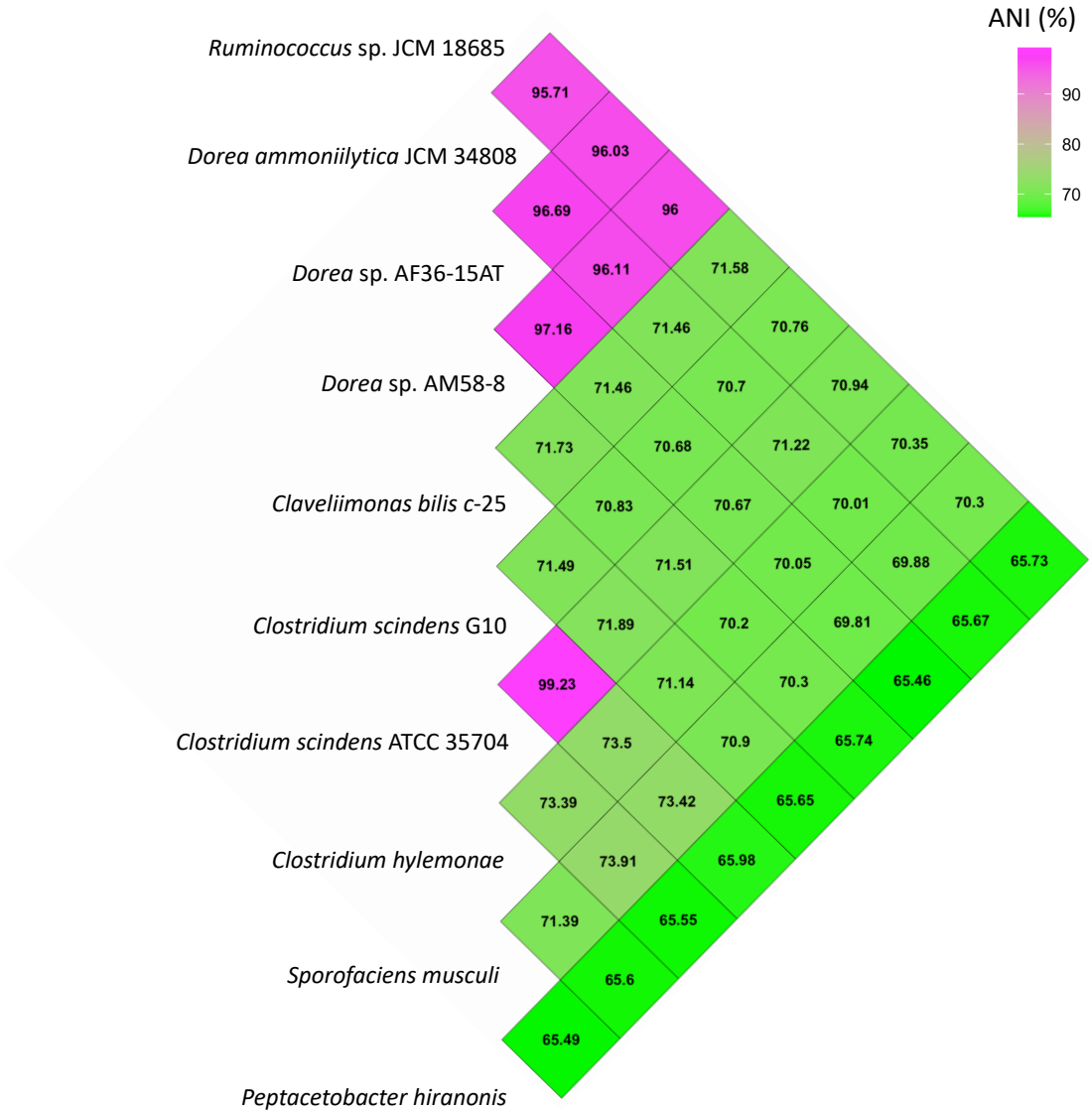

Figure 3-7. Heatmap showing average nucleotide identity (ANI) values between genomes of *Dorea ammoniilytica* JCM 34808^{T}, *Ruminococcus* sp. JCM 18685 and other DCA-producing bacterial strains.

Average nucleotide identity (ANI) between the genomes of DCA-producing bacterial strains. The ANI heatmap displays pairwise comparisons, with colors representing the percentage of nucleotide sequence identity. Pairwise ANI values were calculated using the ANIb method implemented in JSpeciesWS (Richter *et al*. 2016). The resulting ANI matrix was visualized as a heatmap in R using the ggplot2 package (Wickham, 2016). Adapted from Kastawa *et al*. 2025

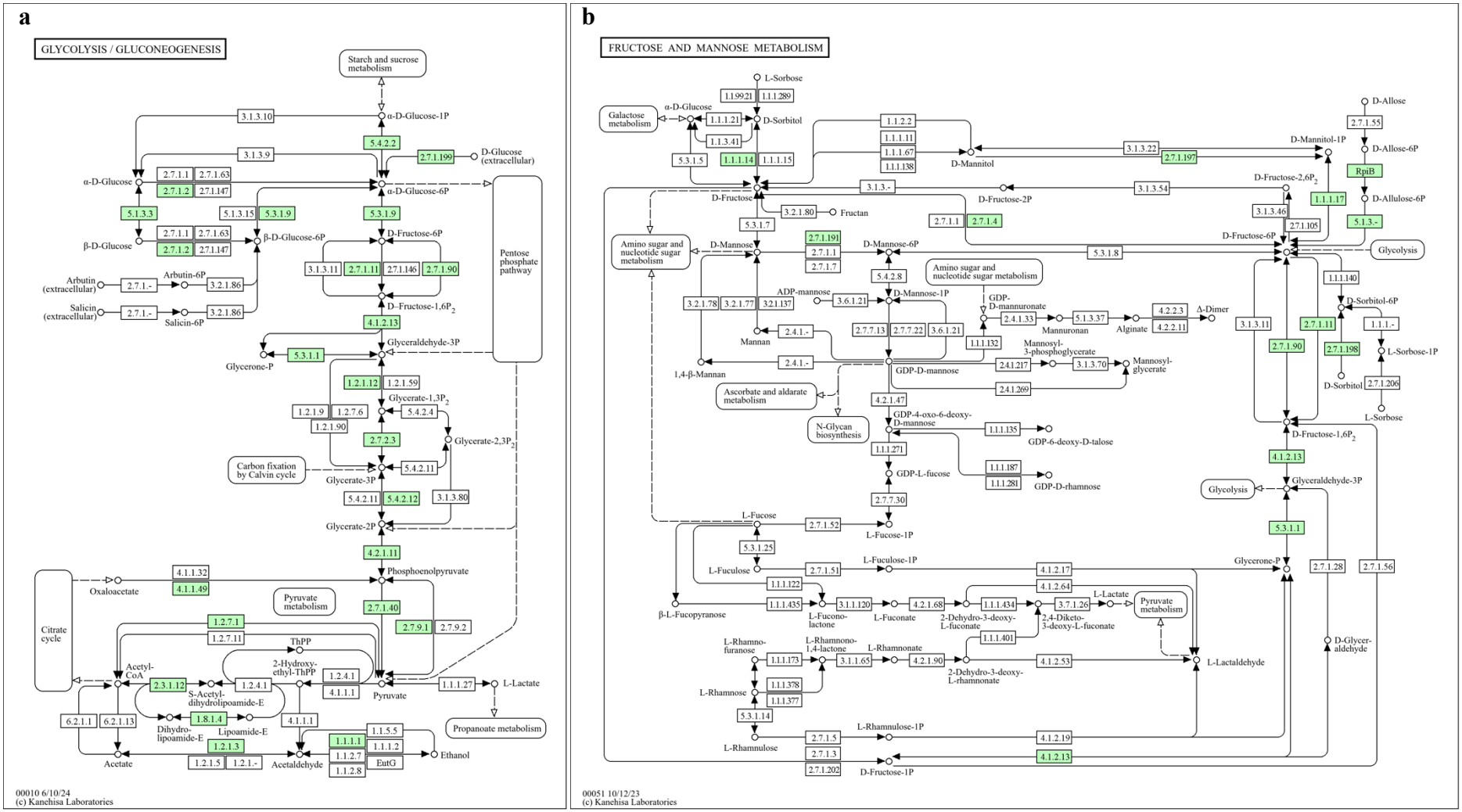
a
GLYCOLYSIS / GLUCONEOGENESIS
Starch and sucrose metabolism
α-D-Glucose-1P
α-D-Glucose
α-D-Glucose-6P
β-D-Glucose
β-D-Glucose-6P
D-Glucose (extracellular)
Arbutin (extracellular)
Arbutin-6P
Salicin (extracellular)
Salicin-6P
D-Fructose-6P
D-Fructose-1,6P2
Pentose phosphate pathway
Glycerone-P
Glyceraldehyde-3P
Glycerate-1,3P2
Glycerate-2,3P2
Carbon fixation by Calvin cycle
Glycerate-3P
Glycerate-2P
Phosphoenolpyruvate
Oxaloacetate
Pyruvate metabolism
Citrate cycle
ThPP
2-Hydroxy-ethyl-ThPP
Acetyl-CoA
S-Acetyl-dihydrolipoamide-E
Dihydro-lipoamide-E
Lipoamide-E
Pyruvate
L-Lactate
Propanoate metabolism
Acetate
Acetaldehyde
Ethanol
EutG
00010 6/10/24
(c) Kanehisa Laboratories
b
FRUCTOSE AND MANNOSE METABOLISM
L-Sorbose
Galactose metabolism
α-D-Glucose
D-Sorbitol
D-Mannitol
D-Fructose
Fructan
D-Fructose-2P
D-Mannitol-1P
D-Allose
D-Allose-6P
RpiB
D-Allulose-6P
D-Fructose-2,6P2
D-Fructose-6P
Glycolysis
Amino sugar and nucleotide sugar metabolism
D-Mannose
D-Mannose-6P
D-Mannose-1P
ADP-mannose
GDP-D-mannuronate
Mannuronan
Alginate
Δ-Dimer
Mannan
1,4-β-Mannan
GDP-D-mannose
Mannosyl-3-phosphoglycerate
Mannosyl-glycerate
Ascorbate and aldarate metabolism
N-Glycan biosynthesis
GDP-4-oxo-6-deoxy-D-mannose
GDP-6-deoxy-D-talose
GDP-L-fucose
GDP-D-rhamnose
L-Fucose
L-Fucose-1P
L-Fuculose
L-Fuculose-1P
Glycerone-P
β-L-Fucopyranose
L-Fucono-lactone
L-Fuconate
2-Dehydro-3-deoxy-L-fuconate
2,4-Diketo-3-deoxy-L-fuconate
L-Lactate
Pyruvate metabolism
L-Rhamno-furanose
L-Rhamnono-1,4-lactone
L-Rhamnonate
2-Dehydro-3-deoxy-L-rhamnonate
L-Lactaldehyde
D-Glycer-aldehyde
L-Rhamnose
L-Rhamnulose-1P
L-Rhamnulose
D-Fructose-1P
D-Fructose-1,6P2
Glyceraldehyde-3P
D-Sorbitol-6P
L-Sorbose-1P
D-Sorbitol
L-Sorbose
00051 10/12/23
(c) Kanehisa Laboratories

Cont.

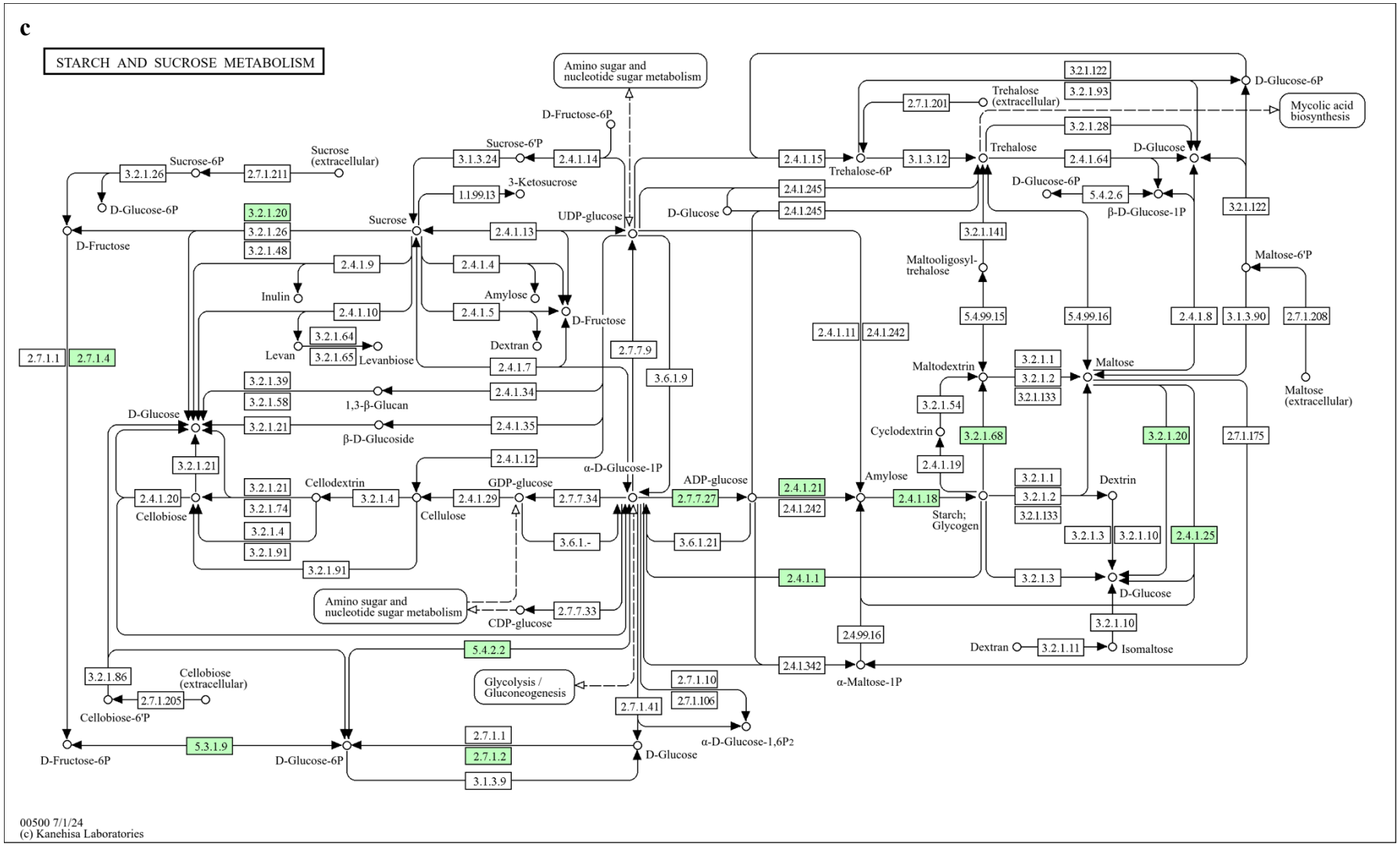
c
STARCH AND SUCROSE METABOLISM
Amino sugar and nucleotide sugar metabolism
D-Fructose-6P
Sucrose-6'P
Sucrose (extracellular)
Sucrose-6P
Sucrose
3-Ketosucrose
UDP-glucose
D-Glucose-6P
D-Fructose
Inulin
Amylose
Levan
Levanbiose
Dextran
D-Fructose
D-Glucose
1,3-β-Glucan
β-D-Glucoside
α-D-Glucose-1P
Cellodextrin
GDP-glucose
ADP-glucose
Cellobiose
Cellulose
Amino sugar and nucleotide sugar metabolism
CDP-glucose
Trehalose (extracellular)
Trehalose
Trehalose-6P
D-Glucose-6P
β-D-Glucose-1P
Mycolic acid biosynthesis
Maltooligosyl-trehalose
Maltose-6'P
Maltodextrin
Maltose
Maltose (extracellular)
Cyclodextrin
Amylose
Dextrin
Starch; Glycogen
D-Glucose
Dextran
Isomaltose
α-Maltose-1P
Glycolysis / Gluconeogenesis
α-D-Glucose-1,6P2
Cellobiose (extracellular)
Cellobiose-6'P
D-Fructose-6P
D-Glucose-6P
D-Glucose
00500 7/1/24
(c) Kanehisa Laboratories

Cont.

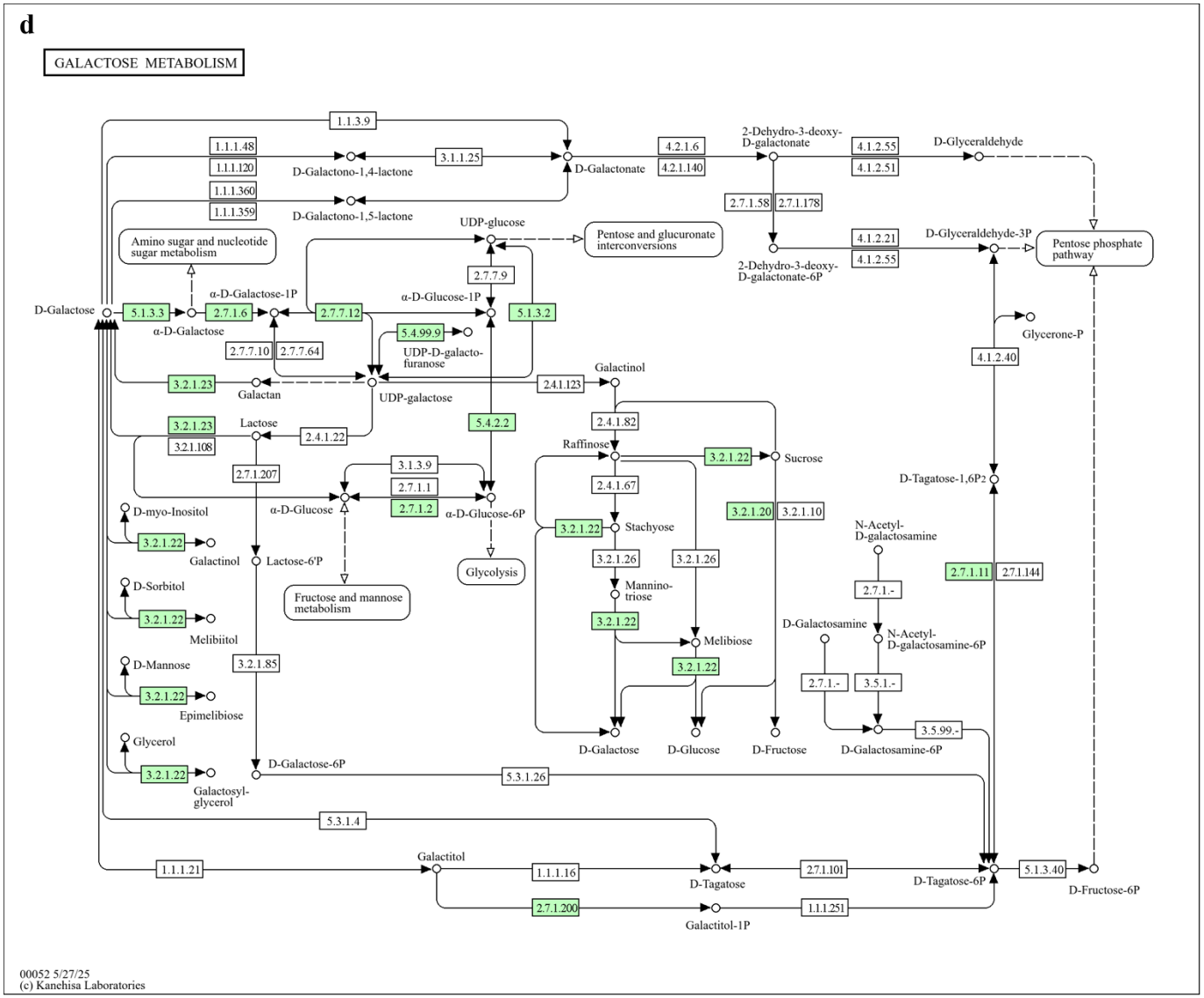
d
GALACTOSE METABOLISM
1.1.3.9
1.1.1.48
1.1.1.120
1.1.1.360
1.1.1.359
D-Galactono-1,4-lactone
3.1.1.25
D-Galactonate
4.2.1.6
4.2.1.140
2-Dehydro-3-deoxy-D-galactonate
4.1.2.55
4.1.2.51
D-Glyceraldehyde
D-Galactono-1,5-lactone
2.7.1.58
2.7.1.178
UDP-glucose
Amino sugar and nucleotide sugar metabolism
Pentose and glucuronate interconversions
4.1.2.21
4.1.2.55
D-Glyceraldehyde-3P
Pentose phosphate pathway
2-Dehydro-3-deoxy-D-galactonate-6P
2.7.7.9
α-D-Galactose-1P
α-D-Glucose-1P
D-Galactose
5.1.3.3
2.7.1.6
2.7.7.12
5.1.3.2
α-D-Galactose
5.4.99.9
Glycerone-P
2.7.7.10
2.7.7.64
UDP-D-galacto-furanose
4.1.2.40
Galactinol
3.2.1.23
Galactan
UDP-galactose
2.4.1.123
3.2.1.23
Lactose
2.4.1.22
5.4.2.2
2.4.1.82
3.2.1.08
Raffinose
3.2.1.22
Sucrose
3.1.3.9
2.7.1.207
2.7.1.1
D-Tagatose-1,6P2
2.4.1.67
D-myo-Inositol
α-D-Glucose
2.7.1.2
α-D-Glucose-6P
3.2.1.20
3.2.1.10
3.2.1.22
Stachyose
N-Acetyl-D-galactosamine
Galactinol
Lactose-6'P
Glycolysis
3.2.1.26
3.2.1.26
2.7.1.11
2.7.1.144
D-Sorbitol
Fructose and mannose metabolism
Mannino-triose
2.7.1.-
3.2.1.22
D-Galactosamine
Melibiitol
Melibiose
N-Acetyl-D-galactosamine-6P
D-Mannose
3.2.1.85
3.2.1.22
2.7.1.-
3.5.1.-
3.2.1.22
Epimelibiose
3.5.99.-
Glycerol
D-Galactose
D-Glucose
D-Fructose
D-Galactosamine-6P
D-Galactose-6P
5.3.1.26
3.2.1.22
Galactosyl-glycerol
5.3.1.4
Galactitol
1.1.1.21
1.1.1.16
2.7.1.101
5.1.3.40
D-Tagatose
D-Tagatose-6P
D-Fructose-6P
2.7.1.200
1.1.1.251
Galactitol-1P
00052 5/27/25
(c) Kanehisa Laboratories

Cont.

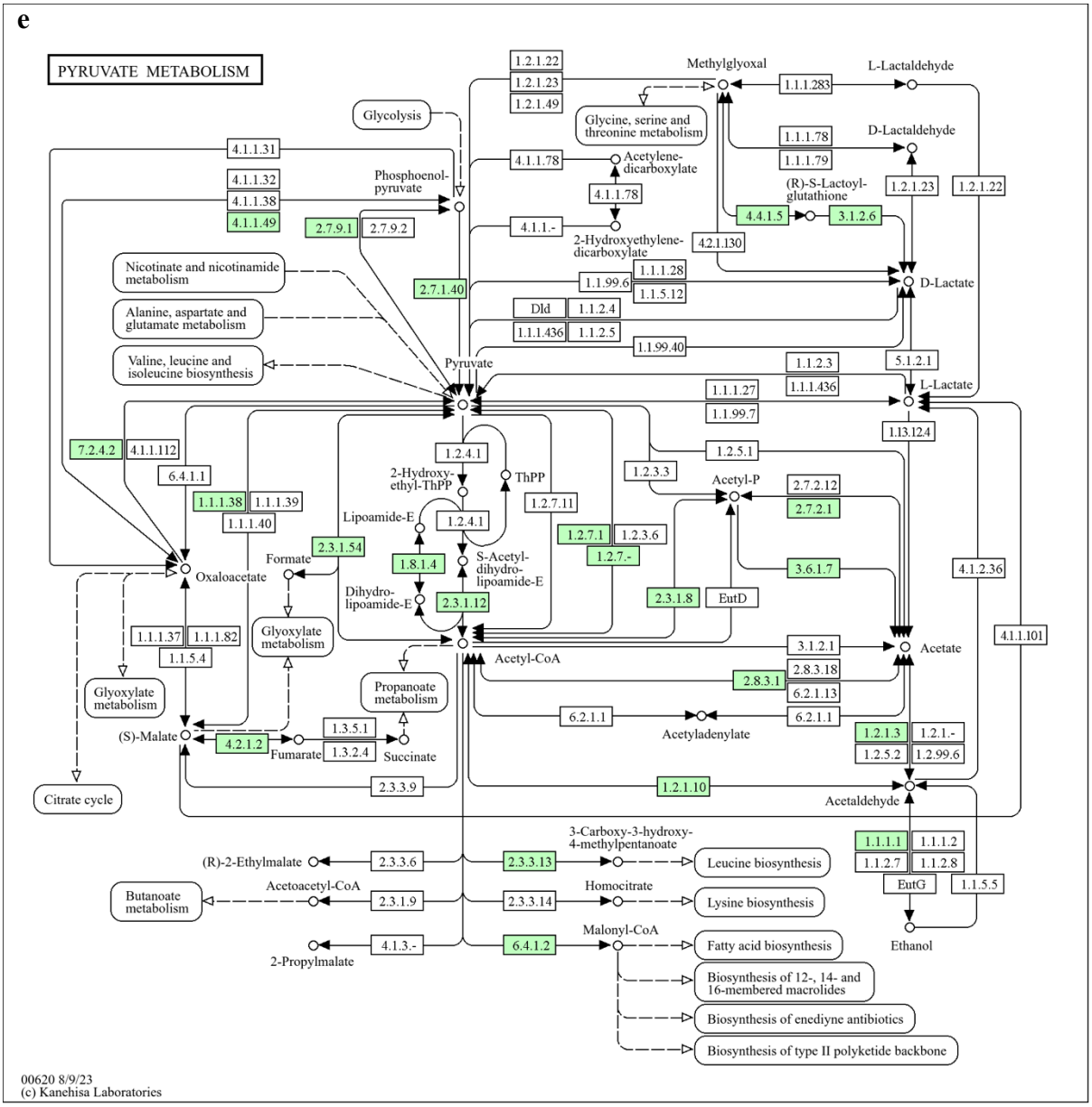

Figure 3-8. Metabolic reconstruction of carbohydrate utilization of *Dorea ammoniilytica* JCM 34808^T

Carbohydrate metabolism pathwyas of *Dorea ammoniilytica* JCM 34808^T were constructed from genome annotation. Key metabolic routes shown in the panels: (**a**) glycolysis, (**b**) glucose and mannose metabolism, (**c**) starch and sucrose metabolism, (**d**) galactose metabolism, and (**e**) pyruvate metabolism. Adapted from Kastawa *et al*. 2025.

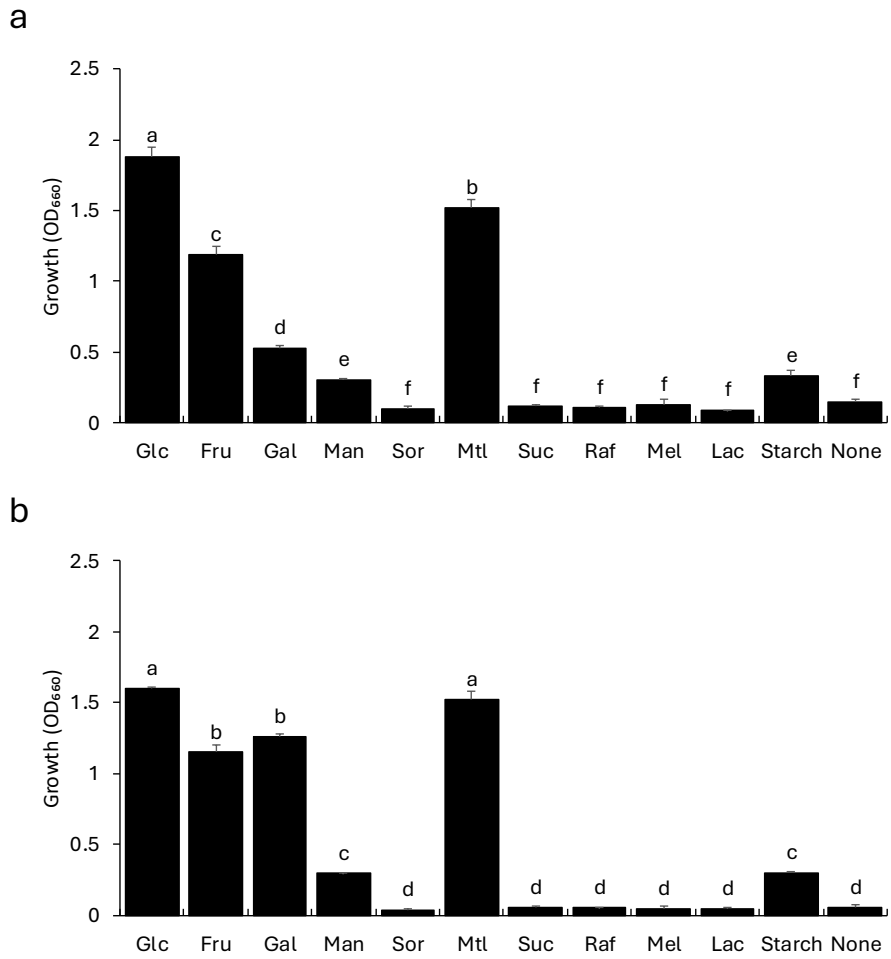

Figure 3-9. Growth of *Dorea ammoniilytica* JCM 34808^T and *Ruminococcus* sp. JCM 18685 in GAM-based medium supplemented with various carbohydrates as a sole carbohydrate source.

D. ammoniilytica JCM 34808^T (a) and *Ruminococcus* sp. JCM 18685 (b) were cultured anaerobically at 37°C in GAM Semisolid without Dextrose medium (agar was removed) containing each sole carbohydrate source for 24 h (black bars). Bars show mean OD_{660} ± standard deviation from three biological replicates. Letters above bars (a-f) indicate statistically significant differences by Tukey-Kramer post-hoc test following one-way ANOVA ($p < 0.05$); bars sharing the same letter are not significantly different. Abbreviations: Glc, D-glucose; Fru, D-fructose; Gal, D-galactose; Man, D-mannose; Sor, D-sorbitol; Mtl, D-mannitol; Suc, sucrose; Raf, raffinose; Mel, melibiose; Lac, lactose; Starch, soluble starch; None, no carbohydrate added. Adapted from Kastawa *et al*. 2025.

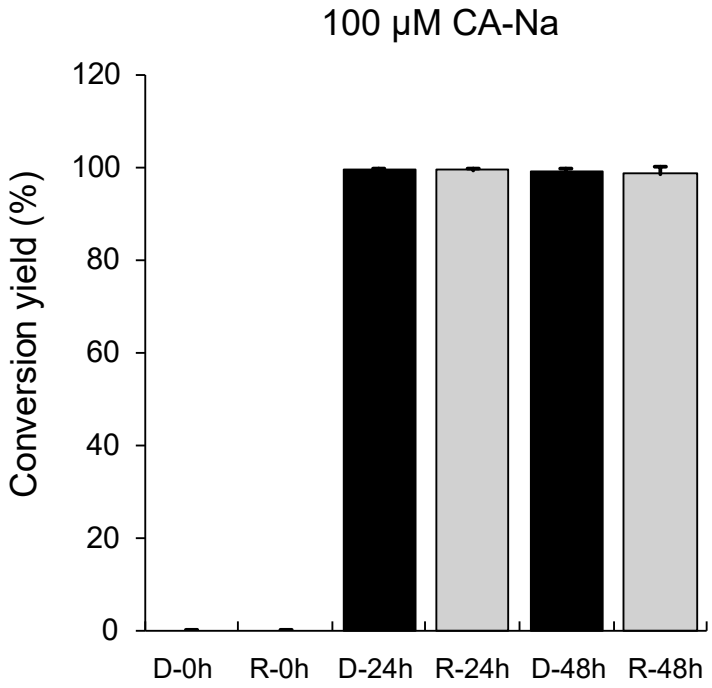

Figure 3-10. DCA production activity of *Dorea ammoniilytica* JCM 34808^T and *Ruminococcus* sp. JCM 18685 in PYG medium

DCA production activity by *Dorea ammoniilytica* JCM 34808^T (D, black bars) and *Ruminococcus* sp. JCM 18685 (R, gray bars). Strains were cultured in the same conditions used in the previous report of Dorea sp. (Bai *et al*. 2022): PYG medium supplemented with 100 μM CA-Na as a substrate at 37°C for 24 to 48 h. Quantification of BAs extracted from the culture was conducted by using LC-MS. Adapted from Kastawa *et al*. 2025.

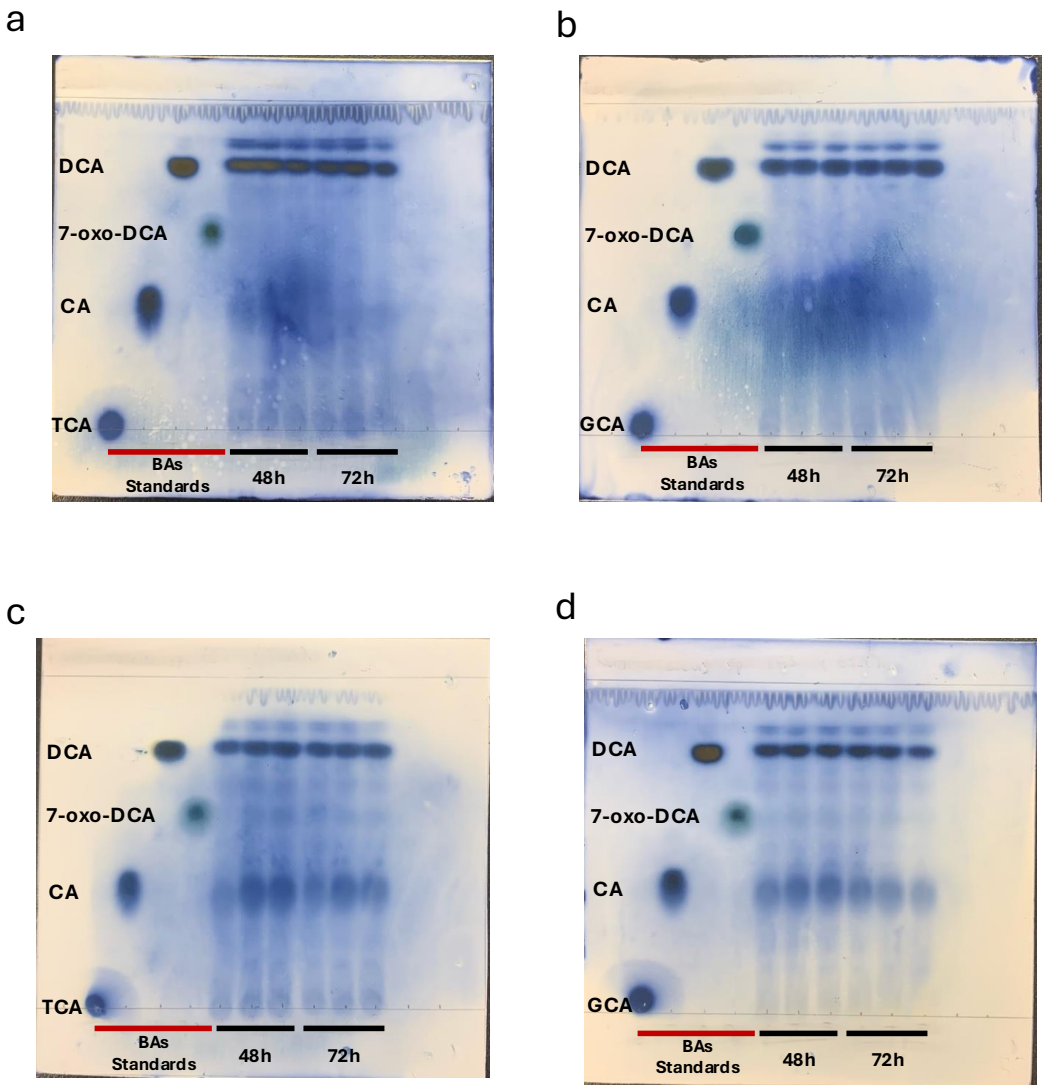

Figure 3-11. Evaluation of the conversion of conjugated BAs (TCA or GCA) to DCA.

Dorea ammoniilytica JCM 34808T (a and b) and *Ruminococcus* sp. JCM 18685 (c and d) were cultured anaerobically at 37°C for 72 h in GAM medium with 1 mM of TCA (a and c) or GCA (b and d) as a substrate (n = 3). BAs were extracted from 48 h and 72 h cultured samples. BA conversion was analyzed by TLC using TCA, GCA, CA, 7-oxo-DCA, and DCA as standards. Adapted from Kastawa *et al*. 2025.

Chapter IV. General Discussion

General discussion

This study successfully established a functional screening framework to identify DCA-producing bacterial communities from human fecal samples, providing direct insight into microbial contributors to DCA production. Moreover, *Dorea ammoniilytica* was identified and characterized as a novel DCA-producing bacteria. This finding substantially expands current knowledge of the diversity of DCA-producing bacteria in the human gut and highlights the importance of exploring undercharacterized microbial taxa in DCA production.

1. Screening of DCA-producing bacteria

DCA, produced through microbial biotransformation in the human intestine, plays significant roles in host physiology, metabolic regulation, and disease. Its formation depends on the presence and activity of specific gut bacteria capable of 7α-dehydroxylation. Despite the recognized importance of this pathway, the diversity of DCA-producing bacteria within the complex gut microbiota remains incompletely understood.

Screening for DCA-producing bacteria in human fecal samples represents a critical step toward identifying the microbial contributors responsible for DCA formation and understanding how this function is maintained under varying ecological conditions. In this study, fecal culture-based approaches were combined with dilution of the microbial community to intentionally reduce population density, thereby increasing the likelihood of detecting DCA-producing bacteria.

In this study, fecal culture analyses revealed considerable variability in DCA production activity among samples from different donors. Some cultures consistently maintained DCA production across serial dilutions, whereas others exhibited diminished or complete loss of activity, indicating that DCA production may depend on donor-specific microbiota structure, including the presence of key taxa. These observations suggest that host-related factors such

as diet, BA pool composition, gut transit time, and prior environmental exposures further influence microbial BA metabolism (Yokota *et al*. 2012; Zheng *et al*. 2017; Hillman *et al*. 2025; Watanabe *et al*. 2025).

Serial dilution of fecal cultures was employed to reduce bacterial population density, allowing identification of DCA-producing bacteria at different cell concentrations. This approach facilitated the identification of ASVs specifically associated with DCA production and enable a more precise comparison between DCA positive and DCA negative cultures. Both fecal and diluted cell cultures were subsequently assessed for their ability to produce DCA (**Table 2-2, Figure 2-3**).

Notably, not all diluted cell cultures retained the ability to produce DCA (**Figure 2-3**). Some cultures maintained DCA production across dilution steps, whereas others progressively lost this capability, suggesting that DCA production depends on the presence of specific bacterial taxa required to sustain this production. Based on this observation, cultures were categorized as DCA-positive and DCA-negative, allowing direct comparison between metabolically active and inactive communities. To investigate the bacterial composition responsible to DCA production, 16S rRNA gene amplicon sequencing was performed on both DCA-positive and DCA-negative cultures. This analysis characterized community structure, identified dominant taxa, and examined compositional differences associated with DCA-producing capability.

Clear differences were observed between the two culture types. At the genus level, several taxa including *Paraeggerthella, Lachnoclostridium, Fusicatenibacter, Escherichia-Shigella, Erysipelatoclostridium, Enterococcus, Dorea, Blautia, Bifidobacterium, Bacteroides*, and multiple uncultured groups were detected in DCA positive culture, whereas other taxa were more prevalent or uniquely detected in DCA-negative cultures (**Figure 2-6**). Species-level analysis revealed that none of the previously characterized DCA-producing bacterial species

were detected in the sequenced samples (**Table 2-5**). The absence of known DCA producers suggests that alternative microbial contributors may be responsible for DCA production in these cultures.

Members of the genus *Dorea* have previously been reported as DCA-producing bacteria; however, their activity has not been characterized at the species level (Bai *et al*. 2022). In the screening study, ASV_44 was detected exclusively in the DCA-positive culture and was annotated by BLASTn as *Dorea ammoniilytica* and *Ruminococcus* sp. 653 (**Table 2-5**). The detection of this ASV only in the DCA-positive culture highlights a specific association between these taxa and DCA production under the experimental conditions used. These findings provide candidate bacterial species for further investigation into their roles in secondary BA metabolism in the human gut.

These screening results support the hypothesis that DCA production in the human gut is not exclusively driven by a small number of well-characterized bacterial species but may involve a broader and more diverse group of microbial contributors (Vital *et al*. 2019). Collectively, this work contributes to expanding the conceptual understanding of BA metabolism by providing a methodology for the screening and identification of novel DCA-producing bacteria within the human gut microbiome.

2. Identification and characterization of novel DCA-producing bacteria

DCA is produced via the microbial 7α-dehydroxylation by a multi-step biochemical pathway encoded by the *bai* operon. Although several bacterial species have been identified as DCA producers, the diversity, ecological distribution of DCA-producing bacteria within the gut microbiota remain incompletely understood.

Previous studies have largely focused on a limited number of well-characterized of known DCA-producing bacteria, leading to the assumption that DCA production is limited to a narrow

phylogenetic group. However, more evidence suggests that gut microbial functions may be more widely distributed across taxonomic boundaries than previously recognized. For example, metagenomic or metatranscriptomic datasets have detected *bai* gene clusters in the majority of individuals, yet these genes are carried by only a small fraction of total intestinal bacteria (<1%), with most reads assigned to uncultivated members of the order Clostridiales, such as Firmicutes bacterium CAG:103. Only minor fractions of *bai*-associated sequences were linked to Lachnospiraceae (4.7%) and Peptostreptococcaceae (1.9%), which include the previously described DCA producers (Vital *et al*. 2019) . Therefore, identifying novel DCA-producing bacteria and clarifying their ecological behavior is essential for advancing the current understanding of BA metabolism in the human gut.

Diluted cell culture and microbial composition analyses, in Chapter 2, have revealed sequences related to *Dorea* genus, *D. ammoniilytica* (ASV_44; **Table 2-5**) was detected only in DCA-positive cultures, highlighting potential uncharacterized contributors to DCA production. Notably, ASV_44 also showed high similarity to *Ruminococcus* sp. 653, suggesting a phylogenetic relationship between these taxa. Based on these observation, *D. ammoniilytica* and *Ruminococcus* sp. 653 was selected for further investigation as a candidate novel DCA-producing bacterium based on its genomic features and functional potential. *D. ammoniilytica* harbors a *bai* operon structure highly similar to that of *Eubacterium* sp. c-25, which has been reclassified as *Cla.bilis*, a known DCA producer (Song *et al*. 2022; Hisatomi *et al*. 2023). This similarity suggested that *D. ammoniilytica* may possess functional 7α-dehydroxylation capability despite not being previously recognized as a DCA producer. To further clarify its taxonomic and ecological relevance, 16S rRNA gene sequence analysis was performed. This analysis revealed that *D. ammoniilytica* is closely related to *Ruminococcus* sp. 653, and this bacterium has not been previously characterized (**Table 3-2**). Prior to this study, no genomic, functional, or metabolic information was available for these strain. Based on its

phylogenetic proximity to *D. ammoniilytica*, its detection in DCA-producing cultures, and the absence of prior characterization, *Ruminococcus* sp. 653 was selected as a second candidate DCA-producing bacterium.

BA conversion analysis revealed that *D. ammoniilytica* exhibited near-complete conversion of CA to DCA, with conversion yields rates approaching ~100%. This level of activity was notably higher than that observed in several previously characterized DCA-producing bacteria under comparable culture conditions. Similarly, *Ruminococcus* sp. 653 demonstrated robust DCA-producing capability, indicating that both organisms possess highly efficient 7α-dehydroxylating pathway. DCA production by D. ammoniilytica and *Ruminococcus* sp. 653 was also compared with previously reported Dorea strains. In PYG medium, both candidate strains yielding nearly ~100% of DCA within 48 hours. In contrast, earlier studies reported that other *Dorea* strains exhibited markedly lower DCA production, achieving only approximately ~5% conversion under similar conditions (Bai *et al*. 2022).

Phylogenetic analysis revealed that *D. ammoniilytica, Ruminococcus* sp. 653, and related *Dorea* strains clustered within the same clade, suggesting close evolutionary relationships (**Figure 3-6**). To reveal their taxonomic assignment, whole-genome comparisons were conducted using ANI analysis. The ANI values among *D. ammoniilytica, Ruminococcus* sp. 653, and *Dorea* strains were slightly above the accepted species threshold (≥95%), indicating that these strains likely represent the same species (**Figure 3-7**). In contrast, ANI values between these strains and known DCA producers were substantially below the species threshold, confirming that they are genetically distinct from previously known DCA-producing taxa (**Figure 3-7**). This finding challenges the assumption that DCA production is restricted to a limited community of bacterial species and highlights the importance of genome-based functional prediction combined with experimental validation.

To determine whether differences in DCA-producing capacity could be associated to structural variation in *bai* genes, comparative analysis of Bai protein amino acid sequences was performed. The results revealed amino acid identity among *D. ammoniilytica*, *Ruminococcus* sp. 653, and *Dorea* strains were above 99% (**Table 3-5**). This high degree of conservation indicates that variation in DCA production is unlikely to result from differences in Bai protein structure alone. These findings suggest that regulatory mechanisms and gene expression levels may play a critical role in determining functional output.

Further genomic analysis revealed that both *D. ammoniilytica* and *Ruminococcus* sp. 653 possess bsh gene, an enzyme responsible for deconjugating conjugated BAs. This capability is particularly relevant in the intestinal environment, where BAs are predominantly present in conjugated forms (Yang *et al*. 2023). Experimental validation using TLC demonstrated that both strains were capable of producing DCA from conjugated BA substrates such as TCA and GCA (**Figure 3-10**). These results indicate that these bacteria can perform both BA deconjugation and subsequent 7α-dehydroxylation, enabling efficient DCA production under physiologically relevant conditions.

Collectively, this study provides the first genomic and functional characterization of D. ammoniilytica as a novel DCA-producing bacteria. These findings significantly expand the known diversity of DCA-producing bacteria.

3. Significance of this study in human gut microbiota research

The identification and characterization of *D. ammoniilytica* from human feces represents a paradigm shifts in gut microbiota research, offering insights that extend well beyond the secondary BA metabolism. While this study primary breakthrough is the identification of *D. ammoniilytica* as a novel and potent producer of DCA, its broader

contribution lies in redefining the functional role of the *Dorea* genus within the complex intestinal ecosystem.

Historically, the conversion of CA to DCA via 7α-dehydroxylation was thought to be the domain of a highly specialized and limited group of bacteria such as *C. scindens* (Morris *et al*. 1985; Tawthep *et al*. 2017; Devendran *et al*. 2019), *P. hiranonis* (Kitahara *et al*. 2001; Chen *et al*. 2020), *C. hylemonae* (Kitahara *et al*. 2000; Ridlon *et al*. 2010), *Dorea* spp. (Bai *et al*. 2022), and *Eubacterium* sp. c-25 (Song *et al*. 2021), which was recently classified as *Cla. bilis* (Hisatomi *et al*. 2023). This study fundamentally shifts that paradigm by demonstrating that high-activity 7α-dehydroxylation is phylogenetically more diverse, existing within a distinct lineage of the Lachnospiraceae family.

Beyond BA transformation, the presence of *D. ammoniilytica* has boarder implications for gut metabolic stability. Member of the Lachnospiraceae family, including *Dorea*, are known for their ability to ferment diverse carbohydrates and dietary fibers into essential short-chain fatty acids (SCFAs) (Peng *et al*. 2009; Lewis *et al*. 2010). These metabolites are critical for maintaining the integrity of the intestinal barrier, modulating the host immune system, and regulating peripheral energy metabolism (Luo *et al*. 2022; Liu *et al*. 2023). By characterizing D. ammoniilytica, this study provides a deeper understanding of how individual bacterial species contribute to metabolic network in the gut, shaping interaction and cross-feeding relationship that influence overall community resilience.

Furthermore, this study provides critical insights into the link between specific microbial taxa and chronic metabolic diseases. Elevated DCA levels has a carcinogenic effect on the liver and colon. Its high hydrophobicity makes it cytotoxic, inducing oxidative stress, membrane disruption, and DNA damage in intestinal epithelial cells. Chronic exposure to elevated DCA levels has been linked to the development of colorectal cancer (Cao *et al*. 2017; Cong *et al*. 2024) and hepatocellular carcinoma (Yoshimoto *et al*. 2013). Over recent decades,

it has become evident that aspect of the ‘western lifestyle’ including diets low in fiber and high processed carbohydrates and saturated fats, increased both the amount of bile entering the GI tract and the hydrophobicity of the BA pool. These changes affect host metabolic function and increase the risk to human health (Wahlström *et al*. 2016; Trauner and Fuchs, 2022). Conversely, some *Dorea* species have been linked to broader conditions such as obesity and inflammatory bowel disease (Alizadeh *et al*. 2025). By identifying *D. ammoniilytica*, researchers now have a specific biological model to experimentally assess how its metabolic activities, including DCA production, influence intestinal homeoastasis and contribute to metabolic or inflammatory disorders.

Finally, the characterization of *D. ammoniilytica* advances the development of precision microbiome therapeutics. Current interventions, such as probiotics or fecal microbiota transplants, often lack target specificity (Tegegne and Savidge 2025) . This research lays the foundation for "next-generation" live biotherapeutics, where *D. ammoniilytica* could be selectively promoted for its beneficial fermentation products or specifically inhibited to mitigate harmful DCA effects. Overall, the discovery of *D. ammoniilytica* does not only fill a gap in our knowledge of BA metabolism, but it also exemplifies how a single, low-abundance species can shape the gut ecosystem and influence host health.

Conclusion

This study establishes a functional screening strategy based on serial dilution of human fecal cultures as an effective approach for identifying DCA-producing bacteria within complex gut microbial communities. By progressively reducing community complexity while monitoring DCA production, this method facilitated the detection of uncharacterized bacterial species from genus Dorea named *Dorea ammoniilytica* in the DCA positive culture.

D. ammoniilytica was subsequently identified and characterized as a novel DCA-producing bacteria, exhibiting higher DCA-producing activity than previously described producers. These findings expand the known diversity of DCA-producing bacteria and highlights the contribution of previously uncharacterized gut microbes to secondary BA metabolism.

Future Perspectives

Future studies should aim to elucidate the regulatory and physiological mechanisms that enable *D. ammoniilytica* to produce high levels of DCA, including the *bai* gene expression and associated metabolic pathways. Co-culture and in vivo experiments will be important for clarifying the contributions of microbial interactions and host factors to DCA production. Extending dilution-based functional screening to larger and more diverse donors might reveal additional, previously unrecognized DCA-producing bacteria and help explain inter-individual differences in BA metabolism. Integrating functional screening with genome-level approaches will further enhance our understanding of how gut microbial activity shapes host physiology and contributes to health and disease.

Summary

Primary bile acids (BAs) are synthesized in the liver and secreted into the duodenum to facilitate dietary fat absorption. In the large intestine, these primary BAs (cholic acid, CA; chenodeoxycholic acid, CDCA) are converted into secondary BAs (deoxycholic acid, DCA; lithocholic acid, LCA) by gut bacteria. DCA is the most abundant BA in the human gut and is produced from CA via a multistep 7α-dehydroxylation pathway that removes the C7 hydroxy group. Elevated DCA concentrations induce gut microbiota dysbiosis and are involved in metabolic disorders such as fatty liver disease, as well as colon and liver cancer. Despite the importance of DCA in our health, DCA-producing bacteria are not fully characterized: to date, only a few species, such as *Clostridium scindens*, *Clostridium hylemonae*, *Peptacetobacter hiranonis*, and *Claveliimonas bilis,* have been characterized as human-derived DCA producers.

Recent metagenomic analyses of human gut microbiota revealed that bile acid-inducible (*bai*) genes, responsible for 7α-dehydroxylation, exist in different taxa not previously identified as DCA producers. This evidence suggests that additional, uncharacterized DCA-producing bacteria may exist in the human gut. Therefore, this study aimed to identify and characterize novel DCA-producing bacteria from human gut microbiota.

1. Screening of DCA-producing bacteria from human feces

Diluted human fecal suspensions (10^{-1} to 10^{-6}) were inoculated into GAM medium supplemented with 1 mM CA-Na and cultured to assess DCA production ability. Thin-layer chromatography and liquid chromatography-mass spectrometry analysis detected DCA production in all fecal dilutions after 72 hours of incubation. Viable cell counts of the DCA-positive fecal cultures were determined, and cultures containing 10^{7}-10^{4} cells were inoculated

into 96-well plates containing GAM and 1 mM CA-Na to evaluate their DCA-producing ability. DCA production was detected in wells containing 10^7-10^5 cells, and the most diluted positive population (10^5) and negative populations were selected for 16S rRNA amplicon sequencing to characterize their microbial composition. Among the 79 detected amplicon-sequence variants, ASV_44 accounted for ~1.13% of the community in the DCA-positive population, and its sequence matched those of the 16S rRNA genes of *Dorea ammoniilytica* and *Ruminococcus* sp. 653 (JCM 18685).

2. Identification and characterization of novel DCA-producing bacteria

D. ammoniilytica possessed *bai* genes in its draft genome, supporting that it is a DCA-producing bacterium. Therefore, both *D. ammoniilytica* JCM 34808^T and *Ruminococcus* sp. JCM 18685 were selected for comparative characterization. Whole-genome sequencing and comparative genomic analyses showed that both isolates contain complete *bai* gene operons, supporting their 7α-dehydroxylation ability. Both strains exhibited strong DCA and LCA production (~100%), clarifying their high secondary BA-producing ability. Average nucleotide identity analysis indicated that *D. ammoniilytica*, *Ruminococcus* sp. JCM 18685, and other *Dorea* sp. (AM58-8 and AF36-15AT) shares values slightly above the commonly accepted intra-species cutoff (≥95%), suggesting they belong to the same species, *D. ammoniilytica*. Phylogenetic analysis showed that the *D. ammoniilytica* clade was distinct from other known DCA-producing bacteria, suggesting that this lineage comprises previously uncharacterized DCA-producers. Metabolic profiling revealed that both strains can utilize simple sugars, D-mannitol, and starch, which further differentiates them from other known DCA-producing bacteria.

In conclusion, this study characterized *D. ammoniilytica* as a potent DCA-producing bacterium that is phylogenetically different from known DCA producers. These findings

expand the diversity of secondary bile acid-producing bacteria and reveal 7α-dehydroxylation capacity within the *D. ammoniilytica* lineage.

Acknowledgements

I am deeply grateful for the privilege of studying at Hokkaido University and for the opportunity to become part of the Laboratory of Microbial Physiology. My time at Hokkaido University has been truly meaningful, both academically and personally, and I am thankful for the supportive and inspiring environment it has provided. This journey has been made possible through the kindness, guidance, and encouragement of many people. I would like to extend my sincere thanks to:

- Dr. Satoru Fukiya, professor of the Laboratory of Microbial Physiology, is my research supervisor. I cannot thank him enough for welcoming me into this laboratory and giving me the chance to pursue my research under his supervision. His thoughtful mentorship, calm presence, and genuine kindness have shaped not only my scientific growth but also my confidence as a researcher. I will always be grateful for the trust he placed in me, especially during challenging moments, and for all the opportunities he gave me to complete this degree.

- Dr. Tomoya Maeda, associate professor of the Laboratory of Microbial Physiology, for his insightful guidance, constant encouragement, and continuous support throughout my research. His thoughtful advice and brilliant ideas helped me navigate complex challenges and strengthened my understanding throughout my studies.

- Dr. Satoshi Ishizuka, professor of the Laboratory of Food Biochemistry, for his time and valuable comments, and constructive suggestions in reviewing my thesis, which have helped improve the clarity and quality of my work.

- Dr. Yasuhiro Gotoh, I am deeply grateful for his tremendous support with the whole-genome sequence analysis. His technical expertise greatly contributed to the progress of my research.

- EXEX Doctoral Fellowship, Hokkaido University, for providing the financial support that allowed me to focus on my research and academic progress.

- Students and Graduates of the Laboratory of Microbial Physiology, who made every step of this journey warmer and more meaningful. Their willingness to share knowledge, offer help, and celebrate small achievements together transformed the laboratory into a place of comfort and optimism. I am sincerely grateful for every conversation, every shared challenge, and every moment of laughter.

- Indonesian community at Hokkaido University (especially Rinda and Yoan), whose constant help, solidarity, and encouragement carried me through both the bright days and the difficult ones. Their presence made life in a foreign country feel less distant and more like home. I cannot thank them enough for the countless forms of assistance that helped sustain me throughout these years.

- My family and friends in Indonesia, for their endless love, patience, and belief in my ability to complete this degree. Their support has been my most significant source of strength. I am forever grateful for their faith in me.

References

Alizadeh M, Wong U, Siaton BC *et al.* The intestinal mucosa-associated microbiota in IBD-associated arthritis displays lower relative abundance of *Roseburia intestinalis*. *Gut Microbes* 2025;**17**.

Bäckhed F, Ley RE, Sonnenburg JL *et al.* Host-Bacterial Mutualism in the Human Intestine. *Science* 2005;**307**:1915-1920.

Bai Y, Zhao T, Gao M *et al.* A Novel Gene Alignment in Dorea sp. AM58-8 Produces 7-Dehydroxy-3β Bile Acids from Primary Bile Acids. *Biochemistry* 2022;**61**:2870–8.

Bengmark S. Ecological control of the gastrointestinal tract. The role of probiotic flora. *Gut* 1998;**42**:2–7.

Bergstörm S, Danielsson H, Kazuno T. Bile Acids and Steroids 98. The metabolism of bile acids in python and constrictor snakes. *The Journal of Biological Chemistry* 1960;**235**(4):983-988.

Bortolini O, Medici A, Poli S. Biotransformations On Steroid Nucleus of Bile Acids. *Steroids* 1997;**62**:564-577.

Cao H, Xu M, Dong W *et al.* Secondary bile acid-induced dysbiosis promotes intestinal carcinogenesis. *Int J Cancer* 2017;**140**:2545–56.

Chen B. Bai Y. Tong F *et al.* Glycoursodeoxycholic acid regulates bile acids level and alters gut microbiota and glycolipid metabolism to attenuate diabetes. *Gut Microbes* 2023;**15**(1):2192155.

Chen XJ, Wang ZQ, Zhou ZY *et al.* Characterization of *Peptacetobacter hominis* gen. nov., sp. nov., isolated from human faeces, and proposal for the reclassification of

Clostridium hiranonis within the genus *Peptacetobacter*. *Int J Syst Evol Microbiol* 2020;**70**:2988–97.

Chiang JYL, Ferrell JM. Bile acid metabolism in liver pathobiology. *Gene Expr* 2018;**18**:71–87.

Chiang JYL, Ferrell JM. Bile Acids as Metabolic Regulators and Nutrient Sensors. Annu. Rev. Nutr. 2019;**39**:175–200.

Chuan J, Zhou A, Hale LR *et al.* Atria: An Ultra-fast and Accurate Trimmer for Adapter and Quality Trimming. *Gigabyte* 2021:1-18.

Coleman JP, Hudson LL. Cloning and Characterization of a Conjugated Bile Acid Hydrolase Gene from Clostridium Perfringens. *Appl. Environ. Microbiol* 1995:2514-2520.

Cong J, Liu P, Han Z *et al.* Bile acids modified by the intestinal microbiota promote colorectal cancer growth by suppressing CD8+ T cell effector functions. *Immunity* 2024;**57**:876-889.e11.

David LA, Maurice CF, Carmody RN *et al.* Diet rapidly and reproducibly alters the human gut microbiome. *Nature* 2014;**505**:559–63.

De Aguiar Vallim TQ, Tarling EJ, Edwards PA. Pleiotropic roles of bile acids in metabolism. *Cell Metab* 2013;**17**:657–69.

Devendran S, Shrestha R, Alves JMP *et al. Clostridium scindens* ATCC 35704: Integration of Nutritional Requirements, the Complete Genome Sequence, and Global Transcriptional Responses to Bile Acids. *Apl. Environ. Microbiol*. 2019;**85**:e00052-19.

Devlin AS, Fischbach MA. A biosynthetic pathway for a prominent class of microbiota-derived bile acids. *Nat Chem Biol* 2015;**11**:685–90.

Di Ciaula A, Garruti G, Baccetto RL *et al.* Bile acid physiology. *Ann Hepatol* 2017;**16**:s4–14.

Fukiya S, Arata M, Kawashima H *et al.* Conversion of cholic acid and chenodeoxycholic acid into their 7-oxo derivatives by *Bacteroides intestinalis* AM-1 isolated from human feces. *FEMS Microbiol Lett* 2009;**293**:263–70.

Funabashi M, Grove TL, Wang M *et al.* A metabolic pathway for bile acid dehydroxylation by the gut microbiome. *Nature* 2020;**582**:566–70.

Garidel P, Hildebrand A, Knauf K *et al.* Membranolytic Activity of Bile Salts: Influence of Biological Membrane Properties and Composition. *Molecules* 2007;**12**:2292–326.

Goris J, Konstantinidis KT, Klappenbach JA *et al.* DNA-DNA hybridization values and their relationship to whole-genome sequence similarities. *Int J Syst Evol Microbiol* 2007;**57**:81–91.

Hardison WGM. Hepatic taurine concentration and dietary taurine as regulators of bile acid conjugation with taurine. *Gastroenterology* 1978;**75**:71-75.

Heuman DM, Hylemon PB, Vlahcwic ZR. Regulation of Bile Acid Synthesis. 111. Correlation between Biliary Bile Salt Hydrophobicity Index and the Activities of Enzymes Regulating Cholesterol and Bile Acid Synthesis in the Rat. *Journal of Lipid Research* 1989;**30**:1161-1171.

Hillman EBM, Baumgartner M, Carson D *et al.* Changing Gastrointestinal Transit Time Alters Microbiome Composition and Bile Acid Metabolism: A Cross-Over Study in Healthy Volunteers. *Neurogastroenterology and Motility* 2025;**37**.

Hisatomi A, Kastawa NWEPG, Song I *et al. Claveliimonas bilis* gen. nov., sp. nov., deoxycholic acid-producing bacteria isolated from human faeces, and reclassification of Sellimonas monacensis Zenner et al. 2021 as *Claveliimonas monacensis* comb. nov. *Int J Syst Evol Microbiol* 2023;**73**.

Hitch TCA, Riedel T, Oren A *et al.* Automated analysis of genomic sequences facilitates high-throughput and comprehensive description of bacteria. *ISME Communications* 2021;**1**.

Islam KBMS, Fukiya S, Hagio M *et al.* Bile acid is a host factor that regulates the composition of the cecal microbiota in rats. *Gastroenterology* 2011;**141**:1773–81.

Jain C, Rodriguez-R LM, Phillippy AM *et al.* High throughput ANI analysis of 90K prokaryotic genomes reveals clear species boundaries. *Nat Commun* 2018;**9**.

Jalil A, Perino A, Dong Y *et al.* Bile acid 7α-dehydroxylating bacteria accelerate injury-induced mucosal healing in the colon. *EMBO Mol Med* 2025;**17**:889–908.

Kanehisa M, Sato Y, Morishima K. BlastKOALA and GhostKOALA: KEGG Tools for Functional Characterization of Genome and Metagenome Sequences. *J Mol Biol* 2016;**428**:726–31.

Kanehisa M, Sato Y. KEGG Mapper for inferring cellular functions from protein sequences. *Protein Science* 2020;**29**:28–35.

Kang JD, Myers CJ, Harris SC *et al.* Bile Acid 7α-Dehydroxylating Gut Bacteria Secrete Antibiotics that Inhibit Clostridium difficile: Role of Secondary Bile Acids. *Cell Chem Biol* 2019;**26**:27-34.e4.

Kastawa NWEPG, Gotoh Y, Song I *et al.* Identification and characterization of *Dorea ammoniilytica* as a novel deoxycholic acid-producing bacterial species in the human gut microbiota. *Biosci Biotechnol Biochem* 2025, DOI: https://doi.org/10.1093/bbb/zbaf190.

Kim GB, Miyamoto CM, Meighen EA *et al.* Cloning and characterization of the bile salt hydrolase genes (bsh) from *Bifidobacterium bifidum* strains. *Appl Environ Microbiol* 2004;**70**:5603–12.

Kim KH, Park D, Jia B *et al.* Identification and Characterization of Major Bile Acid 7α-Dehydroxylating Bacteria in the Human Gut. *mSystems* 2022;**7**.

Kitahara M, Sakata S, Sakamoto M *et al.* Comparison among fecal secondary bile acid levels, fecal microbiota and Clostridium scindens cell numbers in Japanese. *Microbiol Immunol* 2004;**48**:367–75.

Kitahara M, Takamine F, Imamura T *et al.* Assignment of *Eubacterium* sp. VPI 12708 and related strains with high bile acid 7α- dehydroxylating activity to *Clostridium scindens* and proposal of *Clostridium hylemonae* sp. nov., isolated from human faeces. *Int J Syst Evol Microbiol* 2000;**50**:971–8.

Kitahara M, Takamine F, Imamura T *et al. Clostridium hiranonis* sp. nov., a Human Intestinal Bacterium with Bile Acid 7α-Dehydroxylating Activity. *Int. J. Sys. Evol. Microbiol* 2001;**51**:39-44.

Kurdi P, Kawanishi K, Mizutani K *et al.* Mechanism of growth inhibition by free bile acids in Lactobacilli and Bifidobacteria. *J Bacteriol* 2006;**188**:1979–86.

Lee JY, Arai H, Nakamura Y *et al.* Contribution of the 7β-hydroxysteroid dehydrogenase from *Ruminococcus gnavus* N53 to ursodeoxycholic acid formation in the human colon. *J Lipid Res* 2013;**54**:3062–9.

Lefebvre P, Cariou B, Lien F *et al.* Role of Bile Acids and Bile Acid Receptors in Metabolic Regulation. Physiol. Rev. 2009;**89**:147-197.

Lewis K, Lutgendorff F, Phan V *et al.* Enhanced translocation of bacteria across metabolically stressed epithelia is reduced by butyrate. *Inflamm Bowel Dis* 2010;**16**:1138–48.

Liu XF, Shao JH, Liao YT *et al.* Regulation of short-chain fatty acids in the immune system. *Front Immunol* 2023;**14**.

Luo P, Lednovich K, Xu K *et al.* Central and peripheral regulations mediated by short-chain fatty acids on energy homeostasis. *Translational Research* 2022;**248**:128–50.

Macdonald IA, Jellett JF, Mahony ED. *et al.* Bile Salt 3a-and 12a-Hydroxysteroid Dehydrogenases from *Eubacterium lentum* and Related Organisms. App. Environ. Microbiol 1979:991-1000.

Martin G, Kolida S, Marchesi JR *et al.* In vitro modeling of bile acid processing by the human fecal microbiota. *Front Microbiol* 2018;**9**.

Matsuoka K, Moroi Y. Micelle Formation of Sodium Deoxycholate and Sodium Ursodeoxycholate (Part 1). Biochimica et Biophysica Acta 2002;**1580**:189-199.

Modica S, Gadaleta RM, Moschetta A. Deciphering the nuclear bile acid receptor FXR paradigm. *Nucl Recept Signal* 2010;**8**.

Monte MJ, Marin JJG, Antelo A *et al.* Bile acids: Chemistry, physiology, and pathophysiology. *World J Gastroenterol* 2009;**15**:804–16.

Morris GN, Winter J, Cato EP *et al. Clostridium scindens* sp. Nov., a Human Intestinal Bacterium with Desmolytic Activity on Corticoids. *Int. J. Syst. Bact* 1985:478-481.

Murigneux V, Roberts LW, Forde BM *et al.* MicroPIPE: validating an end-to-end workflow for high-quality complete bacterial genome construction. *BMC Genomics* 2021;**22**.

Nishimura Y, Yamada K, Okazaki Y *et al.* DiGAlign: Versatile and Interactive Visualization of Sequence Alignment for Comparative Genomics. *Microbes Environ* 2024;**39**.

Peng L, Li ZR, Green RS *et al.* Butyrate enhances the intestinal barrier by facilitating tight junction assembly via activation of AMP-activated protein kinase in Caco-2 cell monolayers. *Journal of Nutrition* 2009;**139**:1619–25.

Rasmussen TS, Streidl T, Hitch TCA *et al. Sporofaciens musculi* gen. nov., sp. nov., a novel bacterium isolated from the caecum of an obese mouse. *Int J Syst Evol Microbiol* 2021;**71**.

Richter M, Rosselló-Móra R, Oliver Glöckner F *et al.* JSpeciesWS: A web server for prokaryotic species circumscription based on pairwise genome comparison. *Bioinformatics* 2016;**32**:929–31.

Ridlon JM, Bajaj JS. The human gut sterolbiome: Bile acid-microbiome endocrine aspects and therapeutics. *Acta Pharm Sin B* 2015;**5**:99–105.

Ridlon JM, Daniel SL, Gaskins HR. The Hylemon-Björkhem pathway of bile acid 7-dehydroxylation: history, biochemistry, and microbiology. *J Lipid Res* 2023;**64**.

Ridlon JM, Harris SC, Bhowmik S *et al.* Consequences of bile salt biotransformations by intestinal bacteria. *Gut Microbes* 2016;**7**:22–39.

Ridlon JM, Kang DJ, Hylemon PB. Bile salt biotransformations by human intestinal bacteria. *J Lipid Res* 2006;**47**:241–59.

Ridlon JM, Kang DJ, Hylemon PB. Isolation and characterization of a bile acid inducible 7α-dehydroxylating operon in *Clostridium hylemonae* TN271. *Anaerobe* 2010;**16**:137–46.

Russell DW. The enzymes, regulation, and genetics of bile acid synthesis. *Annu Rev Biochem* 2003;**72**:137–74.

Sjövall J. Fifty years with bile acids and steroids in health and disease. *Lipids* 2004;39:703-22..

Solovyev V, Salamov A. *Automatic Annotation of Microbial Genomes and Metagenomic Sequences. In Metagenomics and Its Applications in Agriculture, Biomedicine and Environmental Studies*. Robert W, Li (eds.). Nova Science Publisher, 2011.

Song I, Gotoh Y, Ogura Y *et al.* Comparative genomic and physiological analysis against clostridium scindens reveals *Eubacterium* sp. C-25 as an atypical deoxycholic acid producer of the human gut microbiota. *Microorganisms* 2021;**9**.

Tamura K, Nei M. Estimation of the Number of Nucleotide Substitutions in the Control Region of Mitochondrial DNA in Humans and Chimpanzees. *Mol Biol Evol* 1993;**10**:512-26. https://doi.org/10.1093/oxfordjournals.molbev.a040023.

Tamura K, Stecher G, Kumar S. MEGA11: Molecular Evolutionary Genetics Analysis Version 11. *Mol Biol Evol* 2021;**38**:3022–7.

Tanaka H, Hashiba H, Kok J *et al.* Bile Salt Hydrolase of *Bifidobacterium longum*-Biochemical and Genetic Characterization. *App. Environ. Microbiol* 2000:2502-2512.

Tanizawa Y, Fujisawa T, Nakamura Y. DFAST: A flexible prokaryotic genome annotation pipeline for faster genome publication. *Bioinformatics* 2018;**34**:1037–9.

Taras D, Simmering R, Collin MD *et al.* Reclassification of Eubacterium formicigenerans Holdeman and Moore 1974 as Dorea formicigenerans gen. nov., comb. nov., and description of Dorea longicatena sp. nov., isolated from human faeces. *Int J Syst Evol Microbiol* 2002;**52**:423–8.

Tawthep S, Fukiya S, Lee JY *et al.* Isolation of six novel 7-oxo- or urso-type secondary bile acid-producing bacteria from rat cecal contents. *J Biosci Bioeng* 2017;**124**:514–22.

Tegegne HA, Savidge TC. Gut microbiome metagenomics in clinical practice: bridging the gap between research and precision medicine. *Gut Microbes* 2025;**17**.

Thibaut M.M. Bindels L. B. Crosstalk between bile acid-activated receptors and microbiome in entero-hepatic inflammation. *Trends Mol. Med* 2022;28(3):112-236.

Thompson JD, Higgins^{+} DG, Gibson TJ. CLUSTAL W: Improving the Sensitivity of Progressive Multiple Sequence Alignment through Sequence Weighting, Position-Specific Gap Penalties and Weight Matrix Choice. *Nucleic Acids Res* 1994;**22**:4673-80.

Trauner M, Fuchs CD. Novel therapeutic targets for cholestatic and fatty liver disease. *Gut* 2022;**71**:194–209.

Vital M, Rud T, Rath S *et al.* Diversity of Bacteria Exhibiting Bile Acid-inducible 7α-dehydroxylation Genes in the Human Gut. *Comput Struct Biotechnol J* 2019;**17**:1016–9.

Wahlström A, Sayin SI, Marschall HU *et al.* Intestinal Crosstalk between Bile Acids and Microbiota and Its Impact on Host Metabolism. *Cell Metab* 2016;**24**:41–50.

Watanabe M, Fujita Y, Hagio M *et al.* Bile acid is a responsible host factor for high-fat diet-induced gut microbiota alterations in rats: proof of the "bile acid hypothesis." *Biosci Microbiota Food Health* 2025;**44**:110–21.

Watanabe M, Fukiya S, Yokota A. Comprehensive evaluation of the bactericidal activities of free bile acids in the large intestine of humans and rodents. *J Lipid Res* 2017;**58**:1143–52.

White BA, Cacciapuoti AF, Fricke RJ *et al.* Cofactor requirements for 7α-dehydroxylation of cholic and chenodeoxycholic acid in cell extracts of the intestinal anaerobic bacterium, *Eubacterium* species V.P.I. 12708. J. Lipid. R. 1981;**22**:891-898.

Wickham H. *Ggplot2: Elegant Graphics for Data Analysis*. Verlag New York: Springer, 2016.

Xu H. Fang F. Wu K. *et al*. Gut microbiota-bile acid crosstalk regulates murine lipid metabolism via the intestinal fxr-fgf19 axis in diet-induced humanized dyslipidemia. *Microbiome* 2023;11(1)-262.

Yokota A, Fukiya S, Ooka T *et al.* Is bile acid a determinant of the gut microbiota on a high-fat diet? *Gut Microbes* 2012;**3**:455–9.

Yoshimoto S, Loo TM, Atarashi K *et al.* Obesity-induced gut microbial metabolite promotes liver cancer through senescence secretome. *Nature* 2013;**499**:97–101.

Zhang D. Lv W. Xu Y. *et al*. Microbial bile acid metabolite ameliorates mycophenolate mofetil-induced gastrointestinal toxicity through vitamin d3 receptor. *Am. J. Transpl* 2024;24(7):1132-1145.

Zhao M. Zhao J. Yang H. *et al*. The bile acid-gut microbiota axis: A central hub for physiological regulation and novel therapeutic target for metabolic diseases. Biomedicine and Pharmacotherapy 2025;18:118182.

Zheng X, Huang F, Zhao A *et al.* Bile acid is a significant host factor shaping the gut microbiome of diet-induced obese mice. *BMC Biol* 2017;**15**.